WIND ATLAS OF BAY OF BENGALWITH SATELLITE WIND MEASUREMENT

A Thesis Submitted to
the Graduate School of Engineering and Sciences of
Izmir Institute of Technology
in Partial Fulfillment of the Requirements for the Degree of

MASTER OF SCIENCE

in Energy Engineering

by
Navila Rahman NADI

September 2016
IZMIR

We approve the thesis of **Navila Rahman NADI**
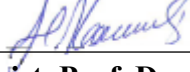
Examining Committee Members:

_____
Assist. Prof. Dr. Ferhat BINGÖL
Department of Energy Systems Engineering, Izmir Institute of Technology

_____
Assist. Prof. Dr. Bergüzar ÖZBAHÇECI
Department of Civil Engineering, Izmir Institute of Technology

_____
Assist. Prof. Dr. Ziya Haktan KARADENİZ
Department of Mechanical Engineering, Izmir Katip Çelebi University

20 September 2016

_____
Assist. Prof. Dr. Ferhat BINGÖL
Supervisor, Department of Energy
Systems Engineering, Izmir Institute of
Technology

Dr. Merete BADGER
Co-Supervisor, Department of
Wind Energy, Technical
University of Denmark (DTU)

_____
Prof. Dr. Gülden Gökçen AKKURT
Head of the Department of Energy
Engineering

_____
Prof. Dr. Bilge KARAÇALI
Dean of the Graduate School of
Engineering and Sciences

ACKNOWLEDGEMENTS

ABSTRACT

WIND ATLAS OF BAY OF BENGAL WITH SATELLITE WIND MEASUREMENT

The objective of this study is to obtain appropriate offshore location in the Bay of Bengal, Bangladesh for further development of wind energy. Through analyzing the previous published works, no offshore wind energy estimation has been found here. That is why, this study can be claimed as the first footstep towards offshore wind energy analysis for this region.

Generally, it is difficult to find offshore wind data relative to the wind turbine hub heights, therefore a starting point is necessary to identify the possible wind power density of the region. In such scenario, Synthetic aperture radars (SAR) have proven useful. In this study, SAR based dataset- ENVISAT ASAR has been used for Wind Atlas generation. Furthermore, a comparative study has been performed with Global Wind Atlas (GWA) to determine a potential offshore wind farm. Additionally, the annual energy production of that offshore windfarm has been analyzed by combining SAR, GWA and ASCAT datasets.

Through ASAR based Wind Atlas and GWA comparison, some differences has been found as less sampled ASAR datasets were achieved for some nodes. Thus, Weibull statistical analysis are performed to have a better Weibull fitting and accurate estimation of Annual Energy production (AEP). The study summarizes that, satellite datasets can be a very useful method to detect potential zone if compared with any long time statistical result and bathymetry data together. In this study, all three datasets comprises similar AEP at the coastal area which indicates beneficiary pace for future wind energy sector of Bangladesh.

ÖZET

UYDUDAN ALINAN RÜZGAR ÖLÇÜMLERİYLE BENGAL KÖRFEZİNİN RÜZGAR ATLASININ OLUŞTURULMASİ

Bu çalışma Bangladeş, Bengal Körfezi'nde bulunan rüzgar kaynakları açısından elverişli açık deniz konumlarını belirleyerek, rüzgar enerjisinin kullanımının daha da geliştirilmesini amaçlamaktadır. Daha önce yayınlanmış çalışmalar analiz edilmiş ve Bengal Körfezi'nde uydu verilerine dayanan açık-deniz rüzgar enerjisi potansiyeli tahminlerine rastlanmamıştır. Bu nedenle, bu çalışma Bengal Körfezi'nde açık-deniz rüzgar kaynakları analizi için ilk adım olarak değerlendirilebilir.

Genellikle, kule yüksekliğine yakın açık-deniz rüzgar verisi bulmanın zor olmasından dolayı bölgenin olası rüzgar enerji yoğunluğunu belirlemek için bir başlangıç noktası belirlemek gerekmektedir. Böyle durumlarda, Sentetik açıklıklı radarın (SAR) açık-deniz rüzgar haritalamasında ki başarısı bilinmektedir. Bu nedenle, SAR tabanlı veri setleri olan ENVISAT ASAR bu çalışmada rüzgar atlası üretimi için kullanılmıştır. Ayrıca bu çalışmada, bir potansiyel açık-deniz rüzgar tarlası belirlemek amacıyla Global Rüzgar Atlası kullanılarak karşılaştırmalı bir çalışma yapılmıştır. Önerilen rüzgar tarlasının konumu dört kritere dayanarak belirlenmiştir. Bu kriterler sırası ile yüksek çözünürlüklü SAR veri seti, en yüksek rüzgar hızı bölgesi, bölgenin sahile yakınlığı ve daha düşük deniz tabanı derinliğidir. Ayrıca, Bengal Körfezi'nde ki belirlenmiş konumun enerji üretim potansiyelini tahmin etmek için söz konusu rüzgar tarlasının yıllık enerji üretimi, SAR, GWA ve ASCAR veri setleri kullanılarak analiz edilmiştir.

ENVISAT ASAR'a dayanan Rüzgar Atlası ve GWA karşılaştırılırken, daha az ASAR veri seti örneklerinin elde edilmesinden dolayı sonuçta bazı farklılıklara rastlanmıştır. Doğru Weibull parametreleri seçildiğinde, rüzgar hızı ölçümleri ve bu uzaktan ölçüm metotlarının enerji yoğunluğu hesapları daha büyük benzerlik göstermektedir. Seçilen alanın yıllık enerji üretiminin ve girdap kayıplarının daha doğru ve yerinde bir analizini yapmak için kapsamlı bir şekilde her iki uydu tabanlı veri setinin Weibull istatistiksel analizi gerçekleştirilmiştir.Bütün bu çalışma özetlemektedir ki, uzun dönem istatistiksel sonuç ve barimetri veri kombinasyonu karşılaştırılırsa, ENVISAT ASAR verisi kullanımı potansiyel alan tespitinde çok kullanışlı bir yöntem olabilmektedir. Bengal Körfezi'ne dair bu çalışmada, ıyılık alanda her üç veri seti de benzer yıllık rüzgar enerjisi üretimine işaret etmektedir ve bu Bangladeş'in gelişen rüzgar enerji sektörü için yararlı olabilir.

TABLE OF CONTENTS

LIST OF FIGURES

LIST OF TABLES

CHAPTER 1

INTRODUCTION

1.1. Wind Energy and Current Scenario

In the 20th century, huge energy demand has emerged because of the rapid increase of population and industrialization across the world. Energy is one of the most important elements of economic sustainability. But to provide sustainable development, the environment and economic conditions should be accounted for. Today, it is commonly accepted that the Earth's fossil energy resources are very limited. If new reserves of global oil, gas and coal could not be discovered, the price of these sources will rise continuously while the production rates show declining tendency. In addition, these fossil fuel power plants load the atmosphere with greenhouse gases and particulates which is around 50 to 60%, resulting in global warming and climate change (Mathew, 2006). With an increment towards usage of energy will lead to a more atmospheric polluted world in near future. And in search of alternative way, the sustainable energies like wind energy has a great impact. Wind Energy is considered as one of the world's fastest emerging renewable energy sources nowadays. Due to the developments concerning in technology, the practice of wind energy is emerging rapidly in onshore and off-shore systems.

Wind Energy is considered as the power extraction from the wind. The source of wind originates in the natural movement of air across the land or sea. The Earth receives around 1.7×10^{14} kW of power from the sun in the form of solar radiation and it is the major source of wind (Mathew, 2006). Land and water areas absorb and release different amount of heat received from the sun. Wind is caused by uneven heating and cooling of the Earth's surface and by the Earth's rotation. Unequal warming of the land masses closer to equator and near the poles causes differences in pressure. When warm air upswings, cooler air moves towards there to submerge its place which causes creation of local winds (Burton et al., 2001). Wind is these large masses of air moving on over the Earth's surface. Depending on the rotation of the Earth, the direction of the flow of air changes accordingly which influences the generation of a patterned large-scale atmospheric

circulation. This is called global winds (Burton et al., 2001). The non-uniformity of the Earth's surface, with its pattern of land masses and oceans, disturbs the global circulation pattern in small-scale variations (Mathew, 2006). These small-scale variations are local winds and caused by two mechanisms such as temperature and altitude difference between lands and seas in day/night period and altitude difference between mountains and lowlands (Burton et al., 2001). Wind is gained through utilization of this available source of nature through wind turbines which converts mechanical power from the wind into electrical power.

A number of assessments confirm that the world's wind resources are extremely large and well distributed across almost all regions and countries. The total available resource that is technically recoverable is estimated to be 53,000 Terawatt hours (TWh)/year (EWEA, 1999). This is over twice as large as the projection for the world's entire electricity demand in 2020 (EWEA, 1999). The excepted growth of renewable energy is being driven by environmental, social, political and economic concerns. Analysis by the EWEA shows that there are no technical, economic, or resource limitations for wind power to supply 12% of the world's electricity by 2020 (EWEA, 1999). With stronger political commitments worldwide, the wind energy industry could install an estimated 1.2 million MW by 2020 (EWEA, 1999).

The recent scenario of emerging wind energy industry represents the social need and awareness of nations to implement emission free technologies in order to mitigate climate change and air pollution. This growing renewable energy's competitiveness relative to other sources of electricity certainly include the economic growth of the world and promotes new successful market of this new form of renewable energy.
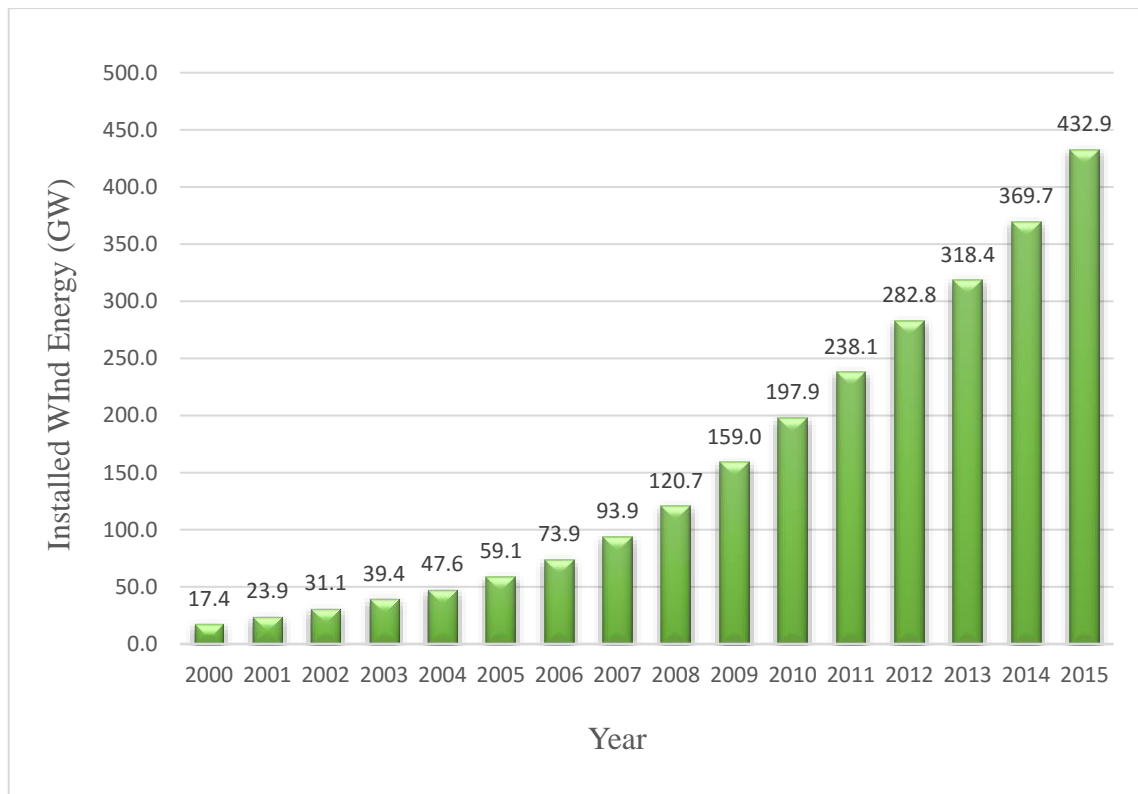
Figure 1.1. Total worldwide installed wind energy capacity
(Source: GWEC, 2015)

Wind Energy Market has been growing in a rapid way throughout the whole world. Based on the recent survey done, worldwide wind capacity reached around 450 Gigawatt by the end of 2015, whereas more than 63 GW were added only in the year of 2015 (GWEC, 2015). This installed amount is higher than 2014 and 2013, when 51.7 GW and 35.7 GW were added annually in each year respectively (GWEC, 2015).
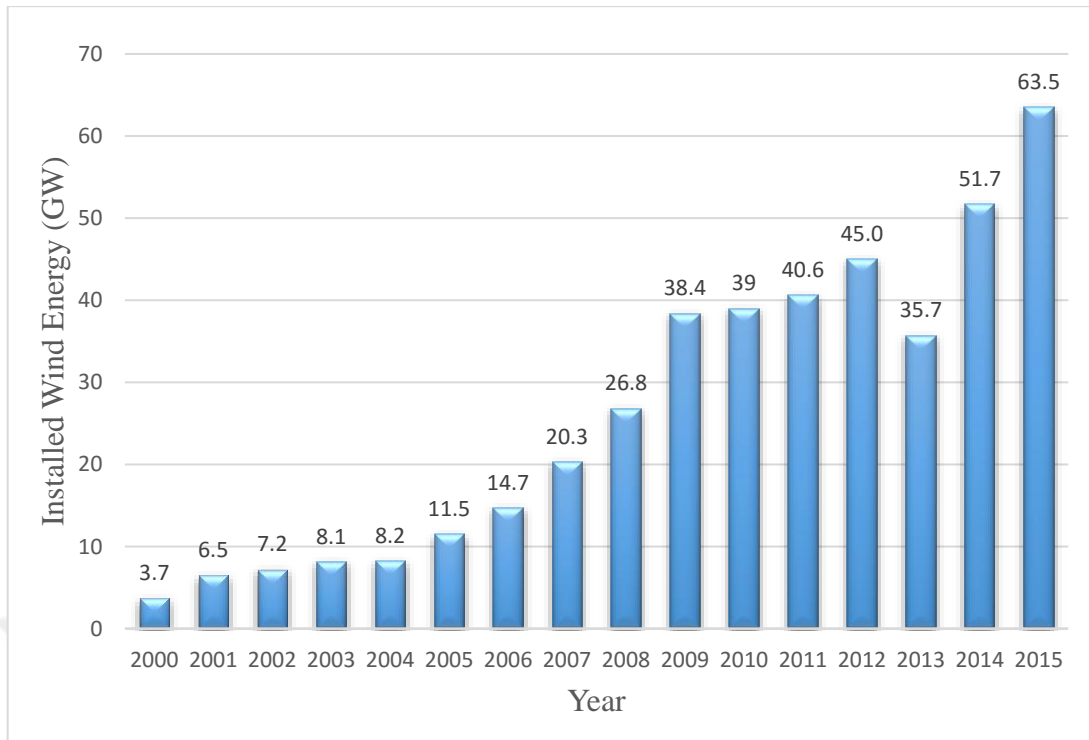
Figure 1.2. Total annual installed wind energy capacity
(Source: GWEC, 2015)

The leading countries of wind energy production are China, USA, Germany, India, Spain, UK, Canada, France, Italy and Brazil. China is holding 33.6 % share of the total installation by having 145.36 GW of wind energy installation capacity (GWEC, 2015). Germany with 10.4 %, India with 5.8%, Spain with 5.3% and UK with 3.1% share of total installation, possessing the top 5 countries in wind energy installation (GWEC, 2015).
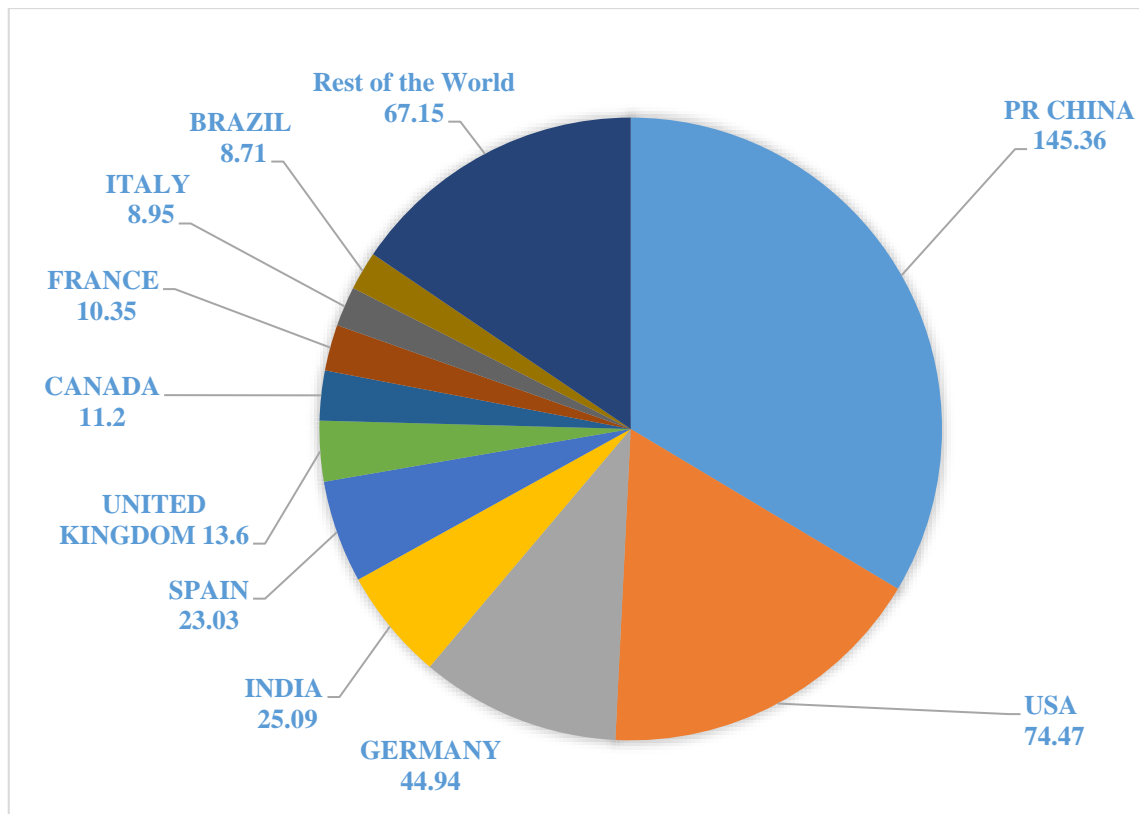
Figure 1.3. Worldwide top ten countries by total wind installation (GW)
(Source: GWEC, 2015)

1.2. Offshore Wind Energy

Offshore wind is a relatively new but potentially valuable technology. This rousing technology has already being assimilated into government's energy planning around the whole world through combining several key benefits such as: higher wind resources than onshore, lower effect of surroundings on wind flow, public acceptance of visual effects, suitability for superior development near to the main demand hubs in coastline, sensibility of installing offshore farms in higher property value densely areas. In 1991, the first ever commercial offshore wind farm was installed in Vindeby, Denmark which consists of 11 numbers of 450kW stall controlled wind turbines and was located approximately 2 km from the coastline (Henderson et al., 2003). From then, this new form of wind energy has been in a raise.
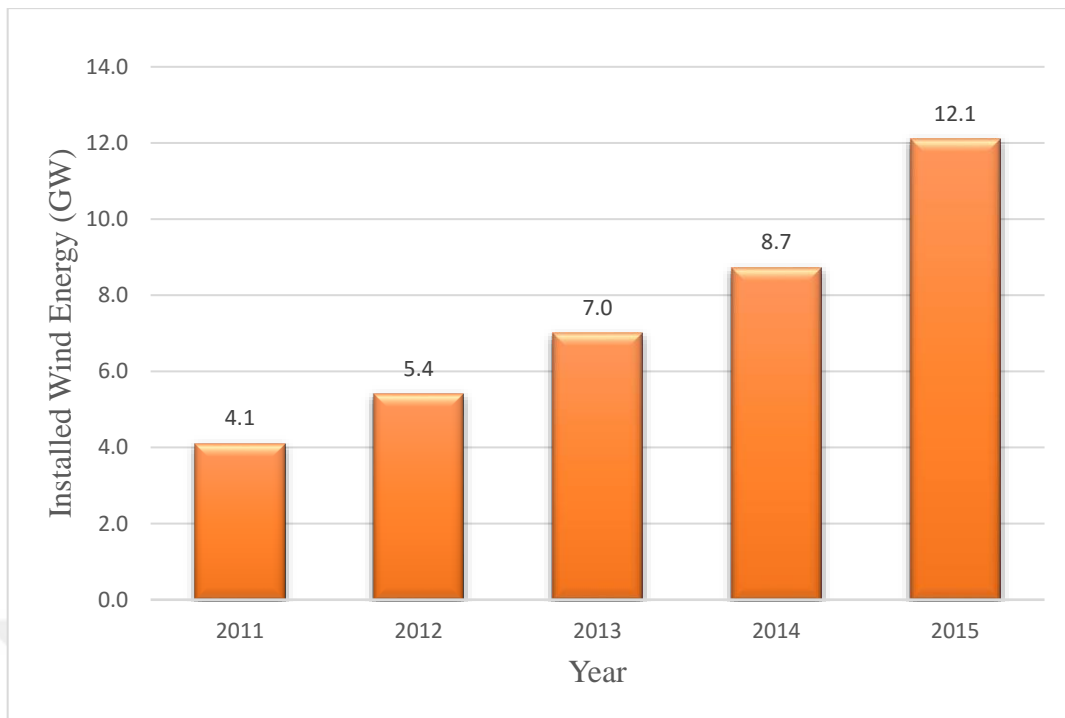
Figure 1.4. Worldwide cumulative offshore wind energy capacity
(Source: GWEC, 2015).

The total offshore wind energy capacity presently is over 12 GW having average offshore wind turbine size as almost 4.2 MW (GWEC, 2015). Currently, more than 91% (11,034 MW) of total offshore wind installations can be found in European waters; largely in UK holding over 5 GW (46%), Germany with 3.2 GW (30%) and thirdly Denmark with 1.2 GW (11.5 %) of total European installations (GWEC, 2015). The new offshore zone has been take off in China, Japan, South Korea and the US. In the row the developing offshore wind roadmap is also getting ready by GWEC (Global Wind Energy Council) for India, and other markets, such as Brazil which lead to future offshore expansion (GWEC, 2015).

	UK	Germany	Denmark	PR China	Belgium	Netherlannds	Sweden	Japan	Finland	Ireland
Total in 2014	4.50	1.01	1.27	0.65	0.71	0.25	0.21	0.05	0.03	0.03
Total in 2015	5.07	3.29	1.27	1.01	0.71	0.42	0.20	0.05	0.02	0.02
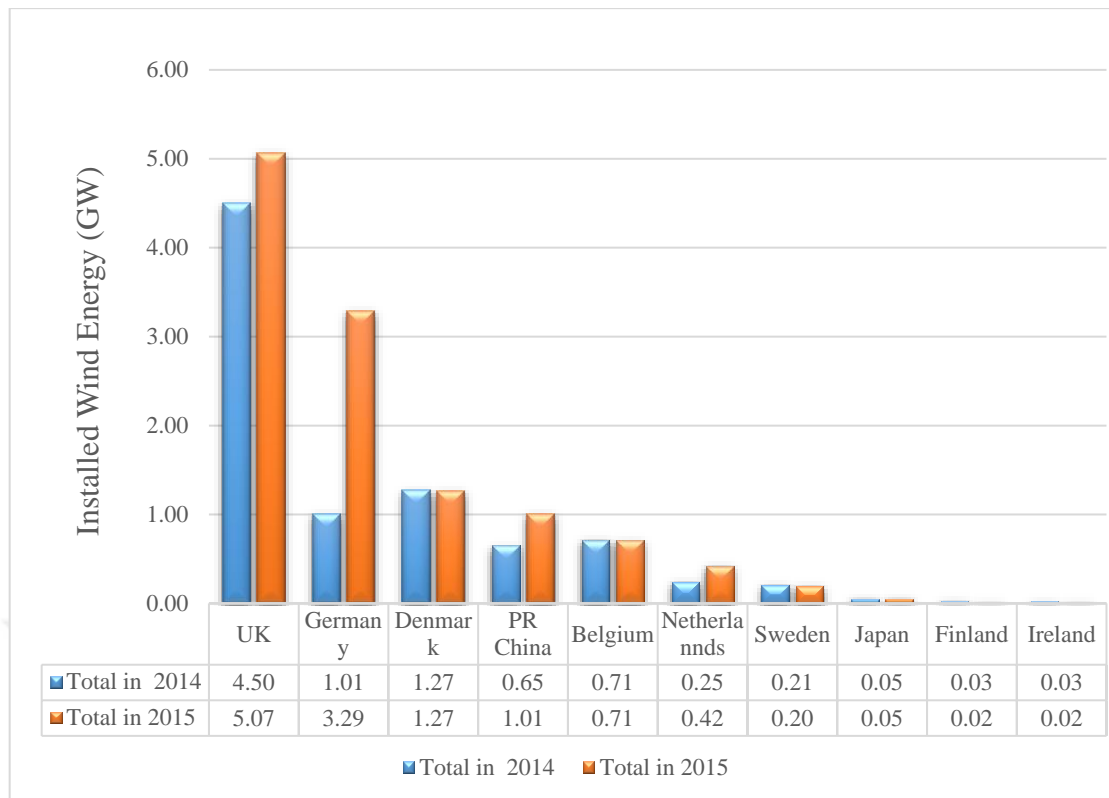
Figure 1.5. Worldwide top 10 countries by total offshore wind installation
(Source: GWEC, 2015)

The average depth covered by these offshore wind turbines is 27.1 meters (GWEC, 2015). Also the latest technology of offshore wind energy is applicable with an average distance of 43.3 km from the coast (GWEC, 2015).

1.3. Conventional Wind Energy Measurement Techniques

A site's wind power potentiality depends on wind speed largely as wind energy production is a cubic function of wind speed. So, really a slight change in wind speed can bring a huge difference in the wind energy estimation as well in production. That is the reason behind precise emphasization on wind speed measurement which represents the higher accuracy in financial estimation of a project also. Basically the measurements are of two types: meteorological tower (met mast) by direct observation of wind resources and remote sensing is done by SODAR (Sonic detection and ranging), LIDAR (Light detection and ranging) and Satellite based instruments.

In direct observation, a met mast is used to measure some aspects of the meteorological conditions such as: wind speed, wind direction, temperature, barometric pressure, relative humidity etc. The core of the measurement technique is the collection of various data through different equipment such as: Anemometer, Wind Vane and other sensors. Anemometer is used to define the wind speed. There are several types of Anemometers basically classified being their rotational methods. Wind vane is the device to measure the wind direction which is necessary to determine the preferred terrain shape and optimizing the layout of the wind turbine in a wind farm.

(a) Tower met mast   (b) Anemometer   (c) Wind vane

(d) Analog sensors (Temperature and humidity-pressure)   (e) Data logger

Figure 1.6. Conventional wind energy measurement equipment
(Source: Pramod, 2011)

Other sensors of conventional measurement techniques consists of temperature sensor, humidity sensor, barometric pressure sensor solar radiation sensor etc. The temperature and pressure sensors compute air density precisely. The temperature sensor is also used to detect icing conditions that can cause the sensors to stop or produce errors in measurement. All of these terms are significantly useful to be measured for the wind farms operating environment and sustainability issues.

There is also an essential part of conventional measurement techniques which includes Data logger. Data logger is a device through which all the sensors are connected. Usually data loggers consist of 12–15 channels to which the measured values by the sensors will be transmitted every 2s (Pramod, 2011). The data logger collects all those values for 10 min. Which means, it collects 300 values (per minute 30 values) and then computes average, standard deviation, maximum, and minimum from the 300 values and these values are being recorded with a specific timeframe (Pramod, 2011).

The remote sensing equipment-SODAR uses sound waves to measure wind speeds in various heights of 50 m to 200 m above ground level. Alike SODAR, LIDAR is used for the same purpose but using light waves. On the other hand Satellite is used to

map wind over water surfaces by measuring the small scale variation of waves of the water.

1.4. Wind Resource Assessment (WRA) and Wind Atlas Methodology

Wind resource assessment (WRA) is the procedure of estimating the strength of wind resources at a planned wind project site. After these assessment the general wind conditions and annual energy production at a project site can be estimated. Meanwhile, a preliminary financial assessment is done through financial model to figure out if the wind project is feasible. WRA is an accumulation of cumulative data that comprises of annual or seasonal WRM (Wind Resource Mapping), Wind rose, average turbulence intensity, average wind shear and Weibull parameters for the distribution of wind speed, Average annual energy production for chosen turbines of a wind farm. Basically wind resource estimation is perceived through fitting a Weibull function towards the time series observations of wind speed and wind direction achieved at least for 1 year in the specific site. This adjusted probability density function is categorized by a scale parameter (A) and a shape parameter (k). These parameters are useful to determine the mean wind speed and the wind power density.
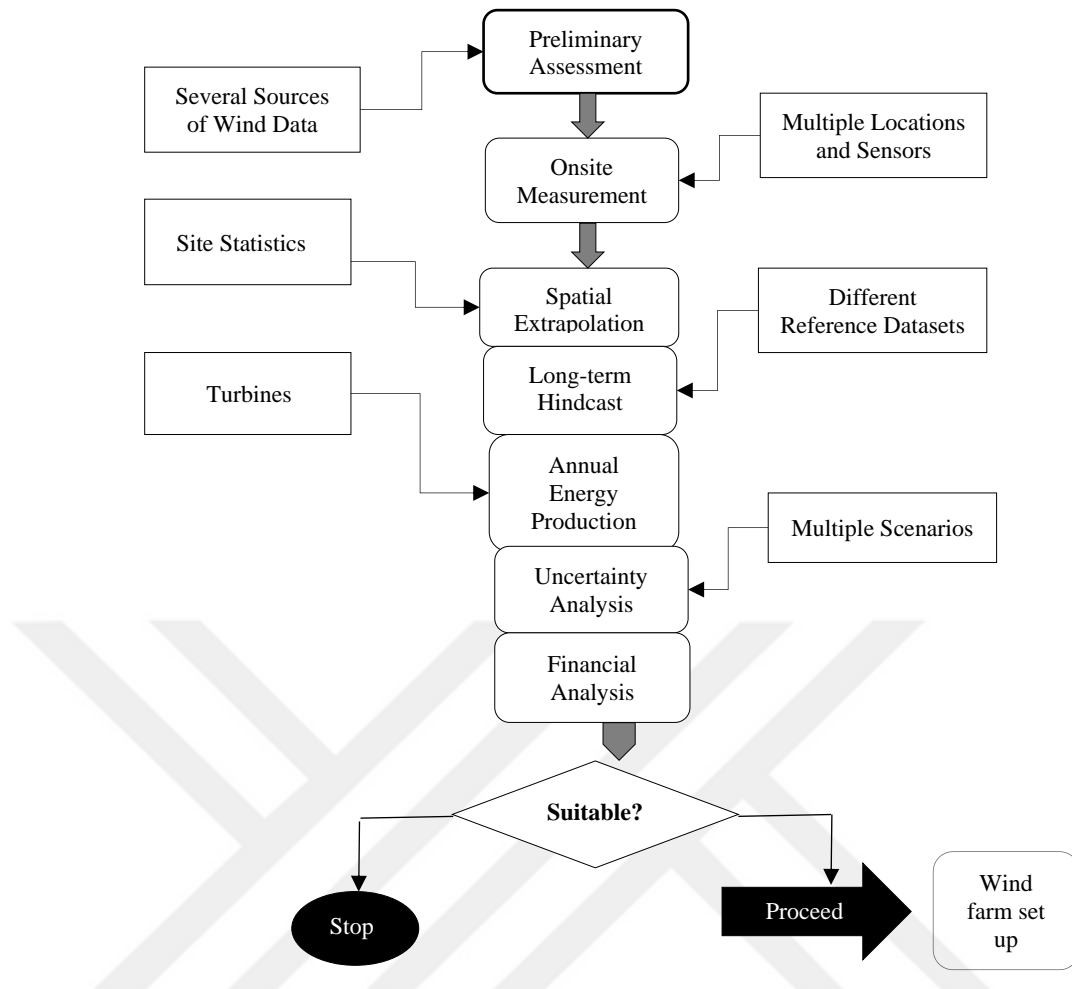
Figure 1.7. Wind Resource Assessment (WRA) and financial analysis process.
(Source: Pramod, 2011)

The first step begins with the evaluation of different sites depending on publicly available wind resource maps and wind data. Depending on the sites suitability, it is being performed with assessments for one year or more years. After collection of the wind data for a satisfactory period, the comprehensive process of WRA begins. In this step the wind speeds over the total project area is estimated by using the measured data at several locations within the area. The following step is to use measure-correlate-predict (MCP). MCP extrapolates the measurement data and produces a long-term dataset which comprises all the time period covered by the reference dataset. The Reference datasets are long-term wind data from a variety of sources like reanalysis data from network of weather stations, airports, and others. The proceeding stage is to estimate the annual energy production (AEP) which is computed with several power production curves from various turbines. The final step is to compute uncertainty of AEP and the whole WRA

data is being input to the financial analysis step, in which the financial feasibility of the project is assessed. Afterwards, if the whole scenario becomes feasible and worthy, the process of wind farm set up starts in a row for electricity production.

Wind Atlas is a mapped version of wind speed, wind direction and wind energy capacity of a specific region. Wind Atlas Methodology is generally a predicted formation of the wind energy potential from high quality wind measurement. It helps to transform comprehensive information about the mean wind climate from one predictor site to predicted site. The predictor site can be a meteorological station, wind-monitoring mast, or a grid point in a mesoscale modelling domain. These atlases provide annual average wind speed categories or wind speed ranges over large areas. The methodology consist of two types: Observational wind atlas methodology where the predictor is a real met-station and Numerical wind atlas methodology whereas the predictor is a virtual met station.
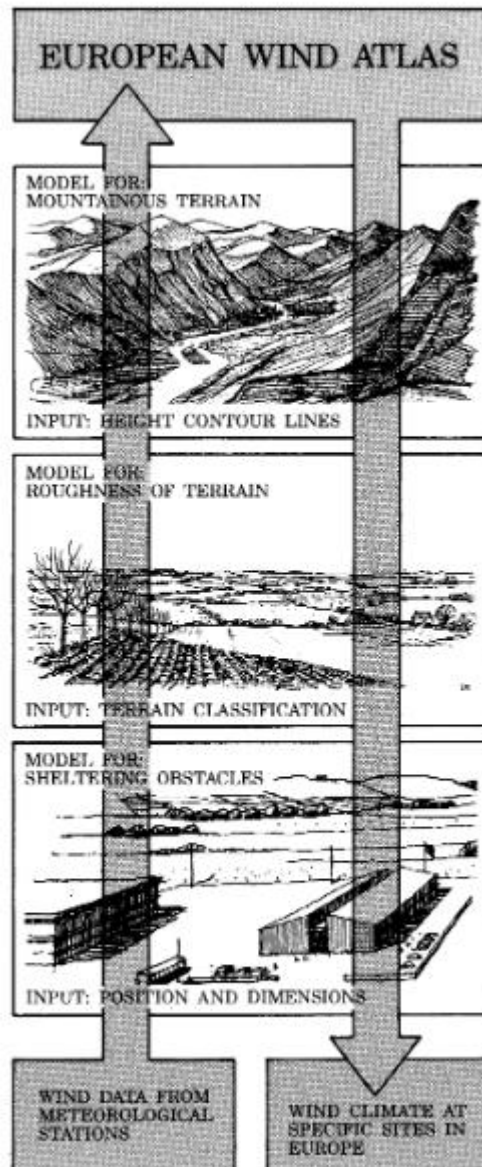
Figure 1.8. WAsP model for Wind Atlas generation
(Source: Mortensen et al., 2007)

Wind Atlas Analysis and Application Program (WAsP) is being widely used for Wind Atlas generation where it turns an observed wind dataset into generalized wind climate and represents the various formation of wind datasets to create the site specific Wind Atlas.

CHAPTER 2

SATELLITE WIND MEASUREMENTS

2.1. New Satellite Technologies for Offshore Wind Measurement

Increasing demand of offshore wind parks in various countries has promoted wind resource mapping over the sea. The original method to estimate the wind energy resource is by installing a meteorological mast at one or more specific sites for minimum one year. This mostly requires more time as well as becomes too costly furthermore. And this drawback leads to find another alternative method which may give preferable indications of wind resources and help in proper decision making of feasibility studies for the prospective wind parks. In such scenario, Satellite remote sensing is useful. Execution of these satellite based images in the early stages of wind farm planning is becoming trustworthy because of its growing improvement and cost effectiveness (Beaucage et al., 2008). This useful method can predict perfect area of higher wind resources which leads to the planning of feasibility studies. Wind maps retrieved from the Satellite datasets can be later fully investigates to provide a faithful supplement to the traditional assessments (Beaucage et al., 2008).

In our study, two types of satellites were analyzed which are: Synthetic Aperture Radar (SAR) and Scatterometer. Our studied datasets were attained from SAR methodology based Advanced Synthetic Aperture Radar (ENVISAT ASAR) and from Advanced Scatterometer (ASCAT). During this study, the SAR methodology has been utilized to create a Wind Atlas for the Bay of Bengal. In addition, using ASAR and ASCAT datasets, the energy density was estimated for a specific location.
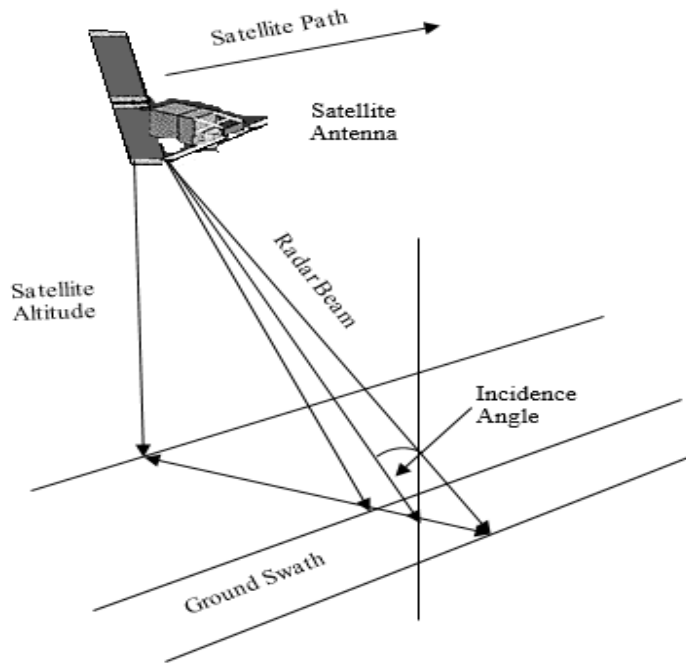
Figure 2.1. Geometry of SAR imaging
(Source: Christiansen, 2006)

Hereafter, it should be mentioned that, this thesis study does not clarify the process of satellite imaging, as the analysis of the study has been started after obtaining the wind retrieval datasets of the mentioned satellite images. Furthermore, the study continued with those datasets to create a Wind Atlas and to perform wind statistical analysis for estimating the energy density and a wind firm production assessment.

2.2. SAR Technology

Synthetic Aperture Radar (SAR) is a remote sensing technique which transmits microwave pulses of energy to illuminate an area of the Earth surface. The pulses gets scattered because of the surface properties and a portion returns to the instrument with a change in amplitude, polarization, travel time and phase (Beaucage et al., 2008). All these backscattered signals[1] for each foot print area stores in the satellite to process a two dimensional image of the surface. For each resolution cell, around 4000 of those backscatter signals added up to distinguish the object (Beaucage et al., 2008). SAR has higher spatial resolution (around 1km) and preferred more for coastal wind energy

---

[1] When the microwave pulses hit the surface of the ocean a scattering effect occurs, known as backscatter.

measurements. (Hasager et al., 2015). The data acquisition from the SAR pulses can be performed in day or night even if it is cloudy or light rainy (Christiansen, 2006). SAR signals are electromagnetic waves with a polarization determined by the orientation of the electric field. (Christiansen, 2006)

The signals of the magnetic waves of the SAR proceed with a polarization which is regulated by electric field alignment. The polarization type can be vertical (V) or horizontal (H) and by recording the backscattered signal in any of the polarization the images of Normalized Radar Cross Section (NRCS)[2] can be formed. (Dagestad et al., 2012) If in both transmitting and receiving cases similar polarization is used, the images are said to be co-polarized and denoted as VV or HH. (Dagestad et al., 2012) On the other hand, if the received and transmitted polarization is different the images are called as cross-polarized and denoted as VH or HV. (Dagestad et al., 2012) Some upgraded SAR systems has the capability of transmitting and receiving both polarization simultaneously, and deliver quad observable SAR images (Dagestad et al., 2012). In addition SAR sensors have also a diverse range of 2-10 cm of wavelength (Table 2.1), though the principle of the technology remains similar just having a reckonable difference in between. (Dagestad et al., 2012)

Table 2.1. Various bands of different wavelength and frequency of SAR
(Source: Christiansen, 2006)

Band	Wavelength (cm)	Frequency (GHz)
L	15-30	1-2
S	8-15	2-4
C	4-8	4-8
X	2.5-4	8-12

2.2.1 SAR History

Satellite SAR systems for wind measurement purpose has been executed approximately 38 years since now. AMERICAN SEASAT was the first space-borne SAR

---

[2] The backscatter signals of each resolution cell across the satellite track (in ground range) and along the satellite track (of azimuth range) is denoted as NRCS

which activated in June-October 1978. SEASAT was designed mainly for ocean and ice applications (Christiansen, 2006). Afterwards, Shuttle Imaging Radars SIR-A and SIR-B in 1981 and 1984 was established. Then European Space Agency (ESA) launched the second satellite SAR in 1991, followed by another identical ERS-2 SAR in 1995. Gradually satellite SARs started to be implemented in the 1990s consisting the Russian ALMAZ, the Japanese JERS-1 and the Canadian RADARSAT-1. The additional capability of ALMAZ and RADARSAT-1 was that it was capable of scanning at numerous radar incidence angles. Furthermore, Advanced SAR launching has been done with ENVISAT by European Space Agency (ESA) in 2002. ENVISAT is being named as advanced SAR (ASAR), because of its capability of scanning the surface in one of the four polarization combinations. Followed by the advances of the technology, in 2006 the L-band PALSAR launched on the Japanese ALOS satellite which is the first fully Polari metric space borne SAR. Polari metric space borne means it can concurrently operate at the four polarization (VV, HH, HH+HV, VV+VH) combinations. In 2007, RADARSAT-2, Cosmo-Sky Med were launched which has same capability of ALOS by having C band Radar system. In the same year, Terra SAR-X was launched as an Advanced SAR method of scanning the surface in one of the four polar combinations. Afterwards, in 2012 HJ-IC was launched in China, having a comparative large incident angle with VV polarization. The latest Satellite launched by ESA is Sentinel 1 which is following the Advanced SAR method having a maximum swath width of 400 km and incidence angle range of 20-45 degrees. Summarization of the history of satellite based SAR systems is shown in Table 2.2 which includes polar orbiting, sun-synchronous satellite series. The meaning of sun synchronous, polar orbiting satellite is, it uses a definite time for ascending and descending over a specified location on the Earth.

Table 2.2. Various SAR satellites applicable for wind retrieval
(Source: Dagestad et al., 2012)

Satellite/ Sensor	Agency/ Country	Year of Operation	Radar Band	Available Polarization	Swath Width (max-km)	Incident Angle Range (Degrees)

ERS-1/ SAR	ESA	1991-2000	C	VV	100	1-2
JERS-1/SAR	Jexa, Japan	1992-1998	L	HH	75	2-4
ERS-2/ SAR	ESA	1995-2001	C	VV	100	4-8
RADARSAT 1	CSA,MDA,Canada	1995-	C	HH	500	8-12
ENVISAT/A SAR	ESA	2002-2012	C	VV,HH, HH+HV, VV+VH	400	15-45
ALOS/PALSAR (2 Satellites)	Jaxa, Japan	2006-	L	Quad	350	8-60
RADARSAT 2 (3 satellites)	CSA,MDA,Canada	2007-	C	Quad	500	10-59
Cosmo-SkyMed (4 satellites)	ASI, Italy	2007-	X	Quad	200	20-60
TerraSAR-X (close formation with TanDEM-X)	DLR, Germany	2007-	X	VV,HH, HH+HV, VV+VH	100	15-60
HJ-1C	CAST, China	2012-	S	VV	100	25-47
Sentinel-1 (2 satellites)	ESA	2014-	C	VV,HH, HH+HV, VV+VH	400	20-45

2.4 ENVISAT ASAR

Environmental satellite based Advanced Synthetic Aperture Radar (ENVISAT ASAR) is an imaging microwave radar appliance which emits microwave radiation to image the surface of the atmosphere, ocean, land and ice (Dagestad et al., 2012). ENVISAT is being named as advanced SAR (ASAR), because of its capability of scanning the surface in one of the four polarization combinations. It is being established by European Space Agency (ESA) in 1 March until 9 May, 2012, when ESA lost the contact with the satellite on 8 April 2012 (Dagestad et al., 2012). The satellite take images and send to the base station down in earth to preserve the images. ENVISAT ASAR provides images at various resolutions. The spatial resolution is around 150 m and swath mode around 400 km (Christiansen, 2006). The total incidence angle coverage is 15-45

degree (Christiansen, 2006). In the scenario of ocean winds, the average of around 1km resolution is processed for SAR images in a purpose to lessen the natural speckle noise and modulation error (Hasager et al., 2015).

From ENVISAT ASAR the data acquisition can be done in different modes like (a) the normal imaging mode (IMG) which is done in a different range of incidence angles, (b) wide swath mode (WSM) having a swath of 400 km, (c) a burst-mode known as alternating polarization (APP) and (d) global monitoring (GM) mode (Small, Rosich, Schubert, Meier, & Nüesch, 2005). In WSM (wide swath mode), it can map a point at mid-latitude (55°N) 15 times per month around (Hasager et al., 2015). The ENVISAT ASAR dataset is freely accessible from the European Space Agency (ESA)[3] achieve from where the required data can be downloaded and used for further research works.

2.4.1. Processing Chain of ENVISAT ASAR

The satellite scenes of ENVISAT ASAR goes through some specific processing chain to create the Wind Atlas. The following Figure 2.2 illustrates the elementary process chain which starts with the downloading and preprocessing of the scenes from the Satellite towards the server. In this precise point a long term black and white general images of the ocean and earth is being stored and preprocessed. The next step belongs to the term wind retrieval which results as wind speed verified wind field images of those Satellite scenes. This whole process of the wind retrieval is done with a patented software called by ANSWRS (Applied Physics Laboratory National Oceanic and Atmospheric Administration (NOAA) SAR Wind Retrieval System) (Christiansen, 2006).

---

[3] http://earth.esa.int/
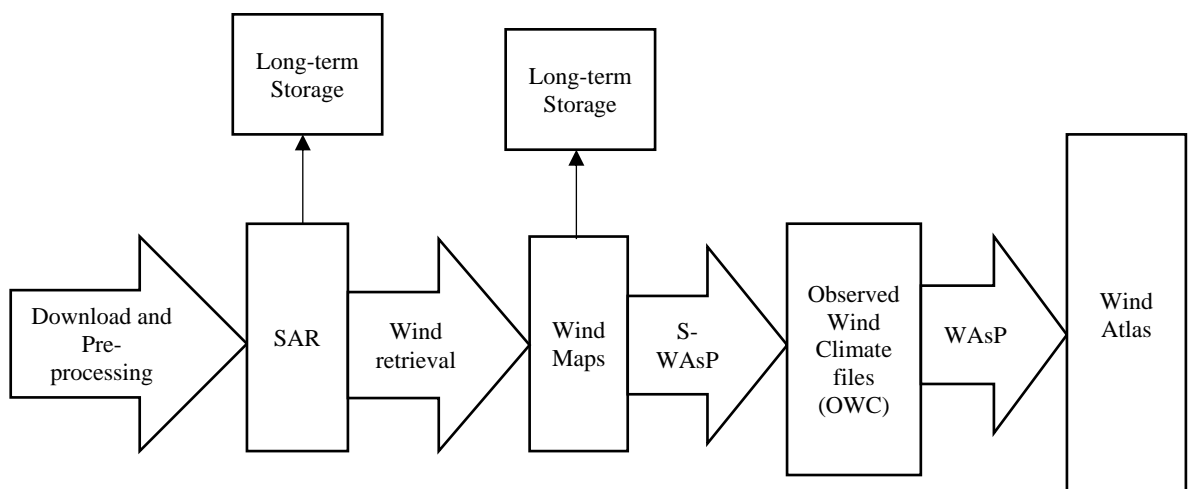
Figure 2.2. Processing chain of SAR images
(Source: Badger, 2015)

In this process a "Satellite Wind Atlas Analysis and Application Program: S-WAsP" is vastly used which is developed at Risø, DTU (Hasager et al., 2008). It takes input of the SAR scenes from ANSWRS to achieve respective wind maps in a database for each nodal point and perform statistical analysis. The end product of this processing is ASCII (text) files with a file name extension 'tab'[4] created for each nodal point. This file comprises wind roses[5] , wind speed bins, height of observation above ground level and the geographical coordinates (latitude and longitude) of the location. The defined files are further analyzed by WAsP to create wind atlas which is actually an offshore wind resource map in various format of wind energy parameters. The Wind Atlas can be in a form of wind speed and wind energy density at 10 m agl.[6] Also the Weibull scale (A) and shape (k) factors can be displayed through this wind atlas.

2.4.1.1. Wind Retrieval of ENVISAT ASAR Scenes

The ENVISAT ASAR possesses long term satellite images in black and white formats. This images are linked with wind datasets by wind retrieval operation. The SAR radar pulses interacts with the waves of the sea by Bragg scattering. There is a relationship between the co-polarized Normalized Cross Section (NRCS) and the strength of the local wind to backscatter forms as equation 2.1 mentioned in (Christiansen, 2006):

$$\sigma^o = U^{\gamma(\theta)}A(\theta)[1 + B(\theta, U)cos\emptyset + C((\theta, U)cos2\emptyset \qquad (2.1)$$

Here, σ^o refers to the normalized radar cross section (NRCS), U as the wind speed at the height 10 m, θ as the local incidence angle, and Φ as the wind direction with respect to the radar direction. In addition, A, B, C, and γ defines the functions of wind speed and the local incidence angle (Christiansen, 2006).

---

[4] Observed wind climate file format.
[5] Frequency of the occurrences of the wind in a number of 12 sectors.
[6] above ground level

In our study, the theory behind the wind retrieval has not been described in detail as it is mentioned before that this study comprises the data analysis after getting the SAR retrieved formats. In addition, already a patented software package named ANSWRS is there to be used for the wind retrieval of the achieved ENVISAT ASAR images. ANSWRS is installed at DTU and DTU holds the user access license of this software. ANSWRS is a well effective software for wind retrieval from the ASAR WSM scenes which has been used in all previous SAR based offshore wind atlas generation (mentioned afterwards in this chapter) and the parameters of this software has been kept confidential.

A series of geophysical model functions (GMF) have been applied to transform the ENVISAT ASAR imagery to wind retrieved speed defined scenes (Christiansen, 2006). GMF is a function which combines the radar observables (NRCS) with the near surface wind speed. Usually in a near neutral atmospheric stability cases, GMFs are being applied to open oceans. In our case, the most recent one CMOD-5.n was used for wind retrieving. CMOD-5.n is an updated version of the CMOD5 which provides neutral condition of wind speed at 10m (Hasager et al., 2015). This CMOD-5.n model functions is valid from lower range towards higher range of wind speed (32 ms^{-1}) that considered as hurricane speed (Soisuvarn et al.,2013).

The SAR wind speed retrieval requires information about the wind direction beforehand, as the SAR images are one directional (Christiansen, 2006). In our study, the SAR wind directional data was attained at 1 degree latitude and longitude resolution from the US Navy Operational Global Atmospheric Prediction System (NOGAPS). NOGAPS is modeled as 6-hourly wind direction provider which were interpolated spatially to be suitable for usage with the SAR images (Hasager et al., 2015). From previous researches it has been found that, the wind retrieval of SAR images for 10-m wind speed has a nominal accuracy of ±2 ms^{-1} (Christiansen, 2006).

2.4.1.2 S-WAsP Application

Satellite wind atlas Analysis and Application program (S-WAsP) is a database which makes a spatial statistics where it collects various scenes in a one dataset. The statistical methodology is same with the WAsP Engineering. A ground based measurement collects data in an interval of 10 minutes average. But, for satellite scenario, at least for 1 year it contains statistical analysis and application parts which possess a

huge bins of wind frequency distribution datasets. For this reason, Satellite WAsP is utilized and over the wind observations, S-WAsP fits a Weibull function for each grid cell of a definite domain. It provides a statistical summary of the observed, specific wind climate by analyzing time-series of wind measurements which results wind speed distribution graph combining mean wind speed and mean power density, frequency distribution of wind speeds, and the Weibull scale (A) and shape (k) parameters for each sector. After the S-WAsP process, the maps along with parameters can be further investigated for detailed statistics of a specific zone by Wind Atlas Analysis and Application Program (WAsP).

2.5. Scatterometer Technology

Scatterometer is a real aperture radar that also uses microwave technology like SAR, which sends pulses and receives the echoed pulses return back to the radar (Dagestad et al., 2012). If the backscattered pulses got reflected by rough surfaces, it producing stronger signals than smooth surfaces. Scatterometers are sun – synchronous polar orbiting satellites similar to SAR. These kind of satellites have a fixed local time of observations for ascending and descending mode. Scatterometers operate in the radar scale of C-band (around 5 GHz) or in Ku-band (around 13 GHz) (Hasager et al., 2006). One of the prime differences in between Scatterometer and SAR is that, Scatterometters take multiple (3 to 4) views of the surface from the antennae while SAR takes only one directional view. Due to this higher area coverage capability Scatterometer's observation rate is higher than SAR. (Hasager et al., 2006)

Table 2.3. Various Scatterometer satellites applicable for wind retrieval
(Source: COAPS, 2003)

Satellite/ Sensor	Year of Operation	Radar Band	Spatial Resolution (km)	Grid Mesh (km)	Scan Characteristics
SeaSat-A Scatterometer	1978/7/7- 1978/10/10	Ku band (14.6 GHz)	50 km	100	Two sided double swath
ERS-1 Scatterometer	1991/7 - 1997/5/21	C band (5.3 GHz)	50	50	One sided single swath
ERS-2 Scatterometer	1997/5/21 - 2011/7	C band (5.3 GHz)	50	50	One sided single swath

NSCAT	1996/9/15 - 1997/6/30	Ku band (13.995 GHz)	25	25	Two sided double swath
SeaWinds on QuickSCAT	1999/7/19 - 2009/11/23	Ku band (13.4 GHz)	25	12.5	Conical scan one wide swath
SeaWinds on ADEOS II	2002/12 - 2003/10	Ku band (13.4 GHz)	25	12.5	Conical scan one wide swath
ASCAT-A	2006/10 - Present	C band (5.3 GHz)	50	12.5	Two sided double swath
ASCAT-B	2012/10/29 -Present	C band (5.3 GHz)	50	12.5	Two sided double Swath
OCEANSAT 2	2009/9/23 - 2014/	Ku band (13.5 GHz)	25	25	Conical scan one wide swath
HY-2A	2011/9- present	Ku (13.256 GHz)	25	25	Conical scan one wide swath
ISS RapidSCAT	2014/09/20- present	Ku band (13.4 GHz)	25	12.5	Conical scan one wide swath

In addition, Scatterometes are aimed to map the ocean winds operationally , but SAR is used for various investigations- like ice monitoring, wave measurements (Beaucage et al., 2008). Moreover, Scatterometers have poorer spatial resolution (around 25km) than SAR (1km) (Hasager et al., 2006).Nevertheless, for both cases, the accuracy rate of wind speed and direction is similar. (Hasager et al., 2006)

.

2.6. ASCAT

In October 2006 the Advanced Scatterometer (ASCAT) was launched on the EUMETSAT (European Organization for the Exploitation of Meteorological Satellites) MetOp-A which is Meteorological Operational satellite program (MetOp) and became completely operational from May, 2007 until now (Ricciardulli, April 2016). From September 2012, MetOp-B became operative, whereas both of these satellites has same ASCAT instruments. ("ASCAT, Metop Meteorological Missions," 2006) In spite of ASCAT's main objective to measure wind speed and direction over the oceans, it has application in monitoring polar ice, soil moisture and snow cover (Hasager et al., 2015) (Ricciardulli, April 2016). Being a C-Band scatterometer, ASCAT operates two times a day (day and night) through its 3 vertically polarized antennas transmitting pulses at 5.255 GHz (Ricciardulli, April 2016). ASCAT has a double swath as the fan-beam antennae is slanted towards 45, 90, and 135° with satellite track where the extended side of antennae

possesses two swaths each consisting of 550 Km wide separated by a gap of about 670 Km nadir gap.

Having two swaths ASCAT can provide mapping of all locations at a midpoint (55°N) around 40 times per month (Hasager et al., 2015). Comparing with ENVISAT ASAR it has more frequent imaging as ASAR maps 15 times per month for the same midpoint. Researchers are expecting that ASCAT instruments (ASCAT-A and ASCAT-B) will provide improved coverage while functioning in tandem in near future. (Hasager et al., 2015) The expected observational mapping is 80 times per month for a location at 55°N (Hasager et al., 2015). The coastal wind product has a resolution of 12.5 km with a mapping capability of 10 km from the coast ("ASCAT, Metop Meteorological Missions," 2006).

Table 2.4 Important features of ASCAT
(Source: Ricciardulli, April 2016).

Geometry	3 beam antenna
Polarization	V
Frequency	5.2 GHz
Radar Band	C
Incidence angle	25°-65° (variable)
Swath	2 swaths of 550 Km each.
Resolution	12.5 (25) and 25 (50) km
Operational Time Period	2007-Current

National Oceanic and Atmospheric Administration (NOAA)'s weather forecasting and warning mission operationally supports the production and utilization of ASCAT ocean surface vector wind products (SAF, 2013). Royal Netherlands Meteorological Institute (KINMI) has developed the ASCAT wind data processor for the standard ASCAT wind by using GMF CMOD5.N (SAF, 2013). KNMI produces the gridded version (cell size of 12.5 km) product of ASCAT wind speed and direction within

EUMETSAT OSI SAF. (SAF, 2013). In our study, ASCAT observations for the year of 2015, are extracted from the ASCAT Level 3 Coastal Ocean Surface Wind Vector Product (MyOcean). L3 daily gridded wind product is available from the MyOcean catalogue after registration at[7] for the defined location.

2.7. Literature on ENVISAT ASAR Wind Resource Mapping

Satellite based offshore wind mapping study has been done in several locations to find out the basic potential of the coastal winds and offshore wind energy of those countries. But ENVISAT ASAR based offshore wind mapping was first implemented in North Sea (Christiansen et al., 2006). Gradually, in some various offshore cases, ENVISAT ASAR based wind resource mapping has been performed. Among those studies, the ENVISAT ASAR datasets were compared with various other satellite based systems (Quick Scatterometer- QuikSCAT, ASCAT) to present a relative comparison between the achieved results. Also some cases, satellite measurements were compared with the In situ (on site) measurement to have a better comparison methodology. But in none of the studies, a specific case study has been performed by finding out a potential zone from those atlases, which makes our study quite distinct than previous studies. Among the satellite based offshore wind energy assessment studies, the main projects having ENVISAT ASAR dataset comparisons, are presented here for a glance.

2.7.1. Wind Resource Assessment in the North Sea

This is considered as the first ENVISAT ASAR used wind resource mapping (Hasager et al., 2015) where a dataset from two SAR satellite technology (ERS-2 and ENVISAT ASAR) was used (Christiansen et al., 2006) to analyze the accuracy of SAR technology in wind resource assessment. In the year among 1999-2005, total 91 scenes were examined against the In situ measurement where 22 were from ENVISAT ASAR and rest from ERS-2 (Christiansen et al., 2006). The images were mostly acquired in image mode rather than WSM for the study site of Horns Rev which is 14–21 km and 2 km far from offshore and one offshore wind farm respectively. (Christiansen et al., 2006) The wind direction from onsite mast and from a local gradient analysis was used for wind

---

[7] http://www.myocean.eu/web/56-user-registration-form.php

retrieval. In the case of wind speed retrieval, 3 GMF ((CMOD-IFR2, CMOD4, andCMOD5) were analyzed and compared throughout the study. The findings of this study lead to ±15% of agreement with the onsite measurements (Christiansen et al., 2006). Also it gives a conclusion of SAR wind mapping can be a reliable method for offshore wind resource assessment as the result fitted well with longer time series of in situ measurements. After this real time experiment of Satellite dataset based offshore wind energy density has gained popularity and furthermore in so many places of the world this technique has been implemented. As, we have focused on ENVISAT ASAR based satellite technology and ASCAT technology throughout this thesis, the studies related to these two types of techniques has been described hereafter. (Christiansen et al., 2006).

2.7.2 Offshore Wind Potential in South India from Synthetic Aperture Radar

The offshore wind energy study has been done based on 164 ENVISAT ASAR scenes where it comprises a small western side of Bay of Bengal under the Indian region (Hasager et al., 2011). The interest area of this study was located from 77° to 80° Eastern longitude towards 7° to 10° Northern latitude in South India (Hasager et al., 2011). The ENVISAT ASAR WSM wind scenes were collected from the year 2002 to 2011. The SAR observations were compared with QuickSCAT (Quick Scatterometer) results to obtain a comparative study analysis. The key finding of the study is around 4 to 5 ms^{-1} wind speed in the coastline, leading to 7.6 ms^{-1} offshore wind speed (Hasager et al., 2011). The study represented a wind energy from 200 to 500 Wm^{-2} for 10 m above sea level (Hasager et al., 2011). Both maps obtained from ENVISAT and QuickSCAT indicated highest mean wind speeds in the location of 78° to 79° eastern longitude to 8°0' to 8°15' northern latitude which is around 7.5 ms^{-1} (Hasager et al., 2011). In addition, general description of the winds and climate with monsoons were presented and five specific areas of special interest were identified in the study.

2.7.3. Satellite SAR Wind Resource Mapping for Offshore in China

The feasibility study of offshore wind farm development in China has been done in a total 147 selected satellite scene for the specific interest region of 119° to 125° Eastern longitude and 29° to 36° Northern latitude (Badger et al., 2014). The main

objective of this study was to create an offshore resource map through satellite measurement in high resolution and by combining this map with other datasets to estimate potential offshore wind farm location in China. From the study, it was found that the mean wind speed at 10 m varies around 7 ms^{-1} near the coastline and increases around 9.5 ms^{-1} in offshore about 100 km from the coastline in China (Badger et al., 2014). The directional wind retrieved was obtained from NOGAPS and China meteorological administration (CMA). CMOD 5 was used as the wind speed retrieval format and was processed in ANSWRS. In addition site statistics were extracted for two locations at 122.5E, 30N and 122.5E, 32.5N correspond to use for model grid points by CMA (Badger et al., 2014). The findings of this study defines that the satellite based wind resouce mapping has realistic value as further from the shore the resources were found to be higher.

Table 2.5. Previous studies based on ENVISAT ASAR

Title/ project	Time Period of ENVISAT Images	Spatial Location	Number of Scenes Used	Comparative Study	Findings
Wind Resource Assessment in the North Sea (Source: Christiansen et al., 2006)	2002-2005	Horns Rev (6.40° to 8.40° Eastern longitude and 55° to 55.80° Northern latitude)	22	Onsite measurement	±15% of agreement with the onsite measurements
Offshore Wind Potential in South India from Synthetic Aperture Radar (Source: Hasager et al., 2011).	2002-2011	South India (77° to 80° Eastern longitude and 7° to 10° Northern latitude)	164	No	Mean wind speed : 3-5 ms^{-1} (coastline) 7.6 ms^{-1} (further offshore) Energy density: 200 to 500 Wm[-2]
Satellite SAR wind resource mapping for offshore in China	2008-2009	South China Sea, Hangzhou Bay to the south and	300	No	Mean wind speed: 7 ms^{-1} to 9.5 ms^{-1}

| | | Yangtze River Delta to the north of Shanghai | | | Energy density: 300 to 100 Wm^{-2} |

Table 2.5. (Cont.)

NORSEWIND satellite wind climatology (Source: Hasager et al., 2012)	2008-2012	North Sea, Irish Sea and Baltic sea	9000	QuickSCAT and ASCAT with onsite wind farms.	Uncertainty on mean wind speed and Weibull k is around 0.04 ms-1 and for energy density from 20 to 50 Wm^{-2}.
South Baltic Wind Atlas (Source: Peña et al., 2011).	2003-2010	Baltic Sea (10° to 22° Eastern longitude and 54° to 59° Northern latitude)	1009	QuickSCAT	Weibull k and energy density ranged from 16 to 30% uncertainty.
Wind Atlas of Aegean Sea with SAR data (Source: Bingöl et al., 2013).	2002–2012	Aegean Sea (22°E to 28°Eastern longitude and 35° to 41°N Eastern latitude)	1286	No	Mean wind speed: 6 to 8 ms^{-1} Energy density: 200 to 500 Wm^{-2}

2.7.4 South Baltic Wind Atlas

In South Baltic wind atlas WRF (weather research and forecasting) mesoscale model has been used and verified by the Danish and German masts. To evaluate the spatial resolution of this WRF model, satellites (ENVISAT and QuickSAT) observables were used (Peña et al., 2011). Around 1009 number of ENVISAT ASAR WSM scenes were investigated for wind resource mapping in the location of 10° to 22° Eastern

longitude and 54º to 59º Northern latitude (Peña et al., 2011). From the key findings it has been observed that though the QuikSCAT and the WRF results matched enough whereas the Weibull k and energy density ranged from 16 to 30% uncertainty depending on the chosen fitting function for the Weibull statistics (Peña et al., 2011).

(a) South India

(b) China

(c) NORSEWIND project

(d) Baltic Sea

(e) Aegean Sea
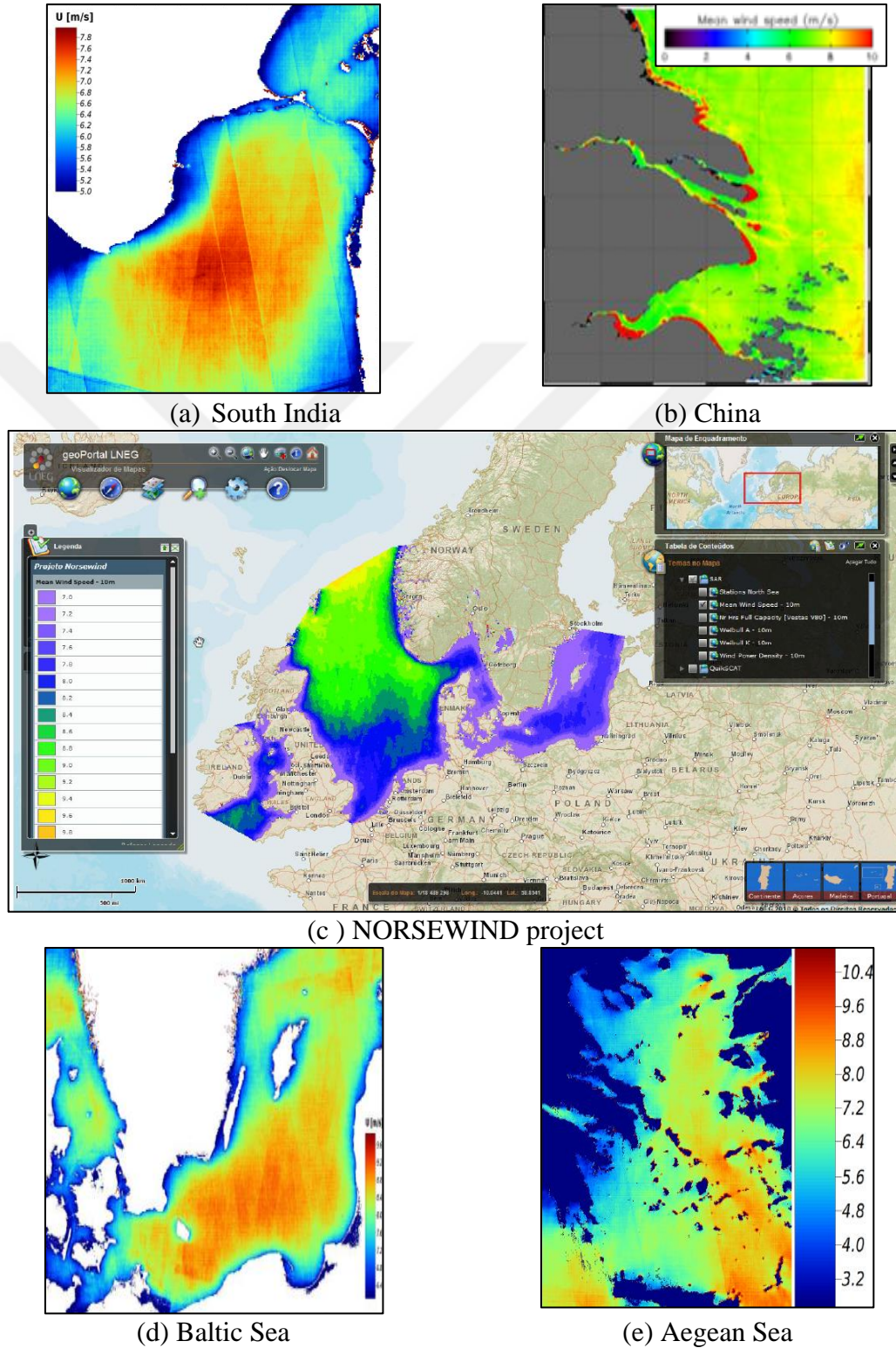
Figure 2.3. ENVISAT ASAR resource mapping of previous studies

(Source: Christiansen et al., 2006; Hasager et al., 2011; Badger et al., 2014; Hasager et al., 2012; Peña et al., 2011; Bingöl et al., 2013).

2.7.5 NORSEWIND Satellite Wind Climatology

This project was based on the Northern Seas Wind Index database which was operated from 2008 to 2012 to promote offshore wind climatology map in the Northern Seas (North sea, Irish Sea and Baltic Sea) based on satellite remote sensing (Hasager et al., 2012). Around 9000 scenes from ENVISAT ASAR was used and compared with QuickSCAT, ASCAT and In situ datasets (Hasager et al., 2012). The resulted value of wind mean speed, energy density, Weibull shape and scale parameters were compared with QuickSCAT obtained results and only mean speed with ASCAT datasets. In addition, to lift the 10m neutral wind to hub height a preliminary method has been suggested. From the project study, the mean wind speed found to be 7 ms^{-1} towards around 9.8 ms^{-1} respectively scattered near coastlines and the northern part of the North Sea (Hasager et al., 2012). The energy density found to be varied from less than 600 to more than 1000 Wm^{-2} respectively from Baltic Sea towards the northern part of the North Sea. (Hasager et al., 2012)

2.7.6 Wind Atlas of Aegean Sea with SAR Data

This study is an elementary analysis of wind energy potentiality in Aegean Sea. In between the coordinate of 22°E to 28°Eastern longitude and 35° to 41°N Eastern latitude of the Aegean Sea around 1286 ENVISAT ASAR scenes were obtained (Bingöl et al., 2013). The mean wind speed were found to be 6 to 8 ms^{-1} and available Energy density as 200 to 500 Wm^{-2} (Bingöl et al., 2013). The study dataset was not compared with any other reliable datasets furthermore (Bingöl et al., 2013).

CHAPTER 3

WIND ENERGY IN BANGLADESH

3.1. Wind Energy Scenario of Bangladesh

The potential wind energy in Bangladesh basically lies to coastlines, off-shore islands and other some main land areas (Khan et al., 2004). Bangladesh power development board (BPDB) handles the procedures of wind farm constructions such as: secure power purchase, selling and land lease, and other agreements. Around 900 KW capacity grid connected wind farm has been installed in Muhuri Dam area in Feni by BPDB ("Development of Renewable Energy Technologies by BPDB,"). In 2008, around 1000 KW capacity of Hybrid Power plant has been finalized in Kutubdia Island which is a wind battery operated Plant to provide grid connected electricity ("Development of Renewable Energy Technologies by BPDB,"). In addition, BPDB is taking further steps to install 15 MW wind power plant in onshore of different coastal regions in Bangladesh. ("Development of Renewable Energy Technologies by BPDB,") Also, 22 potential sites has been identified for comprehensive wind resource assessment and mapping in Bangladesh by Power Division and BPDB ("Development of Renewable Energy Technologies by BPDB,") Which seems that, wind energy of Bangladesh are in its own way to progress in near future. The table 3.1 provides a brief description about the demography, basic energy source and wind energy sufficiency of Bangladesh.

Table 3.1. Demography, basic energy source and wind energy dataset of Bangladesh.

(a)Demographic and Basic Energy Data (Source: "Bangladesh Energy Situation,")	
Population	168,957million
Area	147,570 sq. km
Total Electrical Energy Installed Capacity	6,208 MW
Electrification Rate	47.0%
Major Sources of Electricity	Natural Gas, Oil, Hydro, Coal

(b)Wind Energy Data of Bangladesh (Source: *Solar and Wind Energy Resource Assessment (SWERA)*)	
Total Realizable Wind Energy Potential	Over 20,000 MW
Areas with Good Wind Resource	Coastal areas and offshore islands
Total Installed Wind Energy	1.9 MW (as of 2011)

3.2. Previous Wind Resource Assessment in Bangladesh

Wind resource assessment studies has been performed in Bangladesh by numerous authors where the main focus was on the coastal areas and some specific islands (Khan et al., 2004) (Mukut et al,..2008). Based on Bangladesh metrological department, NOAA and NASA's accessible datasets, the analysis was completed which showed a great potentiality of wind energy in the coastal sides of Bangladesh comprising about 724 km alongside with Bay of Bengal. In addition, by the collaboration of Technical University of Denmark (DTU) and International Renewable Energy Agency (IRENA) a Global Wind Atlas (GWA) is now available online ("Global Wind Atlas," 2015) which is a general wide-ranging mapped form of wind energy potentiality throughout the world. The finding of the Atlas indicates a decent level of wind energy source in the coast lines. In all of those studies the wind energy potential of Bay of Bengal was not purposely focused rather than it was a scanty study. Furthermore, there is no regional wind atlas of Bangladesh or the Bay of Bengal, which can be reliable for the wind energy estimation of the Bay of Bengal, Bangladesh. Moreover, SAR based estimation and feasibility study has not been done in the coastlines and offshore of the Bay of Bengal although those previous studies, which is the main concentration of this research study.
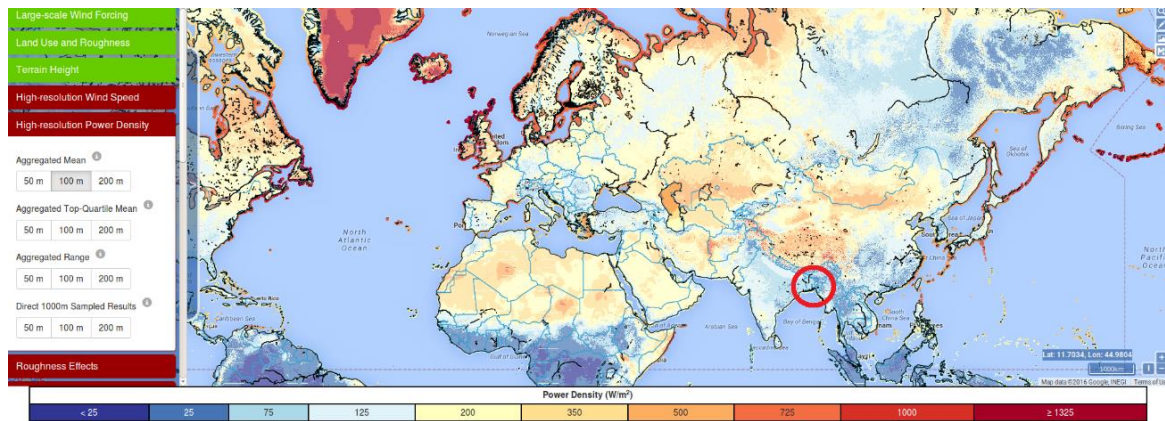
Figure 3.1. Global Wind Atlas Wind Energy Density Map at 100 m above
Ground
Level. Bangladesh has been pointed in red mark
(Source: "Global Wind Atlas," 2015)

Bangladesh Meteorological Department (BMD) has a data archive starting from 1961 which has collection of several weather stations wind speed reading all over the country (Khan et al., 2004). As the collection is done for weather forecasting purposes, the outcome is not applicable for wind energy resource assessment. In recent times, a number of different local and international organizations have team up to start the wind resource assessment projects in Bangladesh. In the below figure 3.2 shows the mean wind speed at 30m above ground level. This map is produced by "National Center for Environmental Prediction (NCEP)" and by a join collaboration with "National Center for Atmospheric Research (NCAR)" as part of world wind map (Khan et al., 2004). The general view of the analysis gives an understanding of higher wind speed in the coastal areas than in the inland. The west part has relatively higher wind energy resources than the east part of the country. But, no offshore studies has been performed by then.
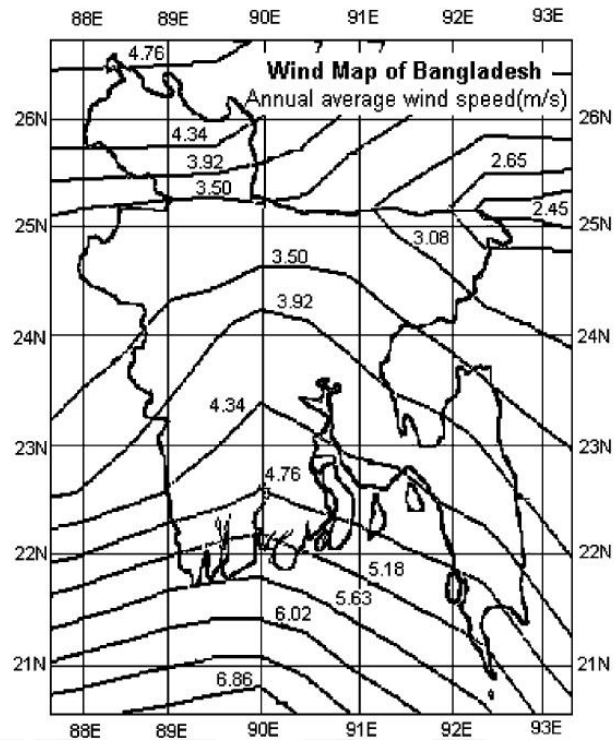
Figure 3.2. Average Wind speed of Bangladesh at 30m above Ground Level.
(Source: Khan et al., 2004).

3.3. The Bay of Bengal

The Bay of Bengal is considered as the largest Bay of the world which comprises around 2090 km of length and 1610 km of width (Kader et al., 2013). The total surface area of Bay of Bengal is around 2,172,000 km^2 and it is bounded by Sri Lanka and India in the west side, Myanmar and Andaman and Nicobar islands in the east side and Bangladesh in the North side (Kader et al., 2013). It has a high depth of 4694 m and average depth of 2600 m which can be an impeccable study area for offshore floating wind turbines (Kader et al., 2013). Though broad wind analysis has not been done yet in this bay to find out the wind energy resources. Few studies has been done in the Indian coasts which just covers a specific western zone of Bay of Bengal. Also, no wind atlas generation and wind energy estimation has been done in the Bay of Bengal which is the main concentration of this study.
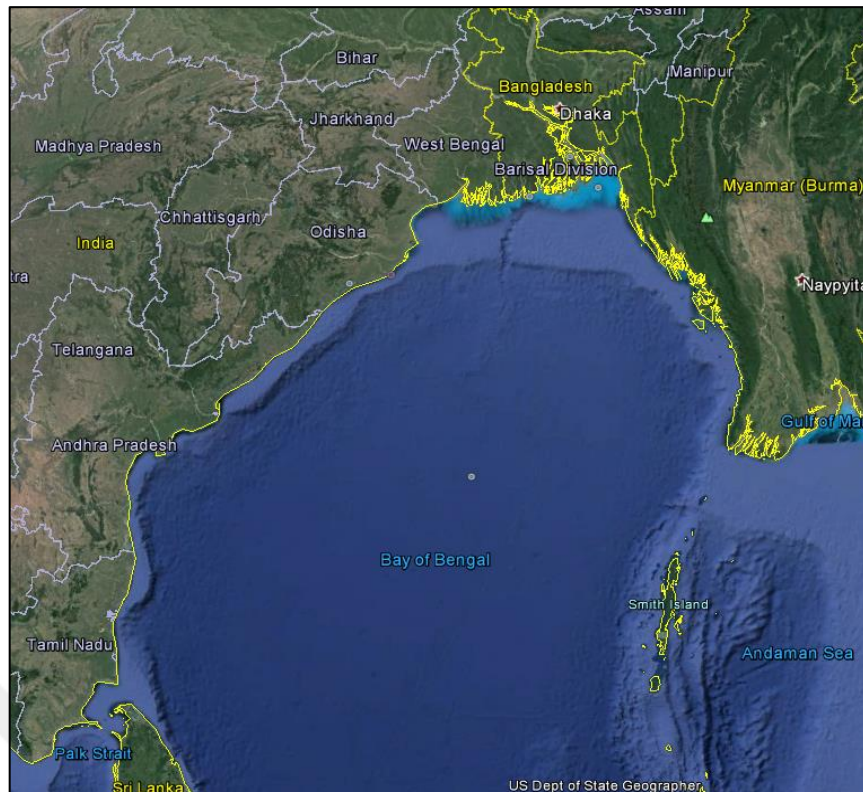
Figure 3.3. Territory of the Bay of Bengal
(Source: "Bay of Bengal,").

3.4 Bathymetry Study of the Bay of Bengal

Bathymetry is the measurement of the water surface in a sea, ocean, river or any water sources. Countries usually have bathymetry maps where the bottom topography of the water surface is briefly represented. Bathymetry mapping can be a helpful source for fisheries, sailors to prevent unwanted hazards. Also, the scientists use this bathymetry map to further research about the natural disaster scenarios, natural flow of waves and current.

In the Bay of Bengal Bathymetry mapping study, it can be seen that, (figure 3.4) it is a U shaped ocean topography divided into specific regions regarding its depth accountancies. It has the largest basin (Bengal basin/ Fan) to be situated at 21.5° Northern latitude and 86.5° Eastern latitude extended towards the Indian Ocean (Kader et al., 2013). It has a length of about 3000 km, comprising 1000 km width and thickness of 16.5 km (Kader et al., 2013). This fan was first notified In the sixties, when Bruce C. Heezen

and Marie Tharp was studying the bathymetry of the Bay of Bengal and resulted as having a canyon form of water source (Kader et al., 2013).
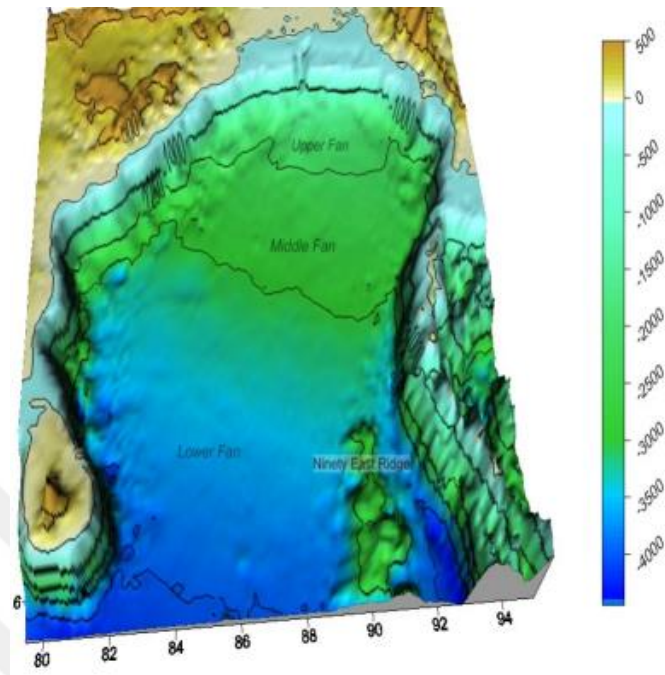
Figure 3.4. Bathymetric study of the Bay of Bengal
(Source: Kader et al., 2013).

In one previous bathymetrical study, three regional division of the Bay of Bengal has been identified calling by Upper fan, middle fan and lower fan (Kader et al., 2013). The first 1000 to 2250 m depth is divided as Upper fan whereas the Middle fan to be extended in a range of 2000 to 3000 m depth and more than 3000 m depth towards end is considered as Lower fan (Kader et al., 2013). Looking at the regional depth and extension, it can be said that, the Bay of Bengal can be a fruitful area for implementation and research study for further offshore new technologies. As, it has a broad oceanic diversity and depth, current and future technology of floating turbines can be precisely investigated and further modified by setting up here. For our research study, an area comprising the lowest depth and near to shore has been precisely investigated for wind farm estimation and further described in chapter 5.

3.5 Maritime Boundary of the Bay of Bengal

The maritime boundary division of Bay of Bengal has been a sensitive issue in between Bangladesh, India and Myanmar. On July 7, 2014, Bangladesh has been awarded around 200 nautical miles (nm) from the coast and over its continent. Beyond this limit, Bangladesh can explore and exploit the mineral and other non-living resources of the seabed and subsoil ("Bay of Bengal Maritime Boundary Arbitration between Bangladesh and India," 2014).This exclusive economic zone (EEZ) can reform a new path for renewable energy sector of Bangladesh. In addition, the area specified under Bangladesh maritime boundary is highly focused for wind energy potentiality throughout this study.

Figure 3.5. Maritime Boundary division of the Bay of Bengal
(Source: "Bay of Bengal Maritime Boundary Arbitration between Bangladesh and India," 2014)

CHAPTER 4

METHODOLOGY

4.1. Methodological Framework

The fundamental of this study is to create a wind atlas for the Bay of Bengal by using ENVISAT ASAR datasets and through a comparative analysis with Global Wind Atlas (GWA), finding a suitable location for wind farm estimation. Based on that, the wind analysis process of the Bay of Bengal has been divided into two major sections. This chapter describes the methodology behind the formation of wind atlas and the comparative study with GWA. Also, the statistical analysis method behind the wind energy estimation has been described in this chapter. Furthermore, the next chapter comprises the case study and wind energy production of the specific chosen location.

In this study wind atlas methodology has been followed to create a wind atlas. This step by step process has been displayed in a flow chart below. The interest area of our study locates in UTM 45N zone, at 82° to 95° Eastern longitude and 16.5° to 23° Northern latitude.
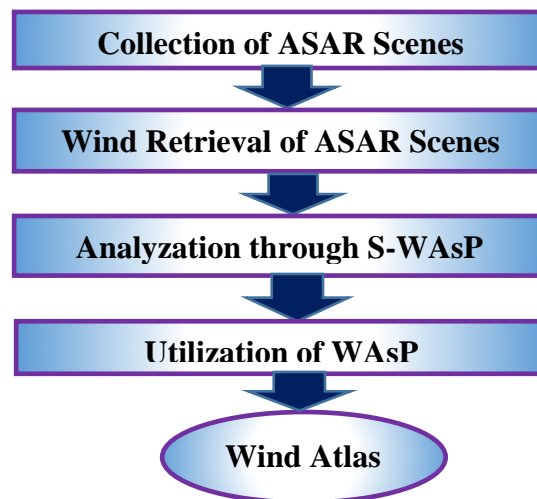
Figure 4.1 Overview of the wind atlas methodology

4.2. SAR Data Analysis of the Bay of Bengal

The Bay of Bengal has been mapped through ASAR on-board by European Space Agency satellite ENVISAT from 2006 until 2012. A total number of 466 Wide Swath

Mode (WSM) scenes from 2002 until 2012 are collected from the ESA's ordering system EOLI-SA (Earth Observation Link) with special request by DTU. Those real time ENVISAT ASAR WSM scenes are received from the ESA for further wind retrieval process. Each of those WSM scenes cover 400 x 400 km. After the wind retrieval process, all the wind maps are delivered as an image file (.png[8] and .tif[9]) and a Google Earth file (.kmz[10]).

The number of those collected scenes of the Bay of Bengal in the region under 82° to 95° Eastern longitude and 16.5° to 23° Northern latitude has been listed in the in figure 4.2, 4.3, 4.4 and 4.5. according to various aspects. The scenes are acquired in an ascending form within 3:32-4:30 UTC in the morning and descending scenes around 15:55-16:30 UTC in the evening. Among those scenes 243 has been observed in early morning and 223 in early evening. The highest scenes are attained from the month of January (72 scenes) and in the year of 2007 (135 scenes). Considering the seasonal variation, in the winter season the scenes are obtained in highest number. The seasonal variation is accounted as the spring (March to May), summer (June to August), fall (September-November) and winter (December-February). The yearly, monthly, seasonal and early morning vs early evening distribution of scenes are shown in figure 4.2, 4.3, 4.4 and 4.5 respectively.

---

[8] Portable network graphics.

[9] Tagged image format file.

[10] Keyhole Markup Language file zipped (KMZ) is a file extension for Google Earth.
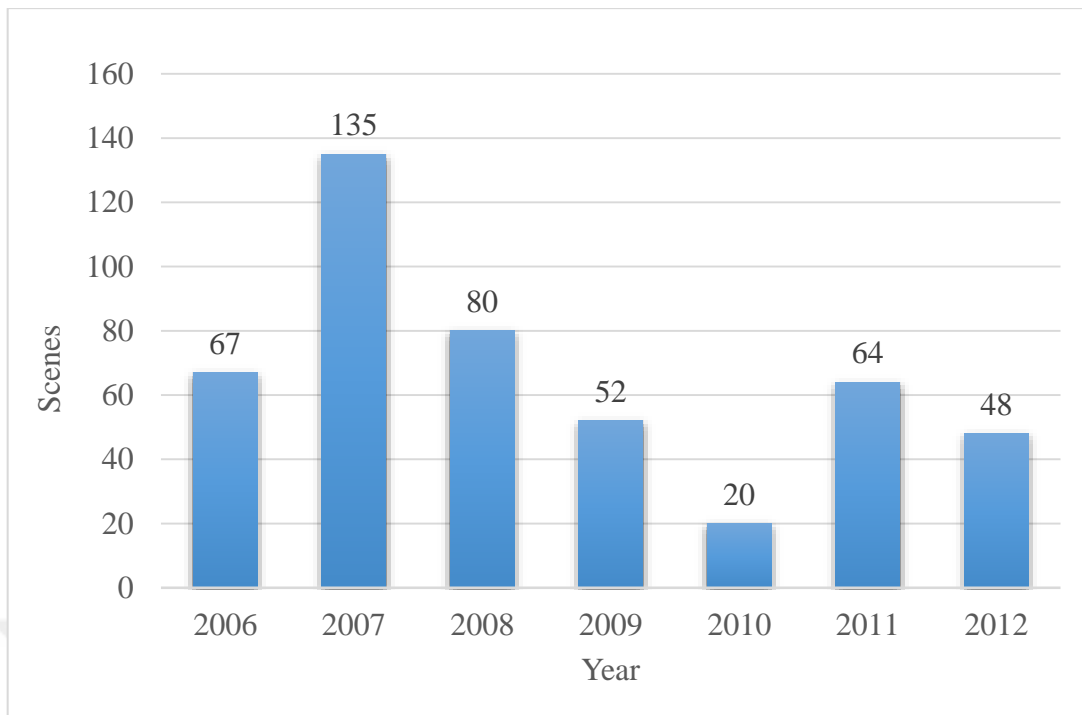
Figure 4.2 Yearly distribution of 466 ENVISAT ASAR WSM scenes.
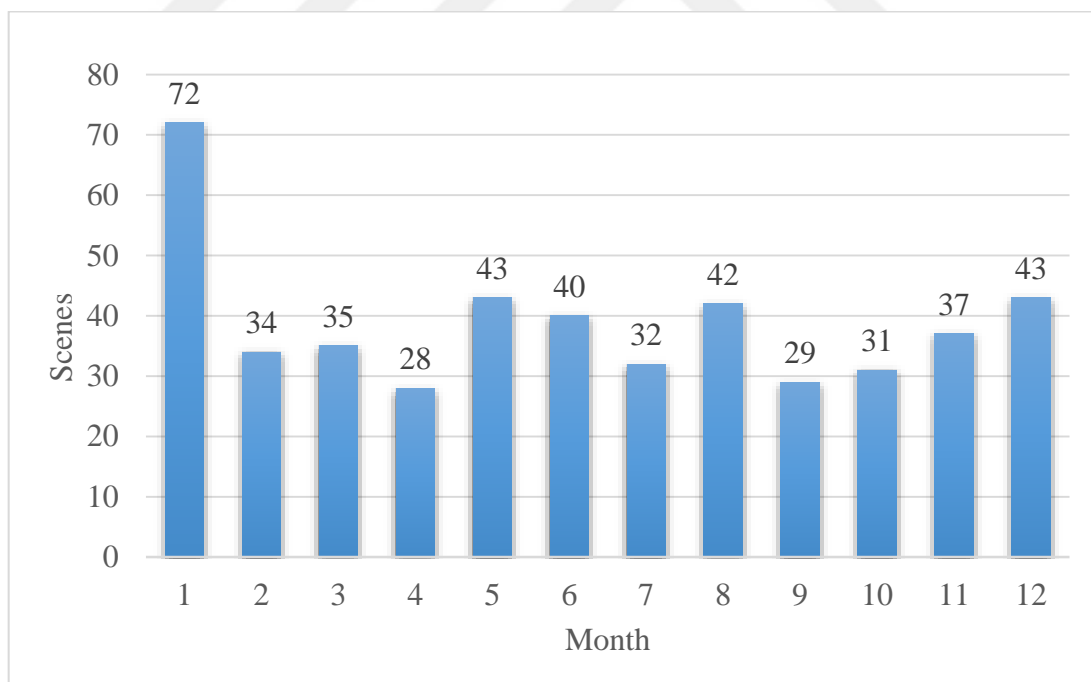
Figure 4.3. Monthly distribution of 466 ENVISAT ASAR WSM scenes.
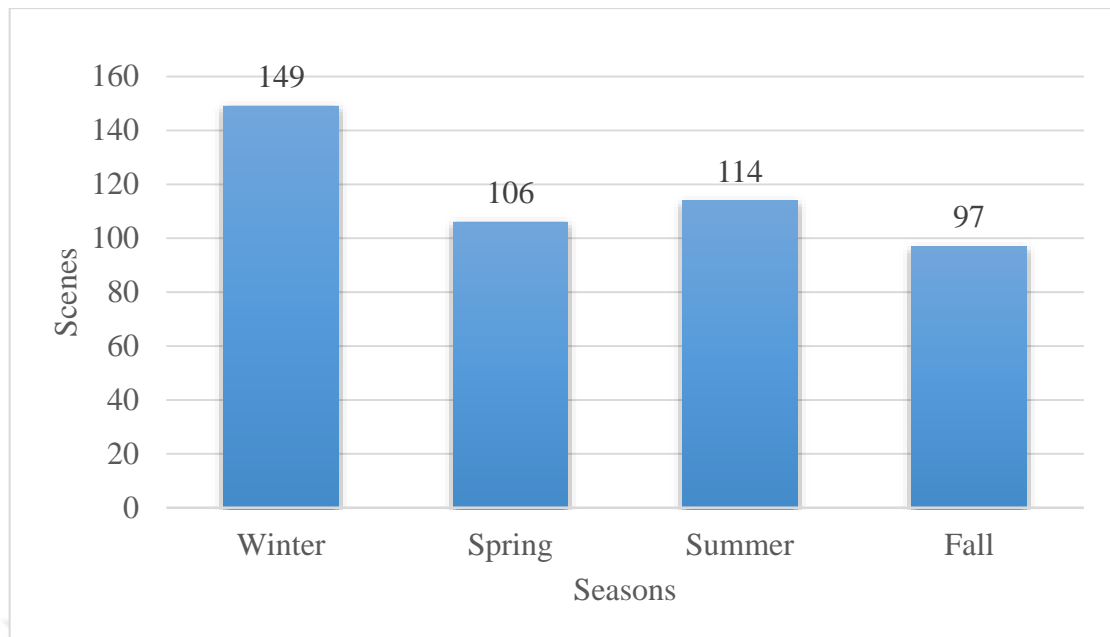
Figure 4.4. Seasonal distribution of 466 ENVISAT ASAR WSM scenes.
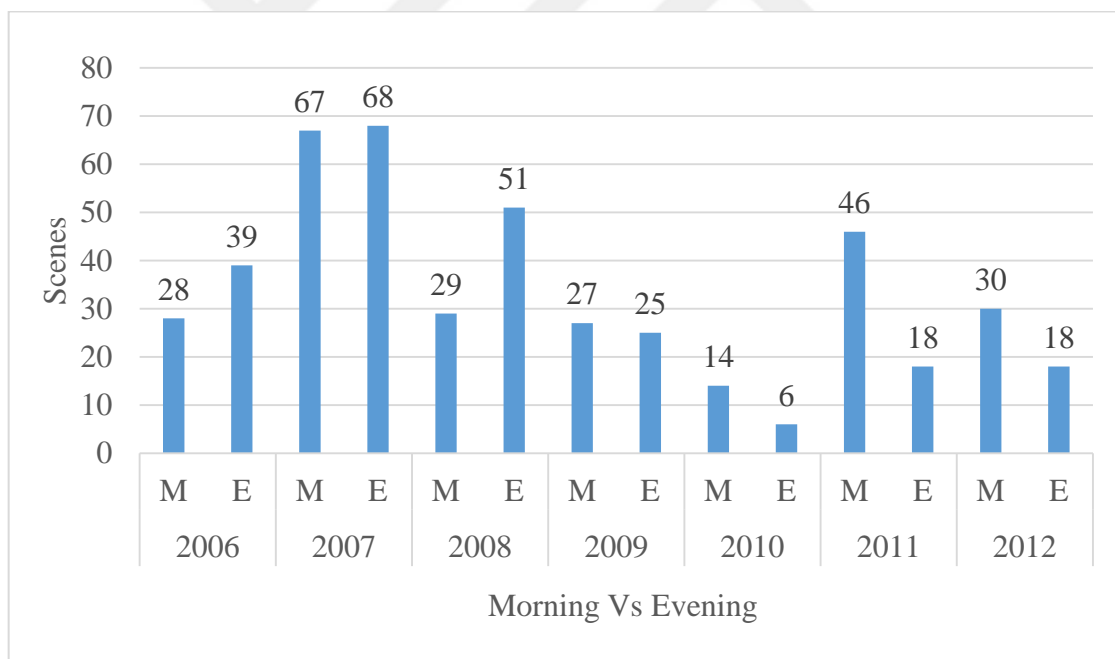
Figure 4.5. Morning vs evening distribution of 466 ENVISAT ASAR WSM scenes.

4.3. Wind Retrieval of ASAR Scenes

After receiving those WSM scenes, the wind retrieval offshore wind maps were produced by ANSWRS software. In this wind retrieval case, from NOGAPS the wind directions were received as previously it has been mentioned that, SAR only takes one directional images. So it cannot detect the wind direction by itself. For geophysical model function CMOD-5.n is being used. In the below Figure 4.6 and 4.7, it represents two ENVISAT ASAR wind maps on the date of 26 June, 2010 and 9 March 2009 respectively in ascending and descending formats. The wind barbs showing in those figures indicates the NOGAPS model wind speed and direction. Here one thing is to be mentioned that the original ENVISAT WSM pixels are re-gridded to 500 m before the wind retrieval to eliminate random noise. (Christiansen, 2006)
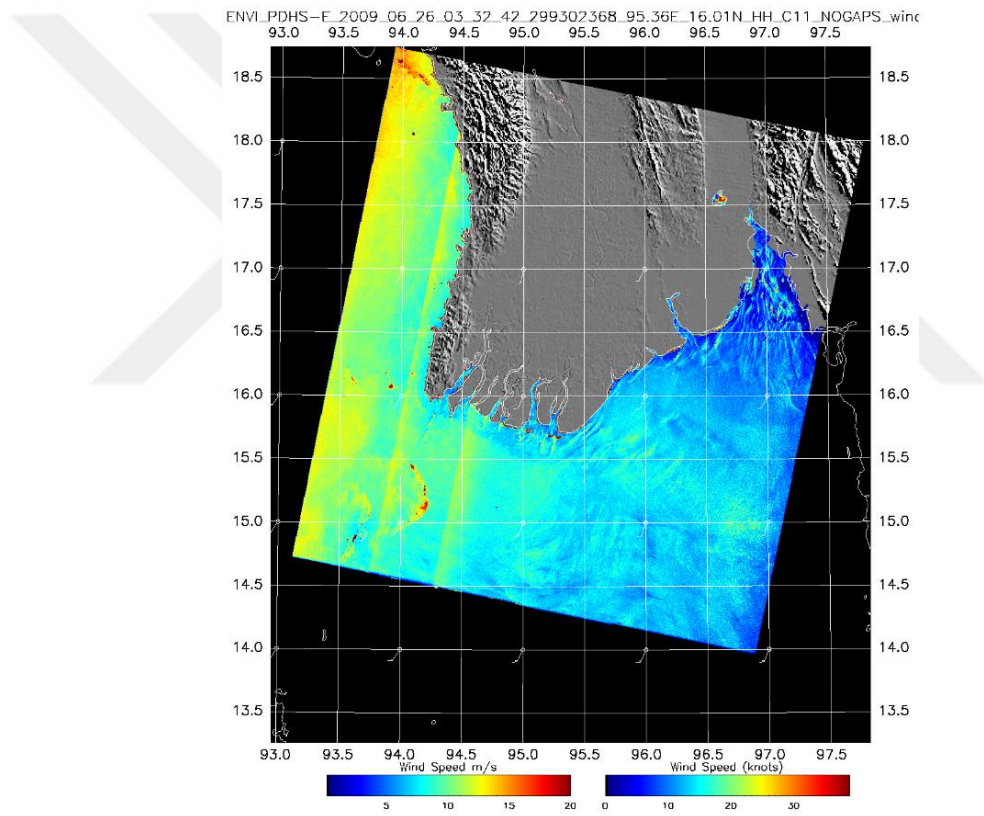
Figure 4.6. ENVISAT ASAR retrieved wind map of 26 June 2010 at 03.32:42 UTC in the

Bay of Bengal
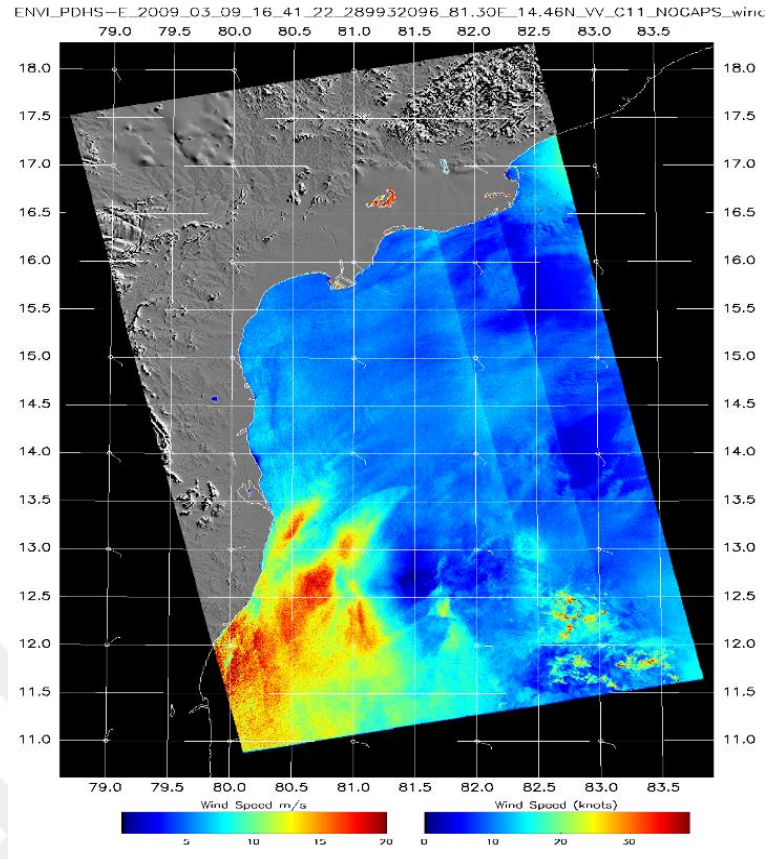
Figure 4.7. ENVISAT ASAR wind retrieved map of 9 March 2009 at 16.41:22 UTC in the Bay of Bengal.

The satellite wind retrieved fields received from the DTU were merged and combined for wind resource mapping using the DTU Wind Enegry S-WAsP.. In S-WAsP, a second moment fitting for the Weibull scale (A) and shape (k) parameters are used to fit a distribution to all data and estimate the two Weibull parameters. For each wind direction, Weibull scale parameter is found by assuming the previously found shape parameter valid for all wind directions. By using the Weibull parameters, gamma function Γ and the air density ρ (~1.245 g m−3) the wind power density is predicted in (Hasager et al., 2015) through equation 4.1:

(4.1)

$$E = \frac{1}{2}\rho A_w^3 . \Gamma(1 + \frac{3}{K_w})$$

4.4. Wind Atlas Generation

43

After S-WAsP mapping, the time-series wind measurement dataset is being generated as .tab files which is a file format for observed wind climate. From then the forming of a generalized wind climate in .lib file format begins. For this instance, a vector map of the whole zonal area is used for specific terrain analysis and a met-station for the site precise location is settled up in WAsP. If the met station location is preferable and specific under that zonal area, the Generalized Wind Climate can be further calculated. For each .tab file, the same procedure is followed to create the respective .lib files.
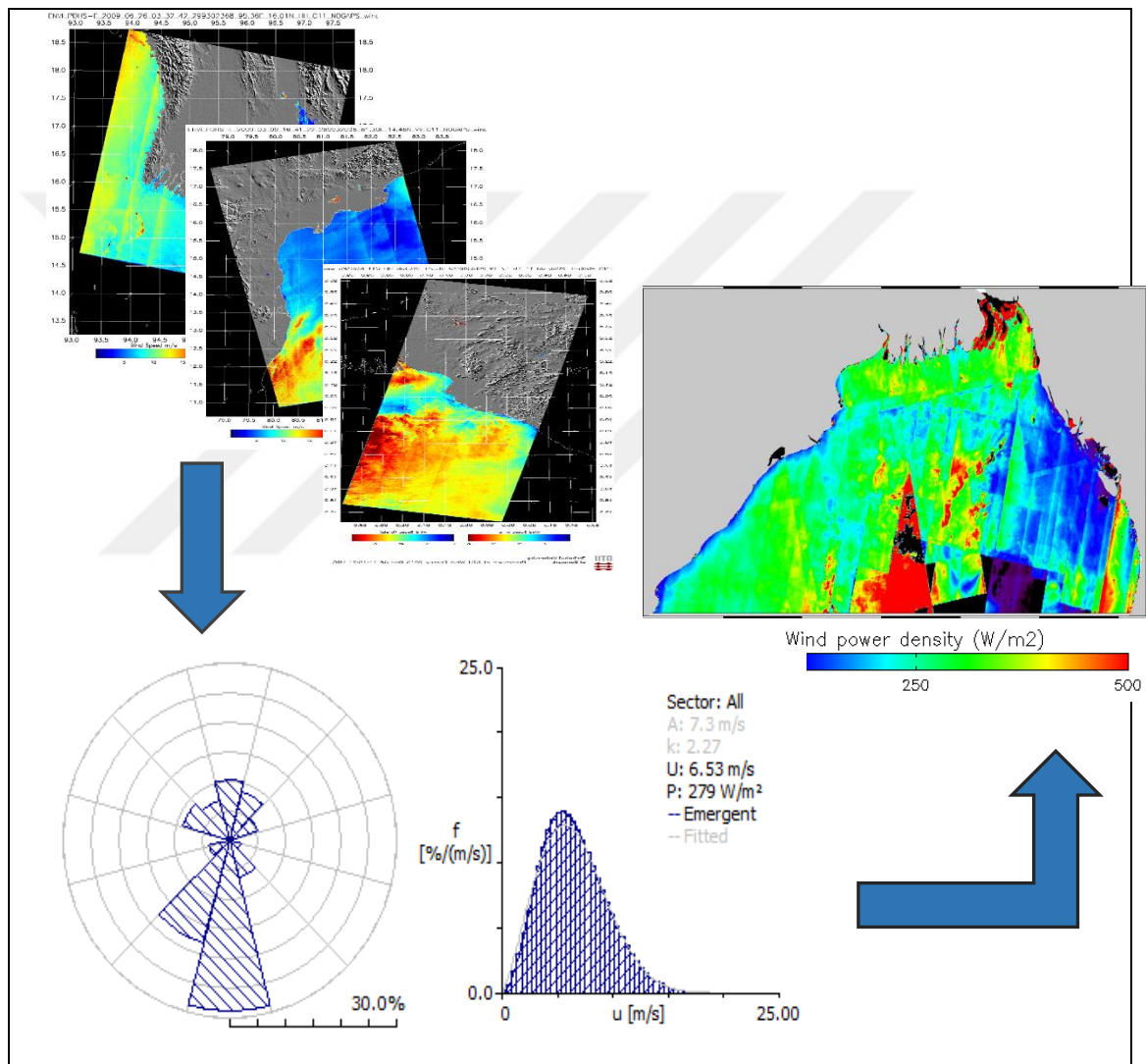
Figure 4.8. Wind resource mapping from ASAR wind scenes

The generated .lib file contains the sectoral wise frequency of occurrence of the wind (the wind rose) as well as the wind speed frequency distributions in the same sectors (as Weibull A- and k-parameters). The wind climates are specified for a number of reference roughness classes and heights above ground level. For specific roughness and

height selection, it provides a combined 12 sectoral wind rose, sectoral frequencies of the wind direction, mean wind speed, mean power density along with Weibull shape (k) and scale (A) parameters. Here, data are stored in an ASCII (text) file with the default file name extension 'lib'. The lib-file is created by WAsP from an observed wind climate, transforming the local (site-specific) wind climate into generalized (site-independent) descriptions of the wind climate.

Figure 4.9. Wind Power density of the Bay of Bengal through ENVISAT ASAR Atlas.

After achieving this .lib files, SAGA (System for automated Geoscientific Analysis) is being operated. The polygon graticule[11] was arranged in 82.33 towards 94.339 Easting and 16.75 towards 22.25 Northing with width distance of 0.667 and height distance of 0.5. At the end a single offshore wind map for the Bay of Bengal at 10m was obtained in the format of wind speed, wind energy density and Weibull parameters. Afterwards, the WAsP .lib files were used for further comparison with Global Wind Atlas (GWA) datasets.

4.5. Global Wind Atlas Analysis

---

[11] A grid of longitudinal and latitudinal lines, on which maps are drawn.

Global Wind Atlas (GWA) provides long-term high resolution wind climatology at 50, 100, 200m hub heights for the whole world including onshore and 30 km from offshore as a free access in online ("Global Wind Atlas," 2015). This wind atlas provides wind resource data at 1 km resolution and contains data at a higher spatial resolution of 250 m ("Global Wind Atlas," 2015). The information provided in the Atlas along with further specific regional studies, supports to identify the prospective areas for additional preliminary assessment of technical possibilities. In this study, the global wind dataset were collected in modern Era-Retrospective Analysis for Research and Applications (MERRA) format from the free access internet as .lib files for definite co-ordinates and then matched those nodal points with the obtained SAR data locations. MERRA is a NASA GEOS-5 data assimilation system; grid point model of 6 hourly datasets. ("Global Wind Atlas," 2015)
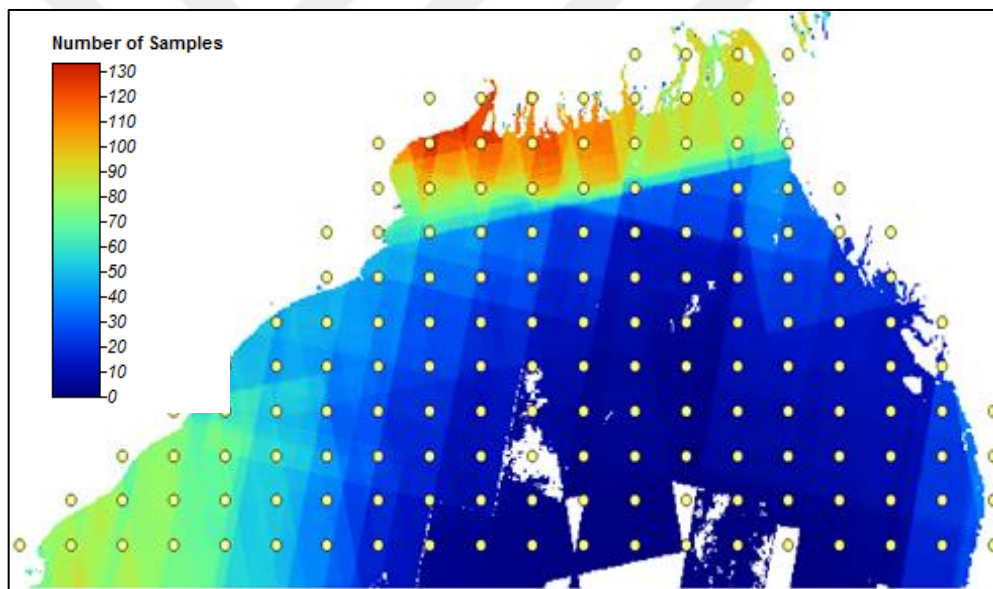
Figure 4.10. Nodal comparison of the Bay of Bengal between GWA and SAR datasets.

In the concerned area, the sample nodal locations of SAR .lib files were matched with the downloaded GWA location defined .lib files for 10m height. The nodal comparison was done in an area basis (60 km by 60 km) keeping the GWA node points in the middle. So these area wise nodal comparison was performed where122 coordinated nodal location points are found in the defined zone. While comparing the Satellite based Atlas with GWA, we have found in further from shore areas, the number of samples are really scanty which leads to a lower data obtain scenario of that particular area. The higher the number of samples, the better the estimation can be provided. In addition, from

previous studies it has been perceived that, wind resources can be predicted well enough through 70 samples considering an uncertainty of ±10% at a confidence level of 90% (Hasager et al., 2002). To gain more accuracy, those ENVISAT ASAR nodal locations were chosen which has more than 70 time series samples. This lead to 26 nodal sample comparison in between GWA and ENVISAT ASAR wind atlas.
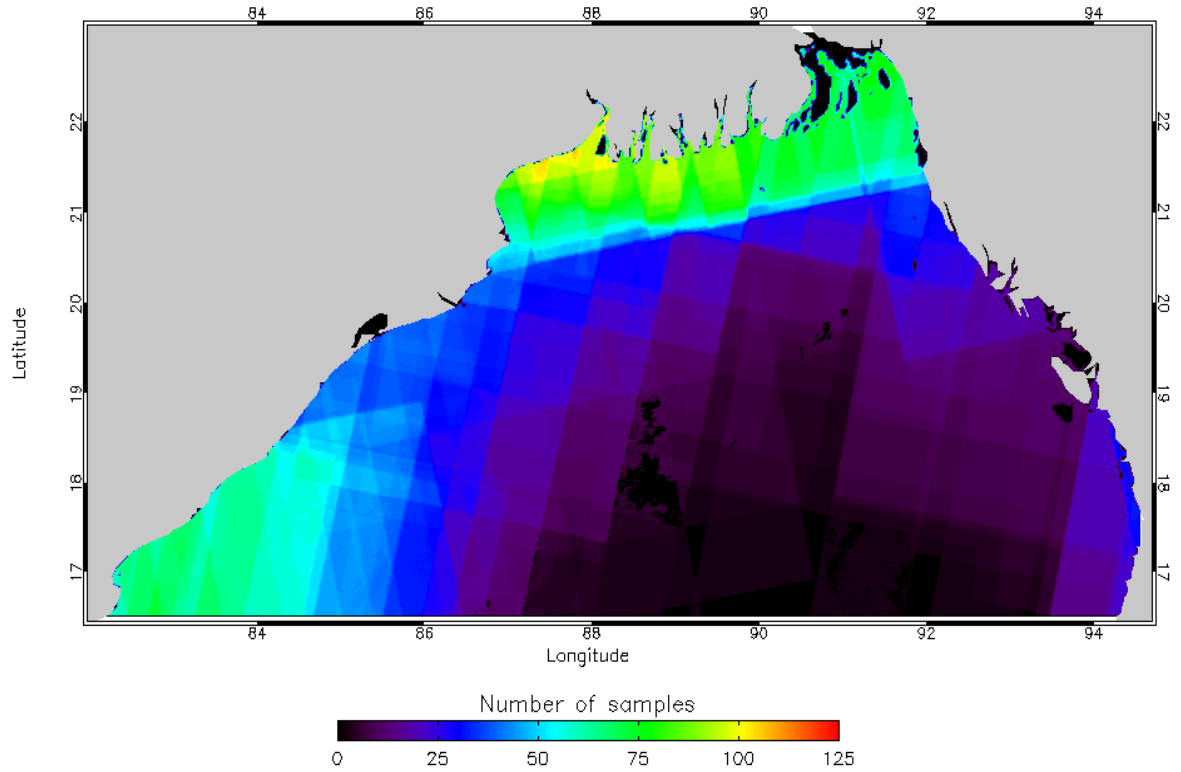
Figure 4.11. Number of samples of the Bay of Bengal from ENVISAT ASAR datasets.

4.6. Observation and Outcomes

The satellite scenes used for the Bay of Bengal offshore area covers as shown in Figure 4.12. Here, the scenes which has more than 70 time series samples has been selected. For this reason other nodal points of deep sea is showing as null values. From the figure it can be seen that the number of overlapping scenes varies highly throughout the whole area. Two particular interest areas can be found from this figure where the number of samples are moderate, which is in the Northern coastal area near Bangladesh and in the Western side of Bay of Bengal near India. The highest sample comprises in the

node at 87.333 Easting and 21.5 Northing. and In the Northern part the overlapping of scenes varies around 83-133 and in the Western side, it varies around 71-92 scenes.
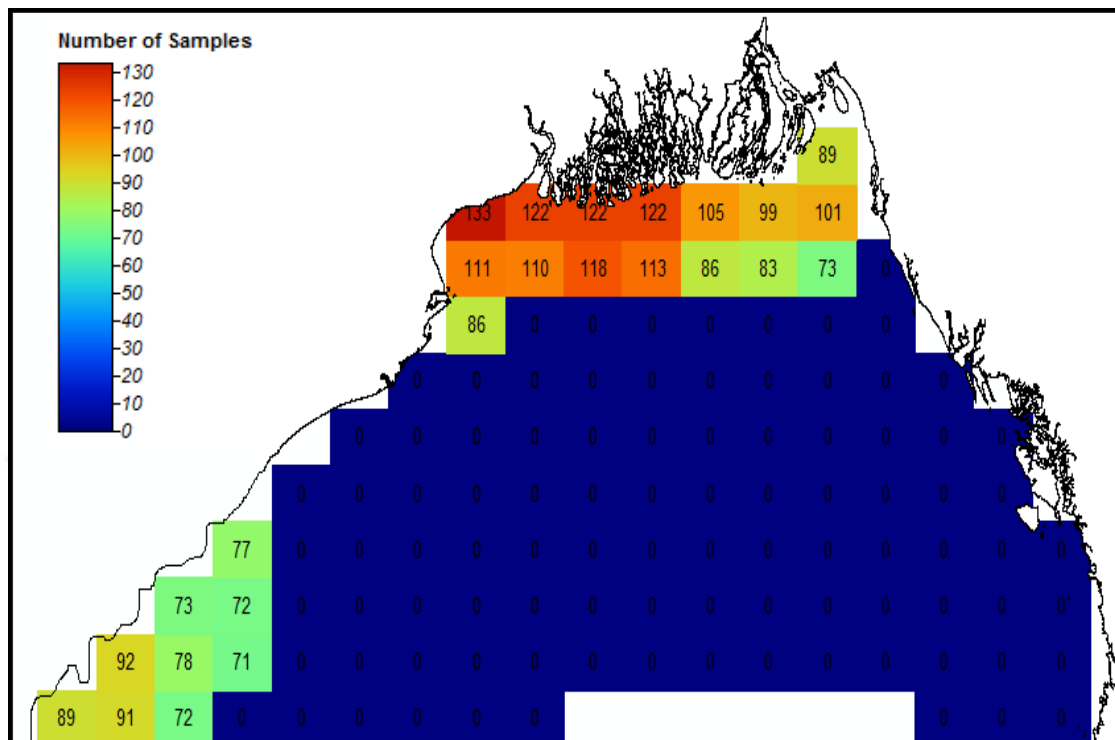
Figure 4.12. Number of samples of the specified location from ENVISAT ASAR

datasets

In the below Figure 4.13 it shows the calculated offshore mean wind speed from ENVISAT ASAR datasets. The color legend shows the variation of mean wind speed availability of that particular zone of the Bay of Bengal. From the legend it is clear that, the color orange to red is the high potential zone whereas the color below are indicating a lower wind speed scenario. As also mentioned before, the higher sample nodal areas are focused hereby, so that, other zones are showing null number.
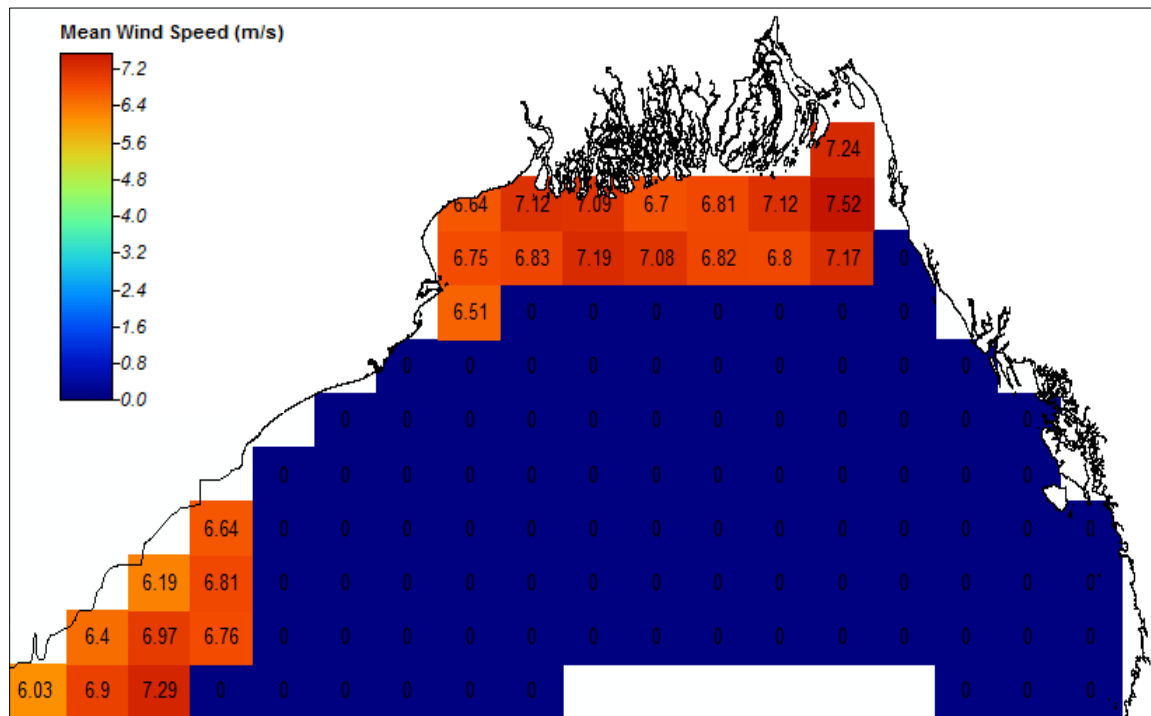
Figure 4.13. Mean wind speed of the specified location from ENVISAT ASAR datasets.

From the above which represents a variation of around 6-7.5 ms^{-1} mean speed. It can be seen that in Northern side of the Bay of Bengal, the mean wind speed is found to be around 6.5-7.5 ms^{-1} where as in Eastern part it varies around 6-7.29 ms^{-1}. This figure shows a moderate wind speed scenario of the Bay of Bengal as a total about 6-7.5 ms^{-1}. All the results described here are for 10 m above sea level.

While comparing the mean wind speed verified ENVISAT ASAR wind Atlas map with GWA, ENVISAT ASAR wind Atlas map shows a moderate result, though the ASAR seems to be over predicting the wind speed and energy entirely, especially in the Northern coastal areas. Figure 4.14 shows the GWA mean wind speed for the same location points where GWA shows a variation of wind speed from 5.05 to 7.82 ms^{-1} whereas from SAR the variation of mean wind speed was around 6.05 to 7.29 ms^{-1}. Alike SAR, It can be seen that in Western side of the Bay of Bengal, the mean wind speed is found to be around 6.5-7.2 ms^{-1}.
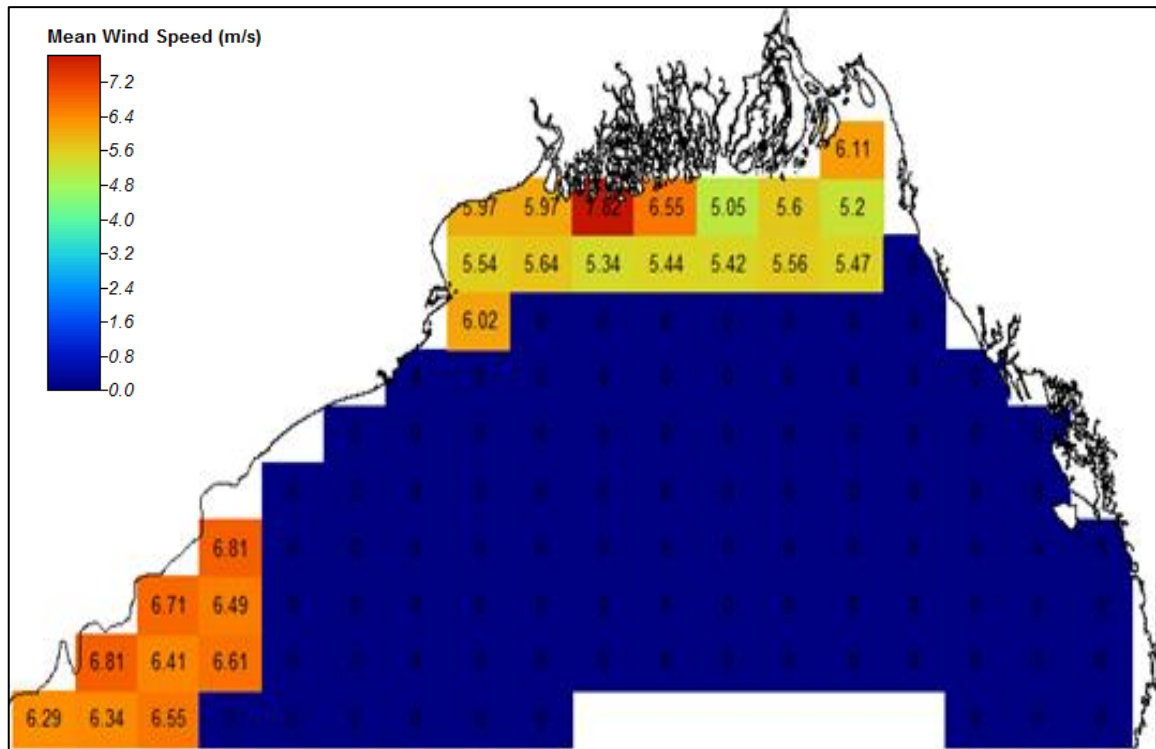
Figure 4.14. Mean wind speed of the specified location from GWA

Figure 4.15 represents the energy density from ENVISAT ASAR datasets for the specific location where it shows a good variation of 225-332 W/m^2 in near coastal area of Northern side of the Bay of Bengal where as in Western coast it is a bit less comparatively. (167-303 W/m^2).
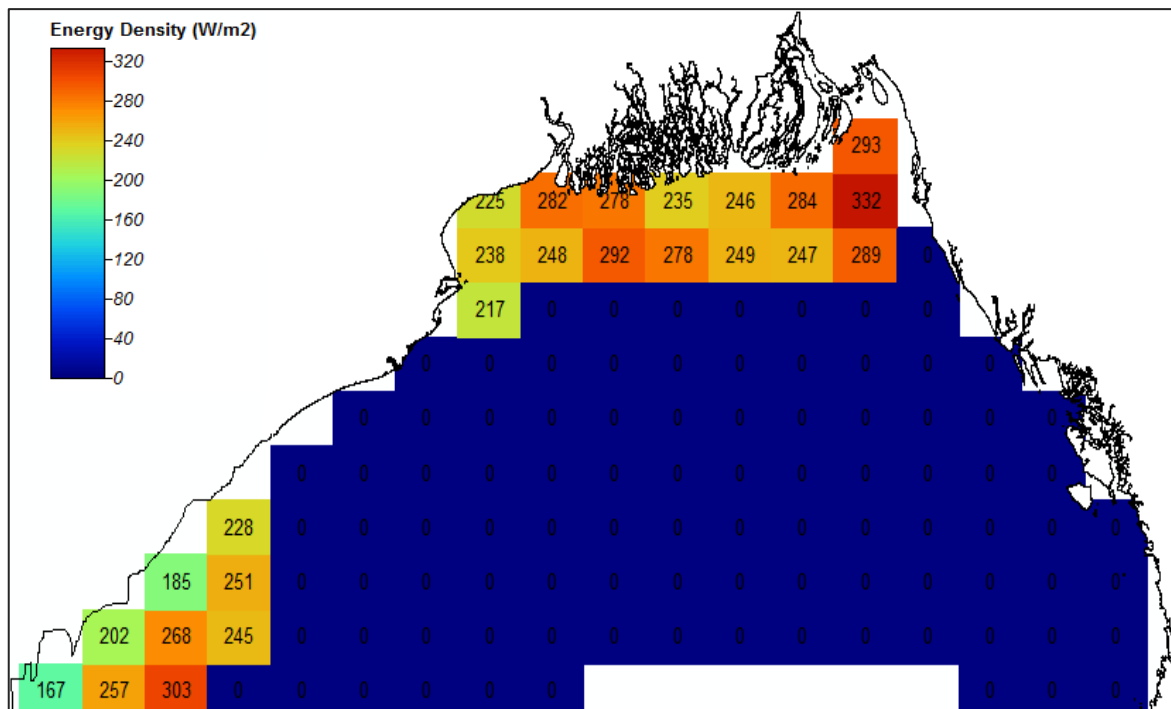
Figure 4.15. Energy density of the specified location from ENVISAT ASAR datasets.

On the other hand, from the wind energy density verified GWA map, the energy density is found to be 162-293 W/m^2 in the Northern nearshore area (Figure 4.16). Where as in a specified location, it is estimated to have around 511 W/m^2 of energy density. Another corner of the map which is situated in the Western coast, the variation of 231-294 W/m^2 energy density has been found.
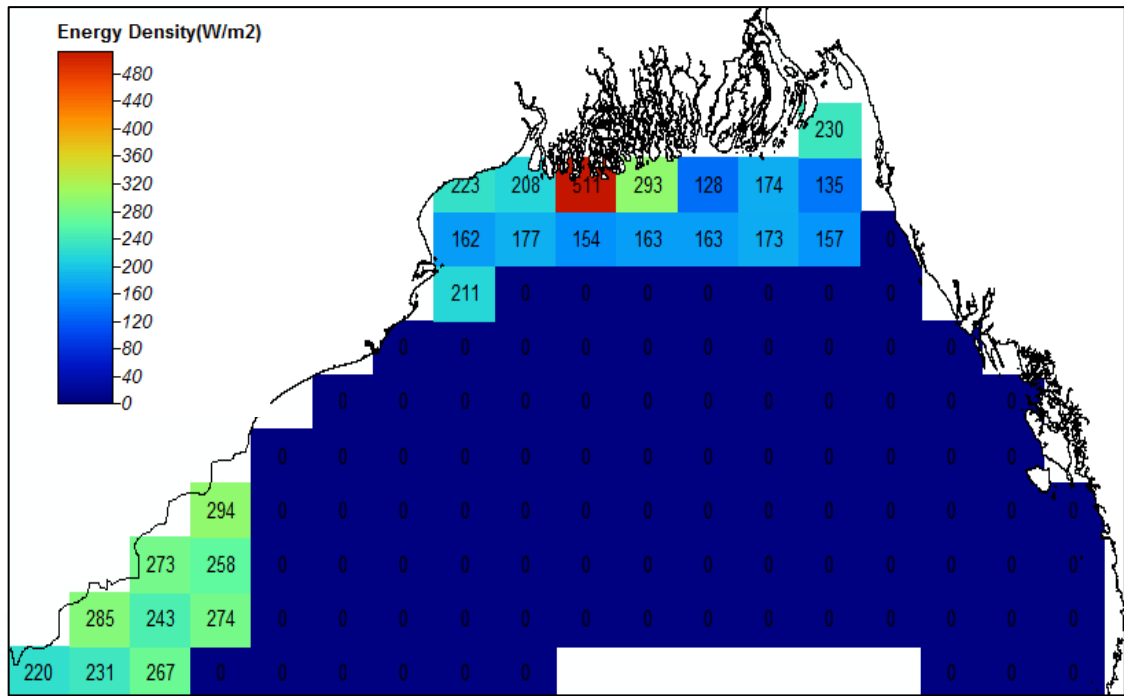
Figure 4.16. Energy density of the defined location from GWA

4.7. Weibull Distribution for Selective Area

After combining the GWA and ASCAT based wind atlas, a specific zone has been chosen for wind farm statistics based on some criterion which is briefly described in next chapter (chapter 5). In this point, various methods of Weibull distribution is performed to estimate the power generation of the defined area more accurately. The Weibull distribution delivers estimated fitting of probability in the case of natural occurrences. In the wind energy sector it is extensively used for predicting wind resource and wind power. This distribution form was entitled by Swedish Physicist Weibull in 1930s (Celeska et al., 2015). In the recent years, it has been used for a better fitting of the experimental data in the wind energy sector. After collecting the data for a particular site, consequently it is very important to estimate the Weibull parameters for modeling the wind energy density of that sector. In our study we wanted to investigate which statistical form fits better in the sectoral division of wind speed. Specially obtaining satisfactory results in the critical sectors this procedure has been emphasized. Mentionable fact of this study is that, as in some datasets the number of samples are too less, Weibull wind statistics is more applicable to predict and estimate the wind resource of the site.

4.7.1. Weibull Probability Functions

For analyzing the wind speed data, the two parameter Weibull Probability distribution function (PDF) is most appropriate and acknowledged. This PDF provides an enhanced fitting to predict high accurate monthly distribution of wind speed. The Weibull Probability function is denoted in (Kidmo et al., 2015) as:

$$f(v) = \left(\frac{k}{A}\right)\left(\frac{v_i}{A}\right)^{k-1}\exp[-\left(\frac{v_i}{A}\right)]^k \tag{4.2}$$

where $f(v)$ is denoted as the probability of observed wind speed, A is the Weibull scale parameter and k is the unit less Weibull shape parameter, v_i is wind speed. The cumulative distribution function (CDF) of the comparative frequency of each wind speed is defined as (Kidmo et al., 2015):

$$F(v) = 1 - \exp[-\left(\frac{v_i}{A}\right)]^k \tag{4.3}$$

The two Weibull parameters and the average wind speed are related by (Celeska et al., 2015)

$$\bar{v} = A.\Gamma\left(1 + \frac{1}{k}\right) \tag{4.4}$$

By using the Weibull parameters, gamma function Γ and the air density ρ (~1.245 g m^{-3}) the wind power density is predicted in (Celeska et al., 2015) as:

$$E = \frac{1}{2}\rho A_w^3.\Gamma(1 + \frac{3}{k_w}) \tag{4.5}$$

where $\bar{v}$ is the average wind speed, E is the power density and Γ is the gamma function.

4.7.2. Data Measurement for Weibull analysis

The wind speed time series format dataset for the specific location from ENVISAT ASAR and ASCAT were statistically analyzed separately. First of all, the

sectoral mean wind speed and standard deviation has been calculated by using equation 4.6 and equation 4.7 from (Kidmo et al., 2015) as :

$$v_m = \frac{1}{N} \sum_{i=1}^{N} v_i \qquad (4.6)$$

$$\sigma = \frac{1}{N-1} \left[\sum_{i=1}^{N} (v_i - v_m)^2 \right]^{1/2} \qquad (4.7)$$

where, v_m is the mean wind speed (m/s), N is the number of measured wind speed data, σ is the standard deviation of the observed wind speed, v_i is the observed hourly wind speed (m/s).

For an appropriate statistical analysis, time series format of wind data were altered into frequency distribution format by defining the wind speed intervals. Wind speed classes (bin) were created to divide those wind speeds in the frequency format and further compared with the frequency of obtained Weibull distribution. In this study, the step is 1 (m/s) starting from 0 to 20 (m/s)

4.7.3. Determination of Weibull Parameters

Four methods of statistical analysis were compared to determine the shape and scale parameters of Weibull wind speed distribution for wind energy resource analysis, these are:

(a) Empirical method
(b) Method of moments,
(c) Moment 3 method.
(d) Power density method.

Each of this method were applied to find out the parameters of Weibull PDF and consequently, the error estimation was estimated using statistical method of analysis.

4.7.3.1. Empirical Method

Empirical method (EM) is a comparison set using the standard deviation and mean wind speed. It is considered as a distinctive situation of Method of moments (MOM). Through EM the parameters of Weibull distribution can be found from (Kidmo et al., 2015) as:

$$k = \left(\frac{\sigma}{\bar{v}}\right)^{-1.086} \tag{4.8}$$

$$A = \frac{\bar{v}}{\Gamma\left(1+\frac{1}{k}\right)} \tag{4.9}$$

where $\bar{v}$ is the average wind speed, σ is the standard deviation and Γ is the gamma function.

4.7.3.2. Method of Moments

In estimating Weibull distribution parameters Method of moments (MOM) is widely used. The equation format is dependent on the arithmetical iteration of mean wind speed ($\bar{v}$) and standard deviations (σ). The equations (Kidmo et al., 2015) are followed as:

$$k = \left(\frac{0.9874}{\frac{\sigma}{\bar{v}}}\right)^{1.0983} \tag{4.10}$$

$$A = \frac{\bar{v}}{\Gamma\left(1+\frac{1}{k}\right)} \tag{4.11}$$

where $\bar{v}$ is the average wind speed, σ is the standard deviation and Γ is the gamma function.

4.7.3.3 Method of Moment 3

By Moment 3 method of Weibull parameter estimation, first the k parameter is being determined from (Amaya-Martínez et al., 2014) through equation 4.12.

$$\frac{\bar{v}^3}{(\bar{v})^3} = \frac{\Gamma\left(1+\frac{3}{k}\right)}{\Gamma\left(1+\frac{1}{k}\right)^3} \tag{4.12}$$

Afterwards the A parameter is determined from

$$A = \frac{\bar{v}}{\Gamma \left(1 + \frac{1}{k}\right)} \quad (4.13)$$

where $\bar{v}$ is the mean wind speed and Γ is the gamma function

4.7.3.4 Power Density Method

The power density method (PDM) is a numerical analysis related to the mean wind speed and for this method initially the Energy Pattern Factor (E_{pf}) should be computed. E_{pf} can be defined as the ratio of mean of cubic wind speed to the cube of mean wind speed. The energy pattern factor (EPF) denoted in (Kidmo et al., 2015) as:

$$E_{pf} = \frac{\frac{1}{N}\sum_{i=1}^{N} v_i^3}{(\frac{1}{N}\sum_{i=1}^{N} v_i)^3} \quad (4.14)$$

Subsequently, the shape parameter (k) and scale parameter (A) can be calculated from the previous E_{pf} equation through below format described in (Kidmo et al., 2015) as:

$$k = 1 + \frac{3.69}{E_{pf}^2} \quad (4.15)$$

$$A = \frac{\bar{v}}{\Gamma \left(1 + \frac{1}{k}\right)} \quad (4.16)$$

where $\bar{v}$ is the average wind speed, v_i is the observed hourly wind speed, E_{pf} is the energy pattern factor.

4.7.4. Accuracy Test

With the aim of evaluating the accuracy of the previously mentioned 4 Weibull methods, 3 types of error estimation has been calculated. Those are:

(a) The root mean square error (RMSE)

(b) Chi-Square Test (χ^2)

(c) Coefficient of determination (R^2)

4.7.4.1. Root Mean Square Error (RMSE)

RMSE estimates the error by considering the deviation between the predicted and the experimental values. The lower the value of RMSE is, the more accurate the values are. RMSE should be as close by to zero as possible to have a successful forecasting of prediction. The equation formula of RMSE is described in (Celeska et al., 2015) as:

$$\text{RMSE} = \left(\frac{1}{N}\sum_{i=1}^{N}(y_i - x_i)^2\right)^{1/2} \tag{4.17}$$

where, y_i is the frequency of the observation , x_i frequency of Weibull (using those statistical methods) and N is the number of observations.

4.7.4.2. Chi-Square Test(χ^2)

This test is considered accurate when the value comes closer to zero. Basically it gives back the mean square of the deviations between the experimental and the calculated values for the distributions. Chi-squared test is calculated in (Kidmo et al., 2015) as following:

$$\chi^2 = \sum_{i=1}^{N}\frac{(y_i - x_i)^2}{x_i} \tag{4.18}$$

where, y_i is the frequency of the observation x_i frequency of Weibull (using those statistical methods) and N is the number of observations.

4.7.4.3. Coefficient of Determination (R^2)

The coefficient of determination (R^2) represents a linear relationship between the calculated values and observed data. The higher value of it represents a better fit and the highest value it can get is 1. The function can be represented in (Amaya-Martínez et al., 2014) as:

$$R^2 = 1 - \frac{SS_{RES}}{SS_{TOT}}$$
(4.19)

$$where, \quad SS_{RES} = \sum_{i=1}^{N}(y_i - f_i)^2$$
(4.20)

$$SS_{TOT} = \sum_{i=1}^{N}(y_i - \bar{y})^2$$
(4.21)

Here, y_i is the frequency of the observation, $\bar{y}$ is the mean of the observed data, N is the number of observation, f_i is the predicted value.

CHAPTER 5

CASE STUDY AND RESULTS

The purpose of this case study is to make a real time experiment via assembling all the obtained datasets (ASAR, GWA and ASCAT). Through an engineering application this test case has been approached to estimate an offshore wind park production for an

appropriate zone at the Bay of Bengal. The main focus is to create a 400 MW wind farm at low depth sea locations but high in power density; which is 4-6 km close to the shore, so that it does not require any supplementary base station and additionally, it will reduce the cost of the offshore wind farm installation. The proceeding steps of this engineering application has been displayed in a flowchart below.

```
┌─────────────────────────────────────────┐
│      Selection of Suitable Location      │
└─────────────────────────────────────────┘
                    │
                    ▼
┌─────────────────────────────────────────┐
│      Statistical Analysis and Creation of│
│      Observed Wind Climate (OWC) Files   │
└─────────────────────────────────────────┘
                    │
                    ▼
┌─────────────────────────────────────────┐
│      Generation of Atlas (GWC) Datasets  │
└─────────────────────────────────────────┘
                    │
                    ▼
       ╭─────────────────────────────╮
       │   Allocation of Wind Turbines│
       │   and Calculation of Energy  │
       ╰─────────────────────────────╯
```
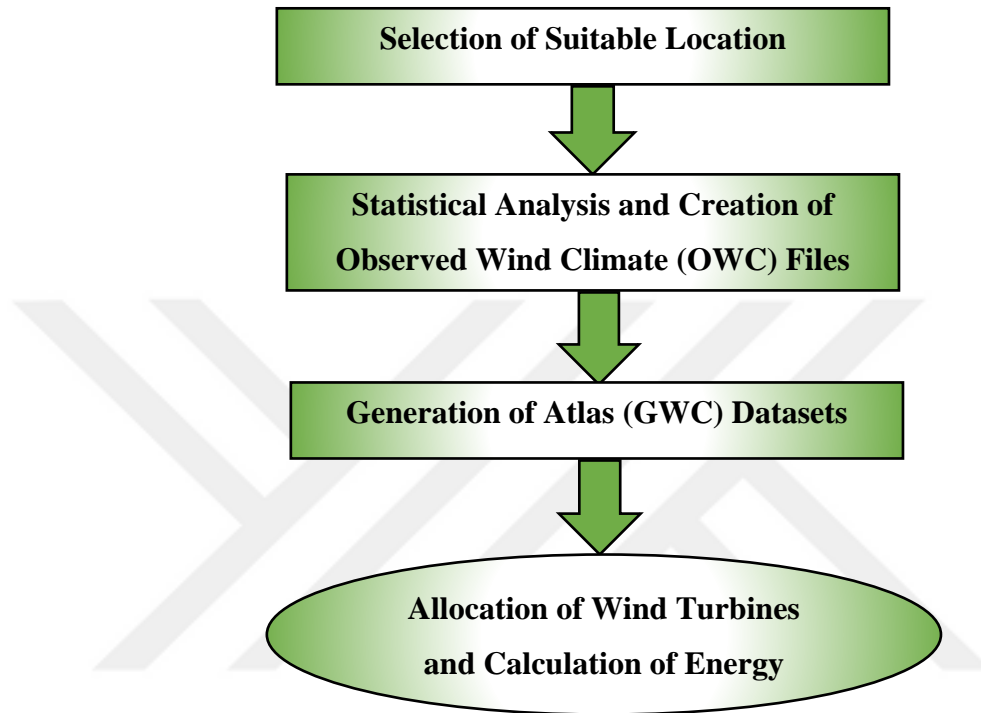
Figure 5.1. Flowchart of Case Study Phases

The sections in Figure 5.1 are briefly introduced below and explained in detailed in coming subsections:

- **Selection of suitable location**

    (a) The coastline map of the Bay of Bengal was attained and digitization is made in the form of WAsP vector map.

    (b) ASAR and GWA power density maps were assessed to choose high density zones. In addition, ASAR datasets with higher sample numbers were preferred as a selection criteria.

    (c) Selected high density zones were matched with low depth area to decrease the cost of installation. For this purpose, bathymetry data was taken from SRTM 30 + and a zone with distance of 5 km to the shore has been selected.

- **Statistical Analysis and Creation of Observed Wind Climate (OWC) files**
  - (a) Subsequently, ASCAT data was acquired for the definite zone.
  - (b) Statistical Analysis steps were performed for the datasets via applying different Weibull fitting functions and furthermore OWC files (*.tab) were created based on those analysis. The associated results are compared and discussed further.

- **Generation of Atlas datasets**
  - (a) A WAsP project has been created to calculate the Atlas values from ASAR and ASCAT OWC files. The Atlas files (*. lib) of ASAR, ASCAT and GWA were compared and discussed further.

- **Calculation of Energy Production**
  - (a) Dominant wind direction for each OWC files was calculated and a 402 MW offshore wind farm occupying 3 MW each, turbines within the selected zone was allocated.
  - (b) Additionally, Generalized Wind Climate (GWC) files (which are ATLAS files) were created by performing step 3 (a) to predict the energy production via WAsP software and the results are discussed and compared as well.

5.1 Selection of Suitable Location

Our achieved SAR and GWA power density maps were analyzed to find a comparable higher energy density area comprising higher sample number of SAR dataset. When a point location has more number of SAR samples that represents more data acquisition in the time domain which can lead to a reliable estimation of wind energy density. Also, another preferences were to find a nearshore, lowest depth and highest potential area for case study purpose. To apply the newest technology of offshore wind turbine in the specified area, it leads to operational uncertainty and more expenses. That is why the conventional turbine installation techniques has been preferred in this section. Therefore, based on four detailed criterion, the zone has been selected:

- Sufficient number of satellite data sample to get more accurate results.
- Highest wind energy density region as an aspect to highest energy production.

- Nearest to shore to not to have a base station in offshore.
- Lowest depth region to deal with the present technology of offshore wind turbine.

5.1.1. Formation of the Vector Map

The coastline map of the Bay of Bengal is processed in Shuttle Radar Topography Mission (SRTM) 30+ version of 30 arc second and digitization is made in the form of WAsP vector map by utilizing WAsP Map Editor. The map editor is a WAsP utility program which inspects, edits and creates digital topographical maps for WAsP. A WAsP digital map contains a topographical terrain description in a vector format (polygons of poly-lines) which can be further used in WAsP analysis for flow modeling. Different height (elevation) and land cover or roughness information are denoted by these different types of lines.

Figure 5.2. Vector Map of the Bay of Bengal for Terrain Analysis

5.1.2. Comparison between ASAR and GWA Power Density Maps

To determine a potential region for wind farm setting, selection of the highest wind energy density location is a must. For this purpose, the attained ASAR based Atlas and GWA power density maps were well analyzed to find out a specific zone with equivalent high power density. In order to perform detailed analysis, the sample number of ASAR datasets were prioritiezed as a purpose of achieving more accuracy in wind energy estimation.

5.1.3. Detecting Nearshore and Lower Depth Area

Currently, only a handful of offshore wind turbines have been installed far from the coastal zone as it requires huge maintenance and operational costs. Apart from that, some established offshore projects are seen to be followed 4 km distance[12] from the shore to avoid setting up a base station. If the wind farm is in a range to 4 km from coastline, it can directly get connected through grid towards the main station. Otherwise, a base station near to the offshore wind farm is needed to take operate as a hub in between turbines and main station. In addition, this formation of base station lead to more wake effects and electricity loss through the cabling. For this reason, we considered the places where wind turbines can easily be placed using the latest technology and deducting the need of further base station. Bearing in mind these effects, the offshore windfarm has been chosen around 5 km from the coastline.
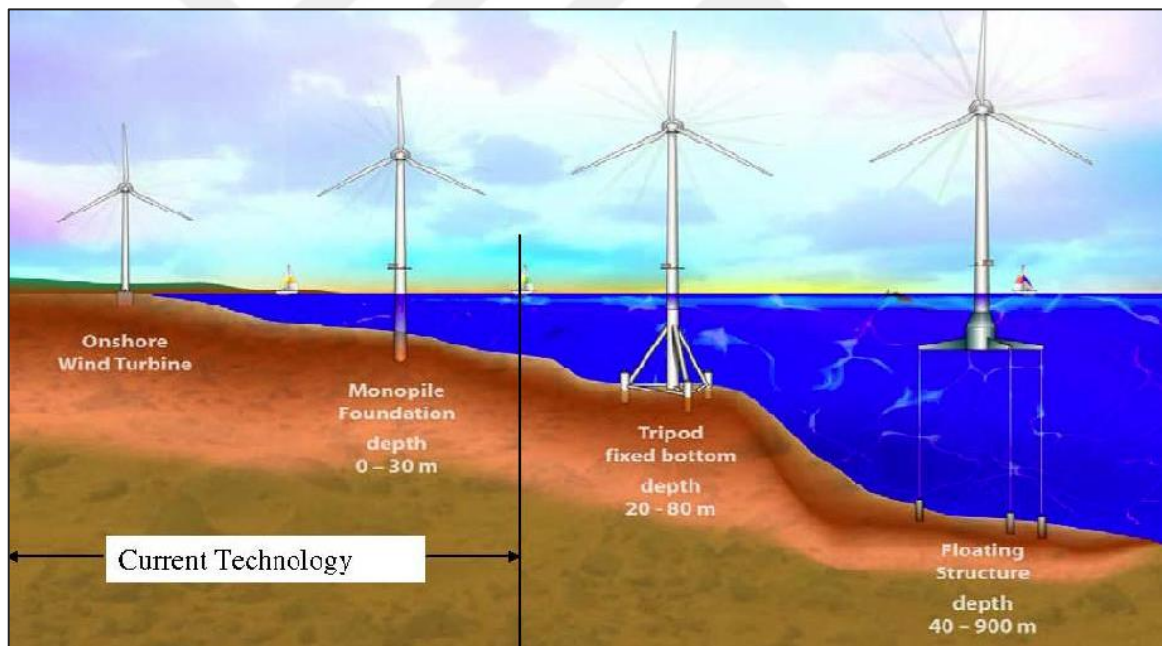
Figure 5.3. Offshore Wind Turbine Development for deep water
(Source: Center for Renewable Energy and Sustainability)

---

[12]http://www.ens.dk/en/supply/renewable-energy/wind-power/offshore-wind-power/nearshore-wind-tenders/six-sites

For a purpose of depth analysis of the Bay of Bengal, the bathymetry map has been downloaded in Shuttle Radar Topography Mission (SRTM) 30+ version of 30 arc second, Global. SRTM 3-arc second resolution digital elevation maps (DEM) have been merged with the vector map of the Bay of Bengal. In our study, the bathymetry for the specified zone of the Bay of Bengal has been investigated by dividing the zone in 6 areas. The 6 areas are considered as: (Displayed in figure 5.4(d))

- Depth less than 0 meter, as Land.
- Depth in between 0-5 meter, as most favorable zone.
- Depth in between 5-10 meter, as favorable zone.
- Depth in between 10-15 meter, as moderate zone
- Depth in between 15-20 meter, as least favorable zone.
- Depth more than 20 meter, as deep water.
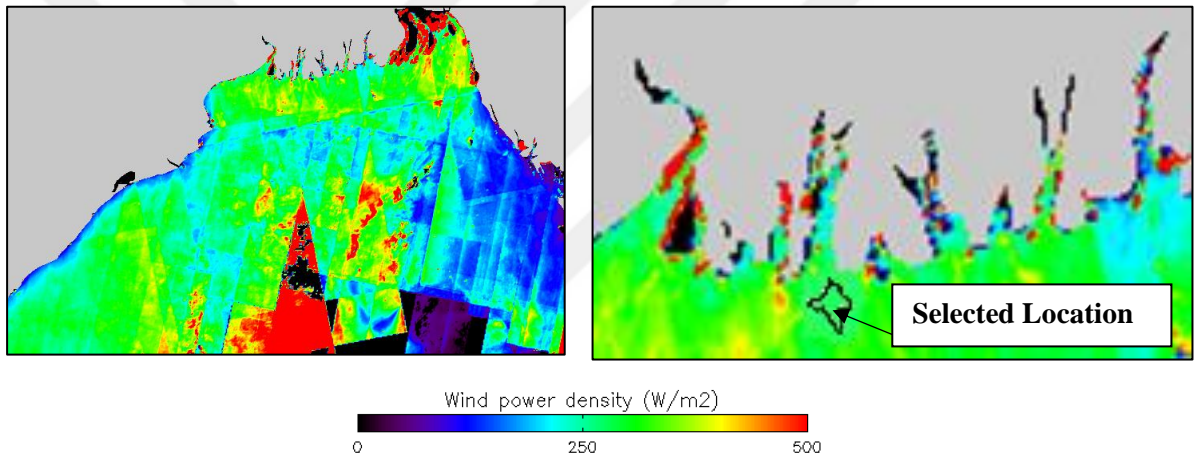
(a) ASAR Wind Power Density Map   (b) Zoomed view with selected location
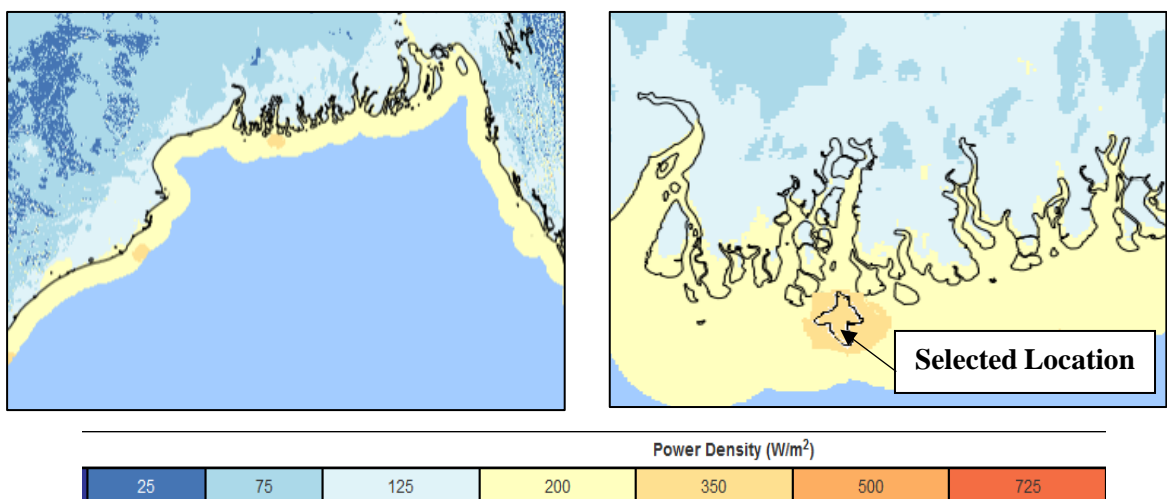
(c) GWA Wind Power Density Map   (d) Zoomed view with selected location
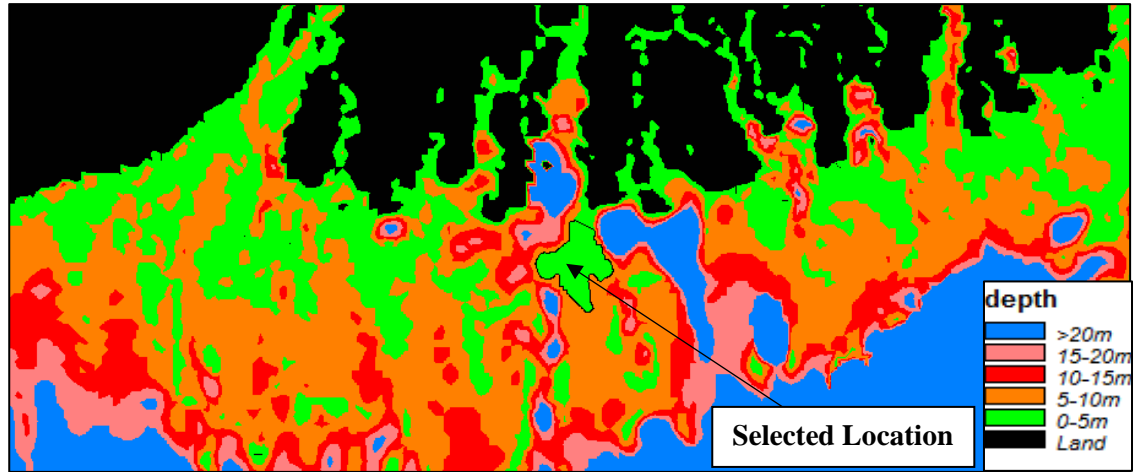
(d) Bathymetrical Segmentation of the Bay of Bengal

Figure 5.4. Selection of suitable location

After investigating the figures of 5.4, such close to shore, higher sample number and lower depth areas with higher wind power density was found to be existed only at the northwest coast of Bangladesh. Therefore, the area has been chosen at the location of 21.5° Northern latitude and 88.667° Eastern longitude. This area is in the depth region of 0-5m, 5 km away from the coastline, comprising one of the highest sample numbers of 122 of ASAR datasets and predicted to have higher wind power density in an assumption from GWA and ASAR based wind datasets.

5.2. Statistical Analysis and Creation of Observed Wind Climate (OWC) files

For the specified location ASAR and GWA data sources are available but additional to that ASCAT dataset is requested from DTU Wind Energy Department as a second satellite wind dataset of that location. Thereafter, statistical analysis was performed with ASAR and ASCAT data time series. In such way, the Observational Wind Climate (OWC) files are created that can be used in WAsP software.

5.2.1. Acquisition of ASCAT Dataset for Selected Location

ASCAT dataset was obtained for the chosen area which comprises a full year of 2015 measurements. The dataset contains 567 time series samples that fairly distributed in every single month and ascending-descending arrangement. This obtained ASCAT

dataset is more frequent than ASAR datasets due to its technological aspects. Both of the satellite datasets were analyzed accordingly to get a broader interpretation. These both datasets yearly, monthly, seasonal and morning vs evening illustrations are shown below respectively in figure 5.5, 5.6, 5.7 and 5.8.

	2006	2007	2008	2009	2010	2011	2012	2013	2014	2015
■ ENVISAT ASAR	16	37	34	14	4	11	6	0	0	0
■ ASCAT	0	0	0	0	0	0	0	0	0	567
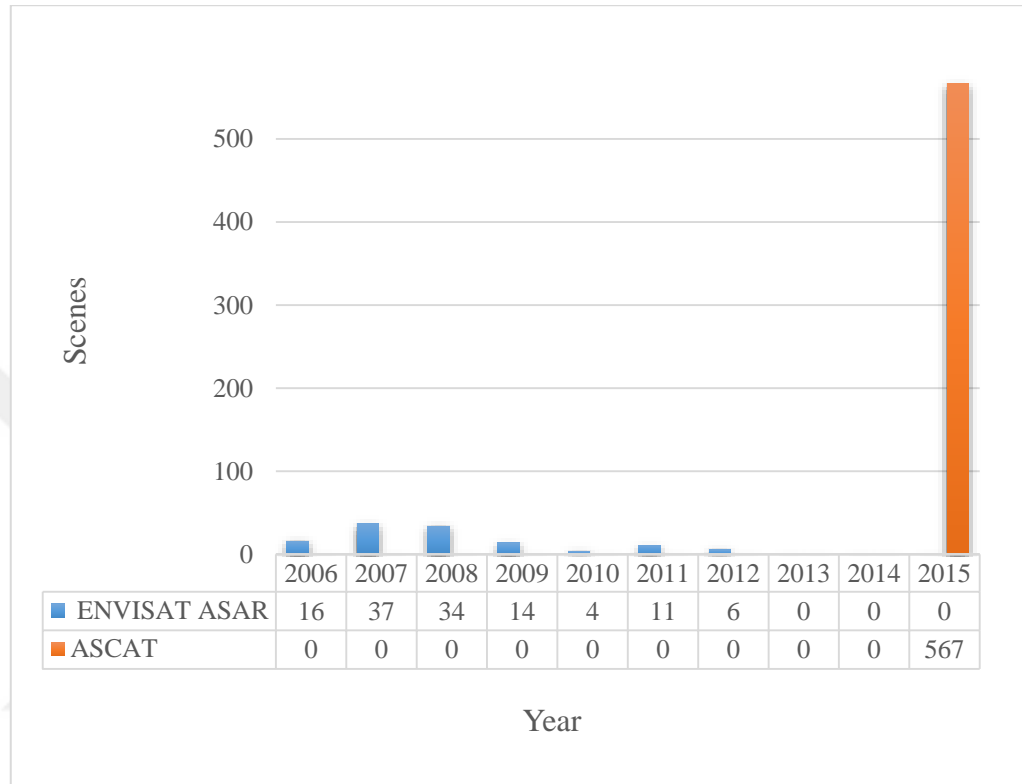
Figure 5.5. Yearly distribution of ENVISAT ASAR and ASCAT scenes for the selected location

As displayed above, The ASAR scenes were obtained from 2006-2012, due to ENVISAT ASAR's non connectivity with ESA after 2012. In contrast, ASAR datasets were possible to be obtained from 2015. For this reason, the datasets were not be analyzed in a same time frame.

In all the comparative illustrations of this chapter, The ENVISAT ASAR datasets are identified in blue color where as ASCAT datasets are identified in orange color. For a better observational comparison this step has been taken throughout the thesis writing.

	Jan	Feb	Mar	Apr	May	June	July	Aug	Sept	Oct	Nov	Dec
ENVISAT ASAR	12	10	7	8	13	15	10	11	7	10	12	7
ASCAT	39	39	40	44	52	50	52	50	50	52	47	52
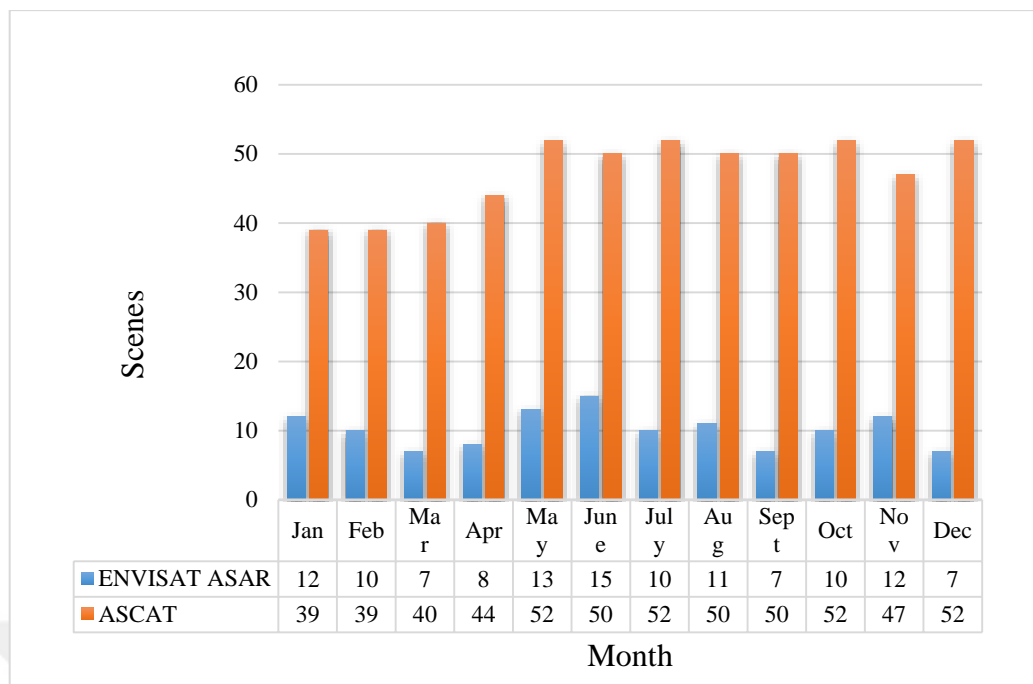
Figure 5.6. Monthly distribution of ENVISAT ASAR and ASCAT scenes for the selected

location

	Winter	Spring	Summer	Fall
ENVISAT ASAR	29	28	36	29
ASCAT	130	136	152	149
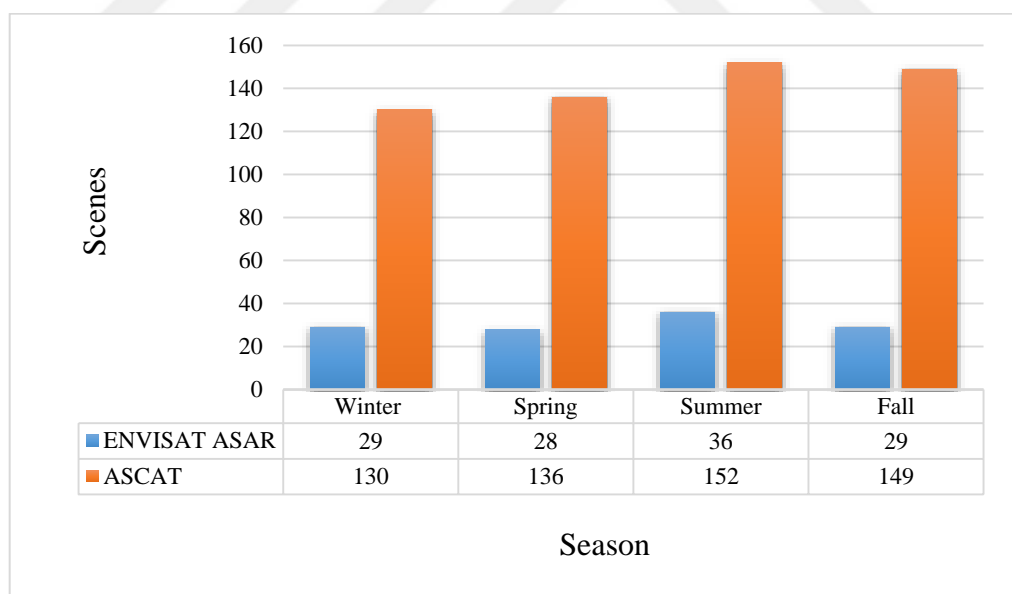
Figure 5.7. Seasonal distribution of ENVISAT ASAR and ASCAT scenes for the selected
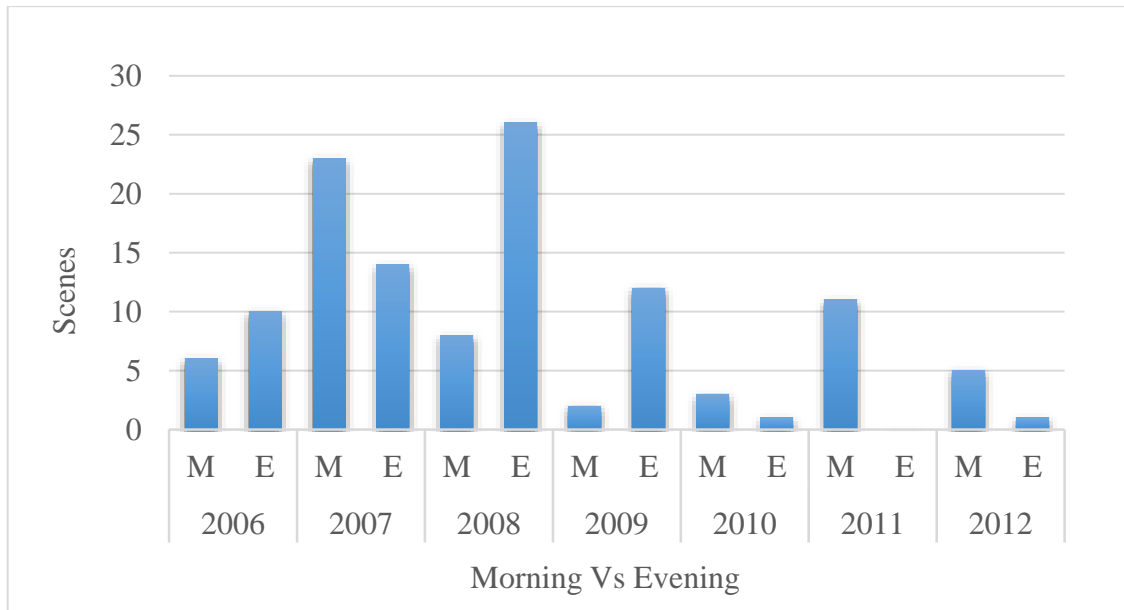
location

(a) ENVISAT ASAR
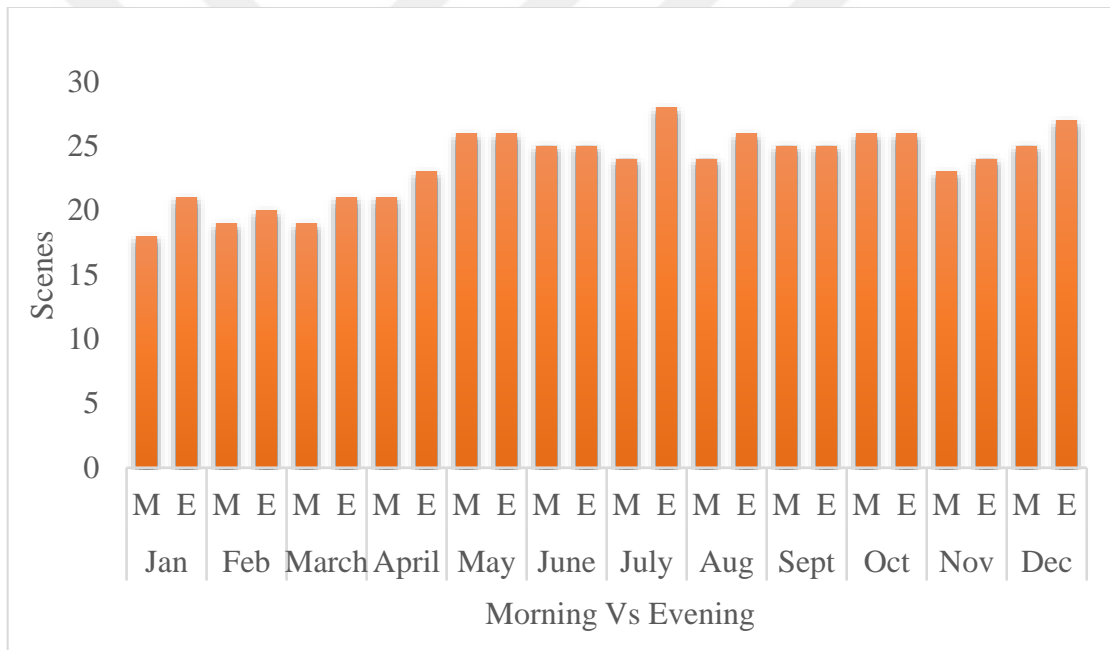
(b) ASCAT

Figure 5.8. Morning vs evening distribution of ENVISAT ASAR and ASCAT scenes for
the selected location

5.2.2. Creation of OWC Files by Fitting Weibull Models

In chapter 4 page 51-56, it has already been mentioned about Weibull probability distribution function and some effective methods of good to fitness. Weibull probability function is a very important term in energy density estimation. So, accuracy of fitting method should also be accounted for a better expectation of estimation. In our study, we investigated Weibull fitting by 4 methods as Empirical method (EM), Moment Method (MOM), Moment 3 method (MOM 3) and power density method (PDM) in the selected zonal area for wind farm. In addition, the relative accuracy test of Root Mean Square Error (RMSE), Chi-Square (χ^2) and Coefficient of determination (R^2) has also performed to predict the energy density uncertainty. Here, it should be mentioned that, RMSE and (χ^2) is considered more accurate when it is near to zero and (R^2) is considered more accurate when it is near to its highest value of 1. The above table 5.1 represents the comparison of the 12 sectoral statistical tests for the four preferred numerical methods. These variation of Weibull fitting has been performed to find out the best Weibull parameters for the purpose of more accurate wind energy estimation. Also the regarding accuracy test results are included in the table to have a greater observation. Here it should be mentioned that, those wind sectors starts with sector 1 (with 0º), North centered and goes clockwise

(a) ASAR   (b) ASCAT
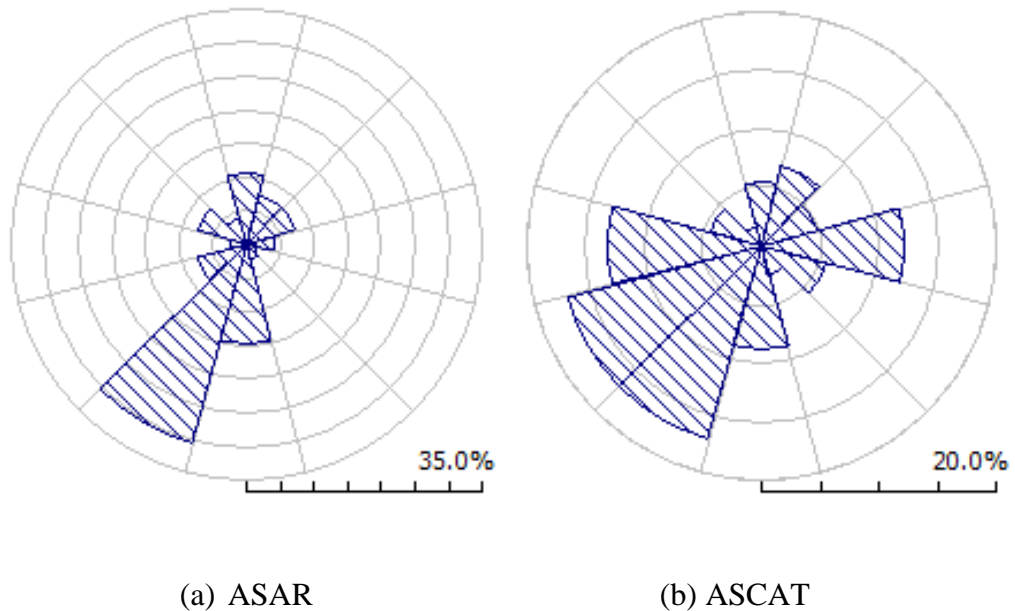
Figure 5.9 Twelve sectoral wind distribution

For ENVISAT ASAR datasets, the twelve sectoral Statistical Weibull analysis along with the accuracy test has been analyzed based on the selective methods and the values are noted in table 5.2 and 5.4 for ASAR and ASCAT datasets accordingly. To have a better interpretation of the analysis, a combined form of all 12 sectors is accomplished

and the values are displayed in the following table 5.1 and 5.3 for ASAR and ASCAT datasets respectively.

Table 5.1. Combined statistical Weibull analysis of ENVISAT ASAR dataset

Method	A	k	v_m	RMSE	χ^2	R^2
EM	7.39133	2.08707		0.00654101	0.104194	0.88102
MOM	7.39083	2.07117		0.00653913	0.103496	0.881089
MOM3	7.39202	2.11759	6.54675	0.00655685	0.106151	0.880443
Epf	7.39219	2.12903		0.00656684	0.1071	0.880079

Table 5.2. Twelve sectoral statistical Weibull analysis of ENVISAT ASAR dataset

Sectors	Method	A	k	v_m	RMSE	χ^2	R^2
	EM	5.38465	2.15348		0.0701325	0.601204	0.557329
	MOM	5.38457	2.13765	4.76868	0.0702083	0.601997	0.556372
Sector 1	MOM3	5.38303	2.28997		0.0695988	0.604699	0.564041
	Epf	5.38292	2.29436		0.0695849	0.605128	0.564215
	EM	5.89862	1.77777		0.104218	1.27545	0.42073
	MOM	5.89575	1.76182	5.24885	0.104433	1.27423	0.418332
Sector 2	MOM3	5.91322	1.8819		0.103038	1.29584	0.433765
	Epf	5.91419	1.89093		0.102954	1.29867	0.43469
	EM	4.98148	1.88269		0.106041	0.872743	0.493987
	MOM	4.97996	1.86671	4.42173	0.106258	0.879731	0.491917
Sector 3	MOM3	4.99085	2.03691		0.104468	0.817377	0.508893
	Epf	4.99123	2.04883		0.104384	0.813979	0.509676
	EM	6.97387	2.3207		0.254655	3.04632	0.168598
	MOM	6.97445	2.30512	6.17893	0.254613	3.04966	0.168874
Sector 4	MOM3	6.96103	2.54217		0.255755	3.02937	0.161403
	Epf	6.9627	2.51904		0.255599	3.02853	0.162426

(Cont. on next page)

Table 5.2. (Cont.)

	EM	6.3527	3.32313		0.410801	2.2526	0.249965
Sector 5	MOM	6.35388	3.31096	5.70048	0.410782	2.25668	0.250035
	MOM3	6.22177	4.81946		0.431584	2.16633	0.172157
	Epf	6.31501	3.71743		0.412807	2.15531	0.242624

Sector	Method	A	k	v_m	RMSE	χ^2	R^2
	EM	4.42517	0.721703		0.381021	19.1561	0.0321513
	MOM	4.35836	0.709743		0.381188	19.4275	0.0313051
Sector 6	MOM3	5.5227	1.0353	5.44571	0.379569	15.5	0.0395179
	Epf	5.67884	1.12147		0.38029	15.2742	0.0358629
	EM	9.23475	2.30297		0.0602831	1.2346	0.288799
	MOM	9.23545	2.28736	8.18133	0.0602996	1.22629	0.288409
Sector 7	MOM3	9.23199	2.35441		0.060242	1.26551	0.289769
	Epf	9.23202	2.3538		0.0602423	1.26512	0.28976
	EM	8.41069	2.82738		0.0290554	1.08853	0.606061
	MOM	8.41233	2.81314	7.49211	0.0291214	1.06824	0.604269
Sector 8	MOM3	8.38637	3.02952		0.0282191	1.45602	0.628413
	Epf	8.40319	2.8913		0.0287705	1.18798	0.613749
	EM	7.5913	1.7847		0.137263	2.11221	0.152154
	MOM	7.58771	1.76875	6.75372	0.137326	2.12322	0.151364
Sector 9	MOM3	7.61968	1.98531		0.136935	2.0093	0.156201
	Epf	7.62053	1.99675		0.136941	2.00531	0.156125
	EM	9.14184	1.46105		0.305257	5.51939	0.0133668
	MOM	9.12846	1.44552	8.28051	0.305159	5.54502	0.0140049
Sector 10	MOM3	9.33917	1.95598		0.309525	5.42337	NaN[13]
	Epf	9.34038	1.96691		0.30963	5.43576	NaN
	EM	7.17885	3.07627		0.112167	2.30762	0.458889
	MOM	7.18028	3.06297	6.41781	0.112342	2.27648	0.457198
	MOM3	7.12821	3.54353		0.106706	4.09942	0.510297
Sector 11	Epf	7.1652	3.20283		0.110551	2.64944	0.474368
	EM	5.20964	2.77267		0.191098	1.1995	0.410992
	MOM	5.21064	2.75825	4.63722	0.190991	1.20126	0.41165
	MOM3	5.19813	2.93181		0.192638	1.18671	0.401459
Sector 12	Epf	5.20609	2.82307		0.191515	1.19416	0.40842

The following table (Table 5.3) represents the whole scenario of the statistical analysis, for ASCAT datasets, by combining all the 12 sectors into one single sector which shows a better combined view of the Weibull statistics.

Table 5.3. Combined statistical Weibull analysis of ASCAT dataset

Method	A	k	v_m	RMSE	χ^2	R^2
EM	6.24514	2.21076	5.53095	0.003134	0.059732	0.914321

---

[13] Not a Number.

Method	A	k	v_m	RMSE	χ^2	R^2
MOM	6.2453	2.19501		0.003104	0.058549	0.915931
MOM3	6.24533	2.18982		0.003095	0.058197	0.916435
Epf	6.24526	2.19938		0.003112	0.05886	0.915497

Table 5.4. Twelve sectoral statistical Weibull analysis of ASCAT dataset

	Method	A	k	v_m	RMSE	χ^2	R^2
Sector 1	**EM**	6.45176	2.79407		0.0197763	0.219554	0.848586
	MOM	6.45301	2.77971		0.0197111	0.216515	0.849582
	MOM3	6.44413	2.87972	5.74452	0.020221	0.240207	0.8417
	Epf	6.45251	2.78541		0.0197366	0.217706	0.849192
Sector 2	**EM**	5.69905	5.29093		0.0335121	1.37804	0.806785
	MOM	5.69895	5.29252		0.033511	1.38086	0.806798
	MOM3	5.68427	5.53749	5.24975	0.0334478	1.90983	0.807526
	Epf	5.79999	3.90199		0.0381155	0.449205	0.750058
Sector 3	**EM**	5.13101	2.91775		0.0441076	0.443099	0.705061
	MOM	5.13203	2.90383		0.0441238	0.439873	0.704844
	MOM3	5.13919	2.80374	4.57643	0.044284	0.423267	0.702697
	Epf	5.1443	2.72886		0.0444572	0.417375	0.700367
Sector 4	**EM**	5.56499	1.9729		0.0122228	0.131865	0.865696
	MOM	5.56396	1.95694		0.0121395	0.129401	0.867521
	MOM3	5.56427	1.96162	4.93319	0.0121634	0.1301	0.866999
	Epf	5.56498	1.97267		0.0122215	0.131827	0.865724
Sector 5	**EM**	6.35837	2.42726		0.0302682	0.314814	0.668347
	MOM	6.35916	2.41189		0.0302023	0.314472	0.66979
	MOM3	6.35356	2.50942	5.63781	0.0306788	0.318976	0.659288
	Epf	6.35471	2.49109		0.0305789	0.317705	0.661504

(Cont. on next page)

Table 5.4. (Cont.)

	Method	A	k	v_m	RMSE	χ^2	R^2
Sector 6	**EM**	5.09409	2.13698		0.0550624	0.422389	0.706142
	MOM	5.09395	2.12113		0.0553496	0.428047	0.703069
	MOM3	5.08958	2.38855	4.51143	0.0515546	0.349694	0.74239
	Epf	5.08972	2.38474		0.0515927	0.35057	0.74201
Sector 7	**EM**	8.17172	3.2842		0.0253551	0.41016	0.692458
	MOM	8.17326	3.27184		0.0253679	0.408887	0.692147
	MOM3	8.151	3.45105	7.3284	0.025288	0.43723	0.694083
	Epf	8.18809	3.15224		0.0255481	0.401283	0.687757
Sector 8	**EM**	8.00198	3.94176		0.0120915	0.138755	0.856665
	MOM	8.00298	3.93304	7.24698	0.0120751	0.138693	0.857056
	MOM3	7.99797	3.97674		0.0121618	0.139155	0.854995

	Epf	8.06518	3.4124		0.0119395	0.161054	0.860247
Sector 9	**EM**	5.7898	1.94776		0.0132791	0.240203	0.799242
	MOM	5.78855	1.93179		0.0132347	0.23547	0.800583
	MOM3	5.7818	1.8635	5.13402	0.0130996	0.219745	0.804634
	Epf	5.78277	1.87195		0.0131112	0.22132	0.804286
Sector 10	**EM**	4.43947	1.7538		0.0154332	0.236653	0.854848
	MOM	4.43709	1.73786		0.0154156	0.231126	0.85518
	MOM3	4.42363	1.66228	3.95338	0.0154153	0.212986	0.855185
	Epf	4.4239	1.66357		0.0154141	0.213197	0.855207
Sector 11	**EM**	3.88262	1.51398		0.0429023	0.963454	0.732898
	MOM	3.87782	1.49834		0.0432093	0.934475	0.729061
	MOM3	3.8358	1.38724	3.50115	0.0455386	0.808265	0.699063
	Epf	3.83755	1.39115		0.0454522	0.810828	0.700204
Sector 12	**EM**	10.2241	3.62901		0.0789631	0.830606	0.433166
	MOM	10.2257	3.61844		0.0789134	0.830078	0.43388
	MOM3	10.2138	3.69658	9.217	0.0793038	0.834948	0.428264
	Epf	10.278	3.28182		0.07788	0.834377	0.44861

Those tables are also illustrated in a relative arrangement, where the color coating shows different types of methods for Weibull fitness. In the following figure (5.10-5.13), each sectoral Weibull frequency is plotted against the frequency distribution of observed wind speed. These curves demonstrate the best fit of Weibull methods for the observed ASAR and ASCAT wind speed datasets. The EM, MOM, MOM 3 and Epf is displayed in the color form of red, black, green and blue respectively.

Sector 1 (0 degree)   Sector 2 (30 degree)

Sector 3 (60 degree)

Sector 4 (90 degree)

Sector 5 (120 degree)
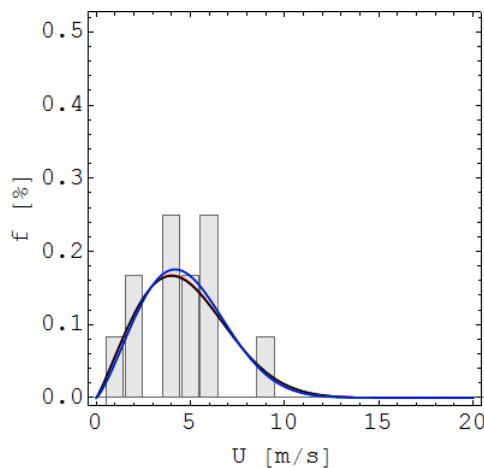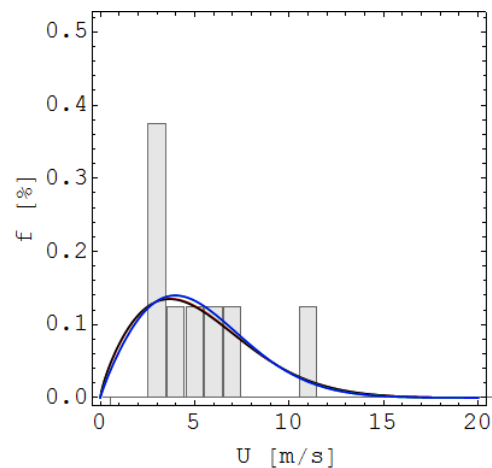
Sector 6 (150 degree)

Figure 5.10. Twelve sectoral Weibull fitting of ASAR datasets (Sector 1-6)

Sector 7 (180 degree)

Sector 8 (210 degree)

Sector 9 (240 degree)

Sector 10 (270 degree)
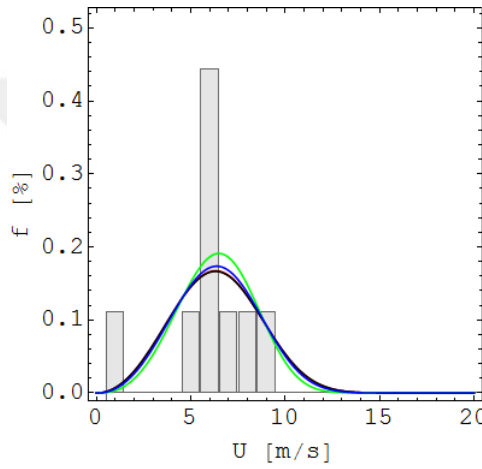
Sector 11 (300 degree)
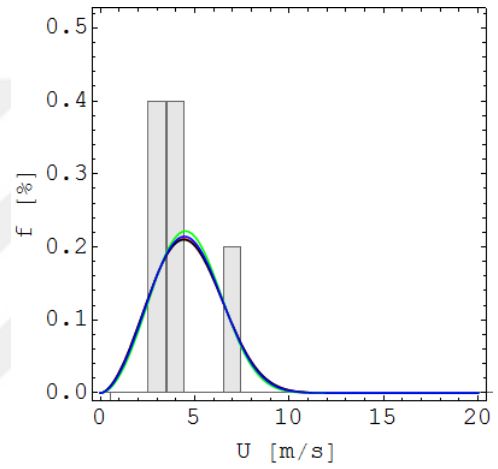
Sector 12 (330 degree)

Figure 5.11. Twelve sectoral Weibull fitting of ASAR datasets (Sector 7-12)
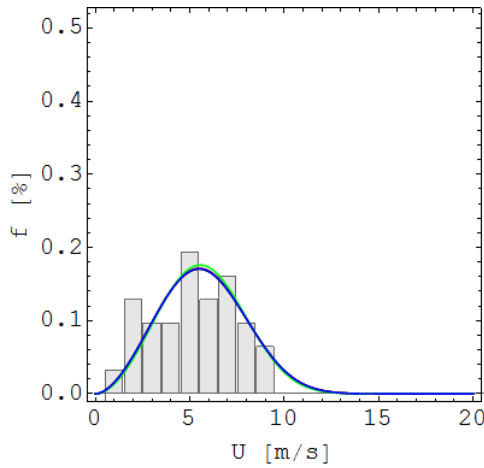
Sector 1 (0 degree)
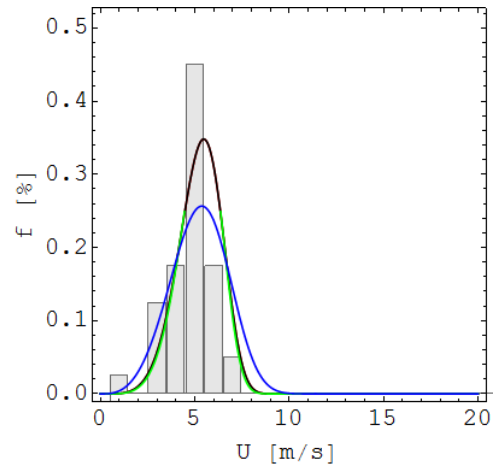
Sector 2 (30 degree)
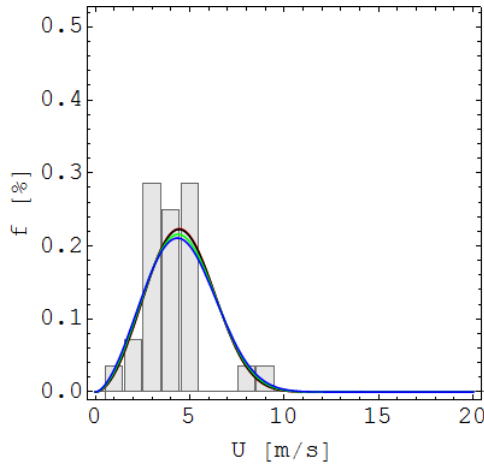
Sector 3 (60 degree)
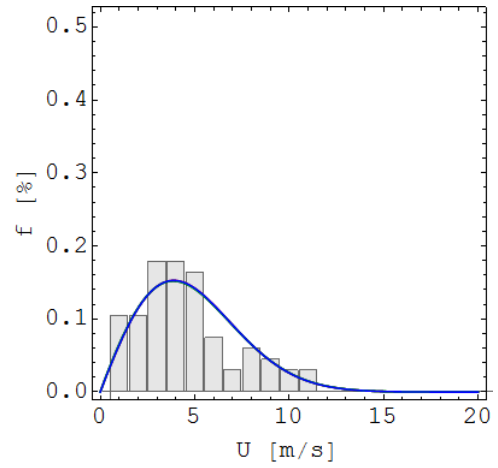
Sector 4 (90 degree)
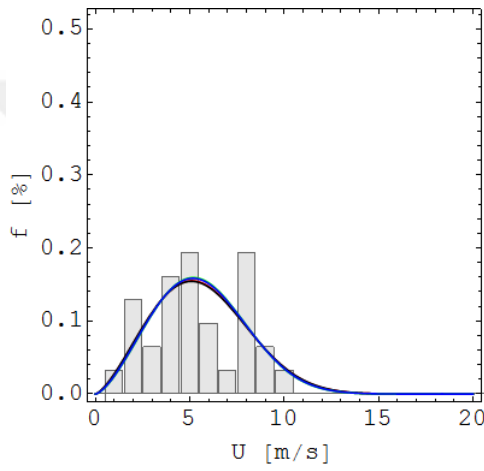
Sector 5 (120 degree)
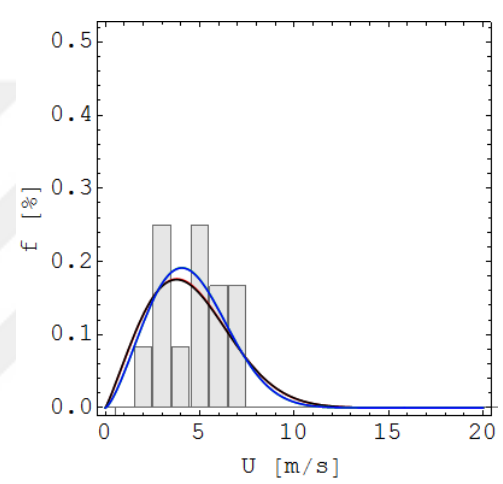
Sector 6 (150 degree)

Figure 5.12.Twelve sectoral Weibull fitting of ASCAT datasets (Sector 1-6)

Sector 7 (180 degree)

Sector 8 (210 degree)

<div align="center">Sector 9 (240 degree)</div>

<div align="center">Sector 10 (270 degree)</div>

<div align="center">Sector 11 (300 degree)</div>

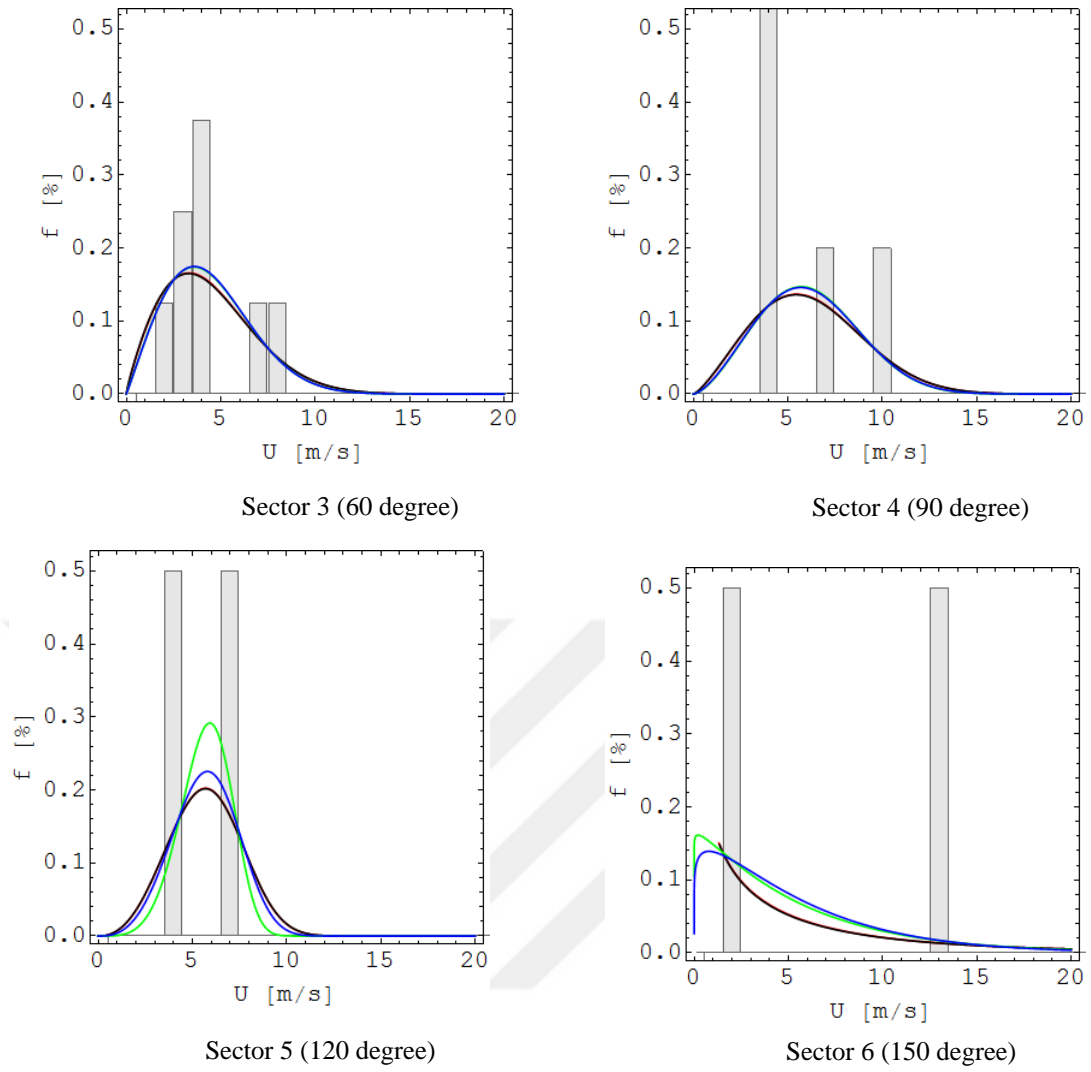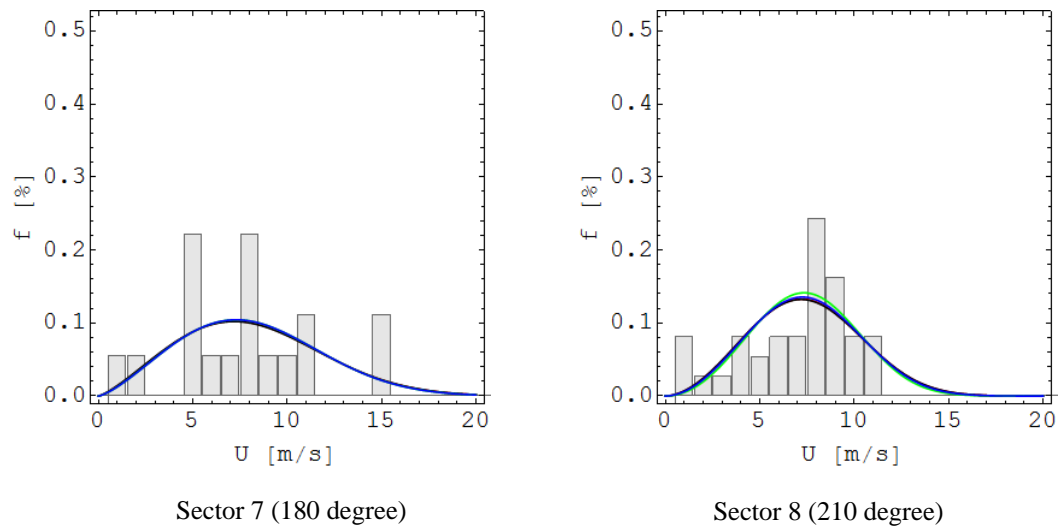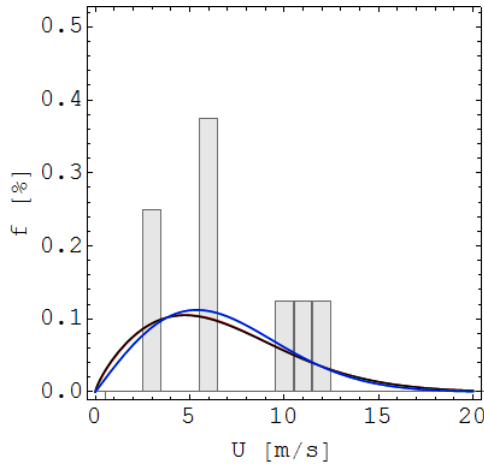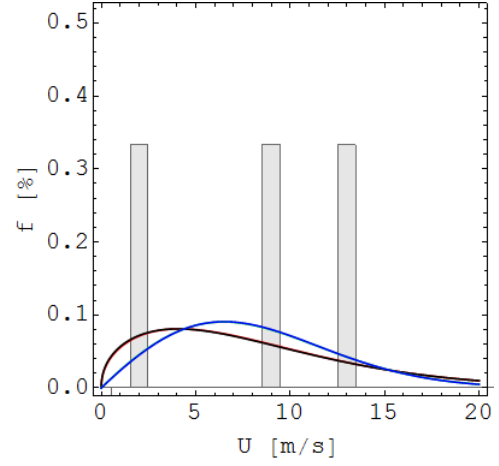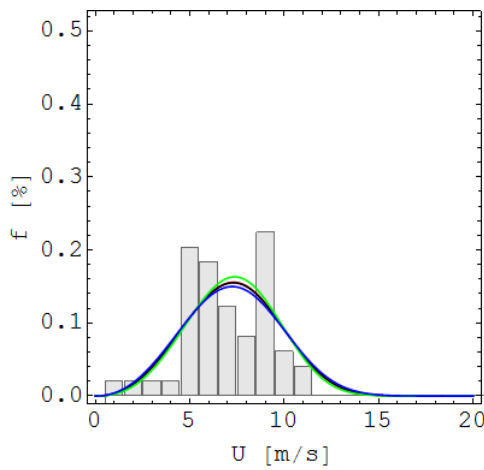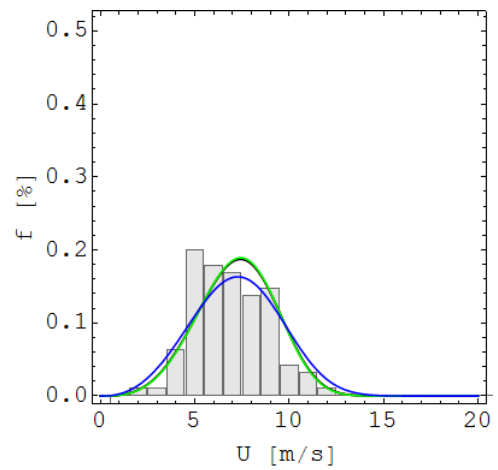<div align="center">Sector 12 (330 degree)</div>
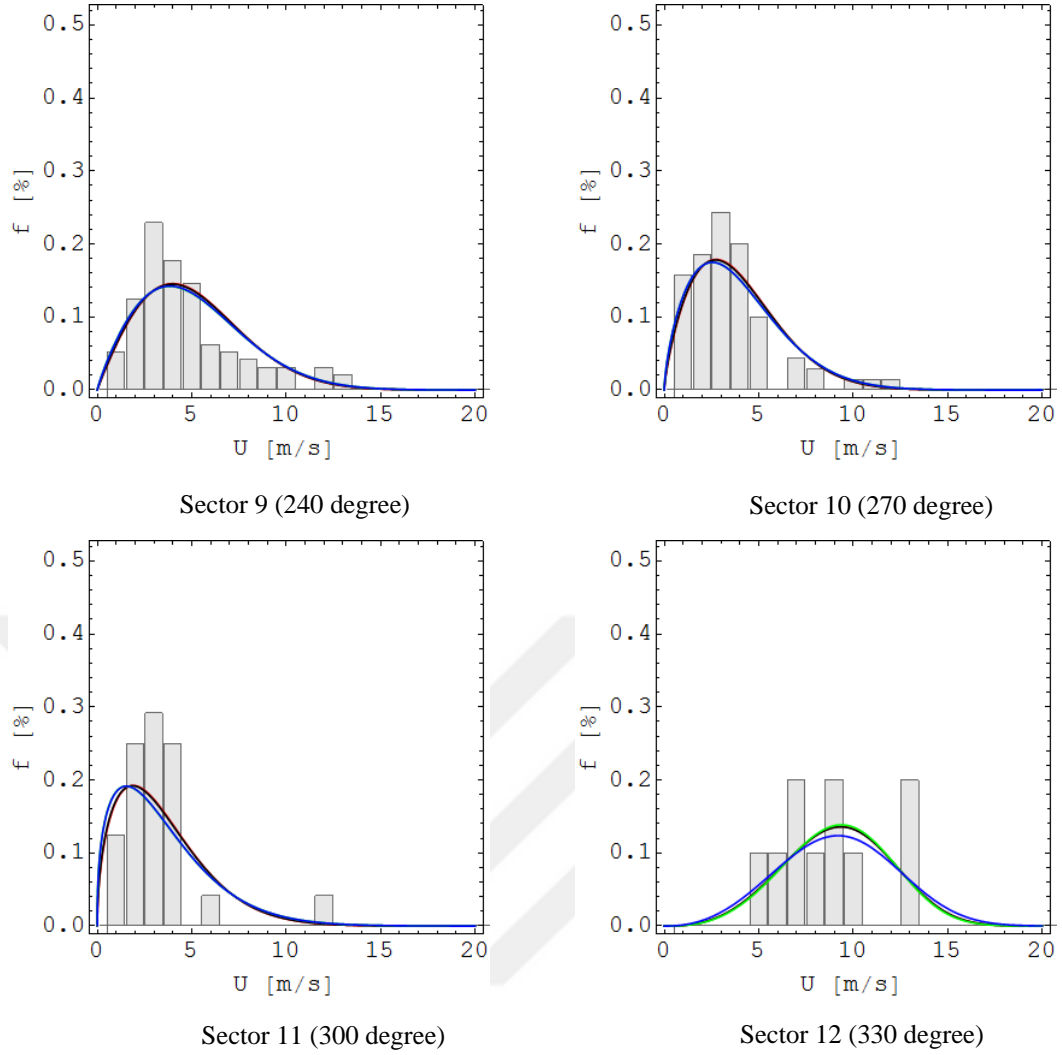
<div align="center">Figure 5.13. Twelve sectoral Weibull fitting of ASCAT datasets (Sector 7-12)</div>

Through comparing the figures it is noticed that, all the statistical fitting methods are well adjusted and similar. Considering MOM 3 method comparatively more accurate than others, the values has been utilized to create OWC files for WAsP project.

As the observed dataset of our study did not have efficient sample numbers for each sector, the samples were too few to count, that is why another proposed idea has been represented here. The proposed idea is to obtain more wind speed datasets in one sector, by reforming the sectoral division to 60 degree from 30 degree. So, in spite of having 12 sectors now, 6 sectoral representation has been investigated. As a result, the number of samples for wind speed calculation increased in every sector and it shows a better result of Weibull fitting.

(a) ASAR   (b) ASCAT
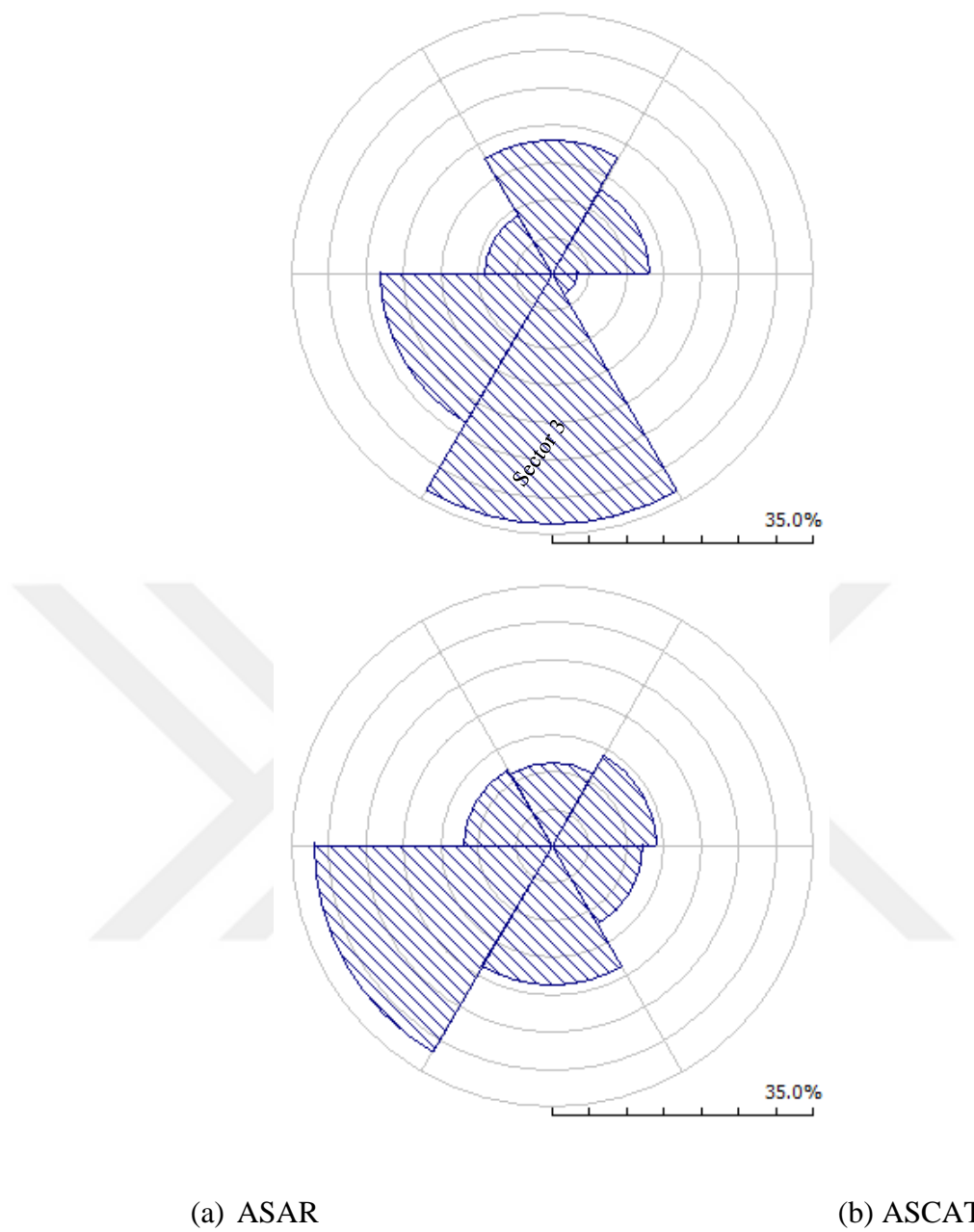
Figure 5.14. Six sectoral wind distribution

Table 5.5. Six sectoral statistical Weibull analysis of ENVISAT ASAR dataset

Sector	Method	A	k	v_m	RMSE	χ^2	R^2

Sector	Method	A	k	v_m	RMSE	χ^2	R^2
Sector 1	**EM**	5.50745	1.98471	4.88157	0.0384736	0.382512	0.716828
	MOM	5.50651	1.96875		0.0386524	0.382699	0.71419
	MOM3	5.5089	2.01335		0.0381659	0.383059	0.721339
	Epf	5.50941	2.02512		0.0380443	0.383624	0.723112
Sector 2	**EM**	5.41977	2.1064	4.80016	0.0813612	0.855438	0.479109
	MOM	5.41949	2.09053		0.081422	0.857126	0.478331
	MOM3	5.42	2.12431		0.0812999	0.853896	0.479894
	Epf	5.42011	2.13563		0.081265	0.853122	0.48034
Sector 3	**EM**	5.39597	1.47392	4.88192	0.344195	6.10465	0.062651
	MOM	5.38838	1.45836		0.344614	6.17142	0.06037
	MOM3	5.50492	1.93983		0.333866	4.67571	0.118069
	Epf	5.50568	1.95042		0.333684	4.65298	0.119028
Sector 4	**EM**	9.07118	2.66903	8.06373	0.0297235	0.600521	0.512678
	MOM	9.07281	2.65427		0.0297591	0.595873	0.51151
	MOM3	9.06607	2.71385		0.0296203	0.616369	0.516056
	Epf	9.07224	2.65943		0.0297466	0.597466	0.511921
Sector 5	**EM**	7.87944	1.98423	6.98403	0.0355017	0.566616	0.395377
	MOM	7.87808	1.96828		0.0354938	0.56199	0.395646
	MOM3	7.88566	2.11243		0.0356467	0.618558	0.390428
	Epf	7.88587	2.12395		0.0356666	0.624582	0.389747
Sector 6	**EM**	7.00936	2.96225	6.25577	0.0793677	1.23627	0.557558
	MOM	7.01076	2.9485		0.0795383	1.22127	0.555654
	MOM3	6.97077	3.33028		0.0751584	1.85139	0.603243
	Epf	6.99692	3.08273		0.0779126	1.38939	0.573633

Table 5.6. Six sectoral statistical Weibull analysis of ASCAT dataset

Sector	Method	A	k	v_m	RMSE	χ^2	R^2
	EM	6.40777	3.4975	5.76516	0.021669	0.246855	0.766533
	MOM	6.40887	3.4862		0.021656	0.245472	0.766811

Sector	Method						
Sector 1	**MOM3**	6.40667	3.50885		0.021682	0.2483	0.766238
	Epf	6.43836	3.18412		0.021586	0.227266	0.76831
Sector 2	**EM**	5.29984	2.37493	4.69734	0.016909	0.254249	0.805849
	MOM	5.30041	2.35945		0.016923	0.250762	0.80552
	MOM3	5.30098	2.3427		0.016941	0.247306	0.805107
	Epf	5.30097	2.34311		0.016941	0.247386	0.805118
Sector 3	**EM**	6.04031	2.19564	5.34942	0.012045	0.111977	0.860322
	MOM	6.0404	2.17986		0.011947	0.111472	0.862594
	MOM3	6.04018	2.20994		0.012139	0.112555	0.858142
	Epf	6.04008	2.21871		0.012198	0.112965	0.856751
Sector 4	**EM**	7.89689	3.16777	7.06943	0.015023	0.250581	0.753235
	MOM	7.89843	3.15487		0.015029	0.251145	0.753055
	MOM3	7.88371	3.27791		0.015019	0.247979	0.753364
	Epf	7.91069	3.05132		0.015112	0.257603	0.750319
Sector 5	**EM**	6.14938	2.16004	5.44591	0.006438	0.113565	0.883152
	MOM	6.14931	2.14422		0.006363	0.11006	0.885852
	MOM3	6.14908	2.12002		0.006254	0.105191	0.889739
	Epf	6.14921	2.13142		0.006304	0.107412	0.887945
Sector 6	**EM**	4.70771	1.39874	4.29132	0.026579	0.542946	0.647285
	MOM	4.69935	1.38336		0.026649	0.541176	0.645413
	MOM3	4.67739	1.34612		0.026845	0.539265	0.640193
	Epf	4.68202	1.35362		0.026802	0.539389	0.641323

While considering those values of table 5.5 and 5.6, it can be said that, it has lesser error values (RMSE and χ^2 near to zero and R^2 near to 1) in both ASCAT and ASAR scenarios comparing with the 12 sectoral scenario (table 5.3 and 5.4).Which indicates a better fitting of suggested Weibull statistical methods. These tables illustrative representation is given here after (figure 5.15 and 5.16) which defines the scenario more precisely.

Sector 1 (0 degree)

Sector 2 (60 degree)

Sector 3 (120 degree)

Sector 4 (180 degree)

Sector 5 (240 degree)

Sector 6 (300 degree)
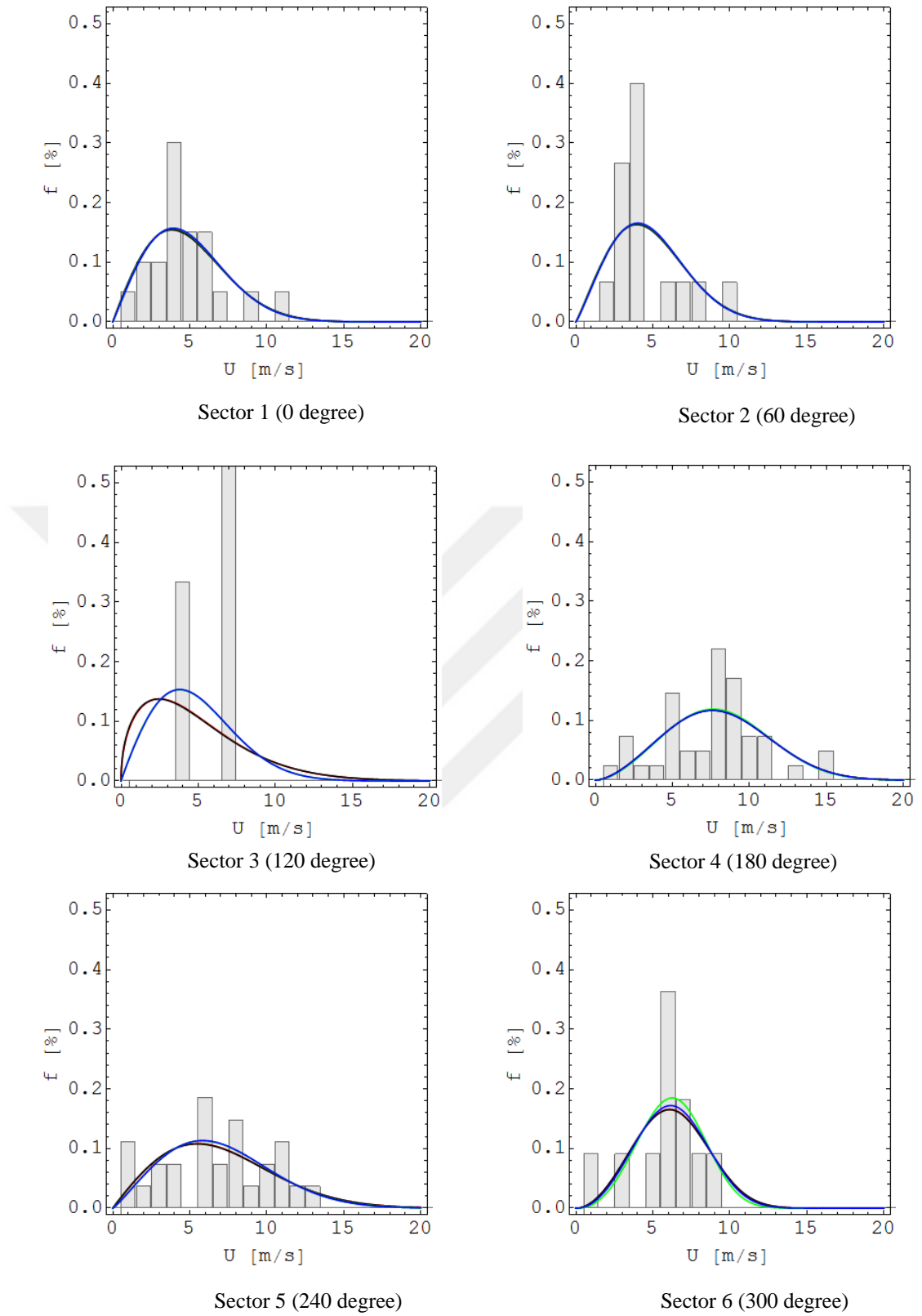
Figure 5.15. Six sectoral Weibull fitting of ASAR datasets

Sector 1 (0 degree)

Sector 2 (60 degree)

Sector 3 (120 degree)

Sector 4 (180 degree)

Sector 5 (240 degree)

Sector 6 (300 degree)

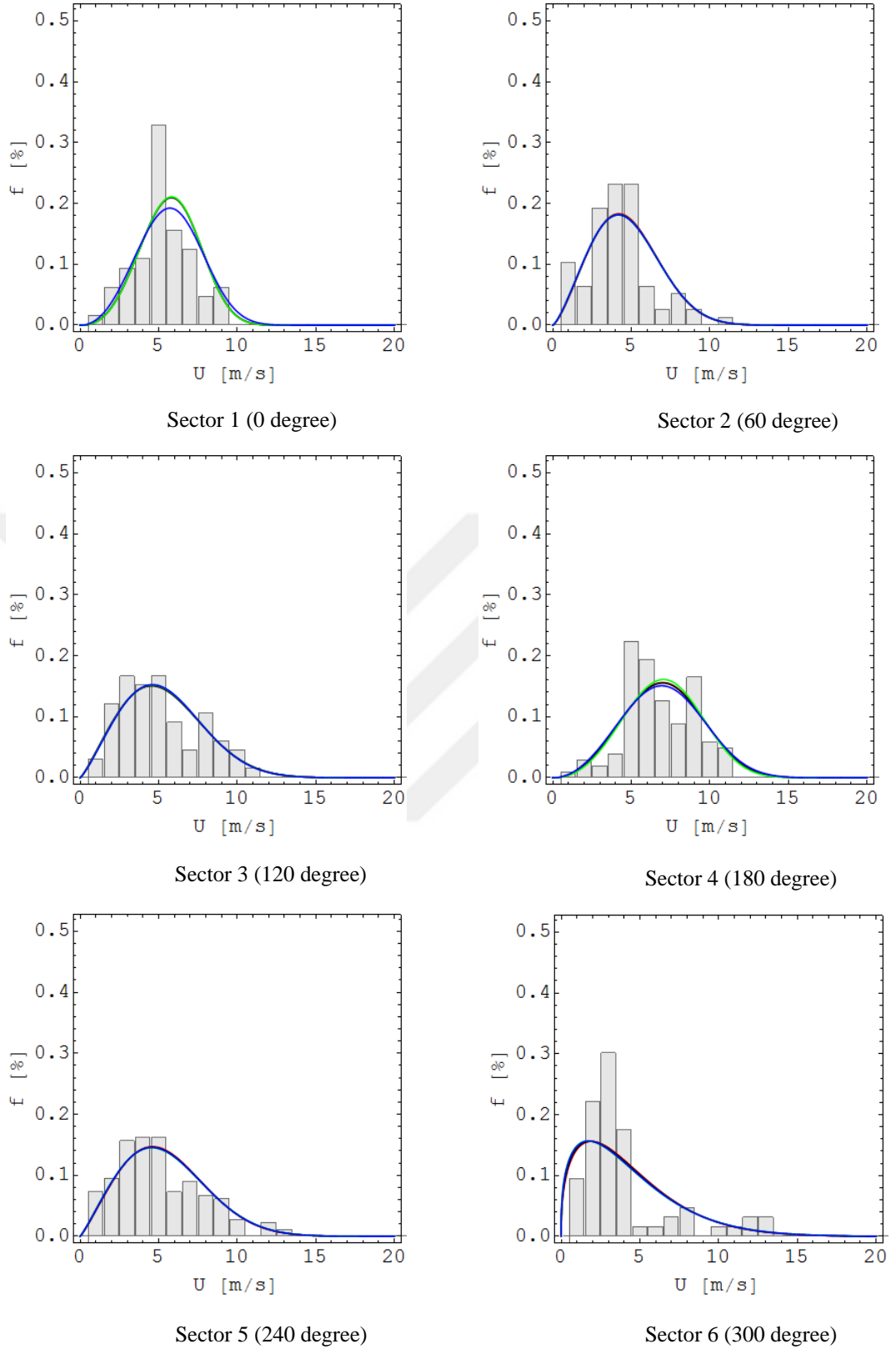Figure 5.16. Six sectoral Weibull fitting of ASCAT datasets

5.3. Generation of Atlas Datasets

In this phase of case study, the WAsP project to calculate the Atlas (GWC) values from ASAR and ASCAT was created. As mentioned before, MOM 3 method was utilized to create the OWC files and from those specific OWC files the generalized wind climate files (.lib) were produced. In addition, GWC files of GWA were also used to have a comparative study with ASCAT and ASAR. For this process, all 3 generalized wind climate files (.lib) for ASAR, ASCAT and GWA for the specific chosen locations are inserted in WAsP.

5.4. Calculation of Annual Wind Energy Production (AEP)

In WAsP software when Atlas files are used as input with the help of the flow model, the software can predict the wind climate on different location on the map. Given turbine locations are one-by-one calculated and each information is combined with the turbine characteristics in order to predict the annual production. This production is called Gross which means the total amount of energy that could be generated if the turbine is single. In wind farm, each turbine will effect each other based on the wind direction and create wake losses. This is also done by WAsP software and the results are altered due to these losses. The final result, so called NET AEP is the expected production as a total. It is preferred to have maximum 5-10% wake losses in wind farms and this is only related to turbine allocation.

Wake effect is the impact of turbines or blockades on each other which turns towards lesser wind speed and energy production in a wind farm. WAsP uses N.O. Jensen's (1984) wind farm model which is based on momentum-deficit theory (Mortensen et al., 2007). Katic and others prolonged this wind farm model in real life wind farms afterwards in 1986. (Katic, Højstrup, & Jensen, 1986). This wake model theory considers liner expansion of the wake behind the rotor by accounting the velocity deficiency at the starting of the wake to be the only variable. In the overlapping fraction of a wake, different rotor diameters and hub heights are considered with a down-wind rotor plane. [14](Katic et al., 1986).

---

[14] The rate of expansion (break-down) of the wake.
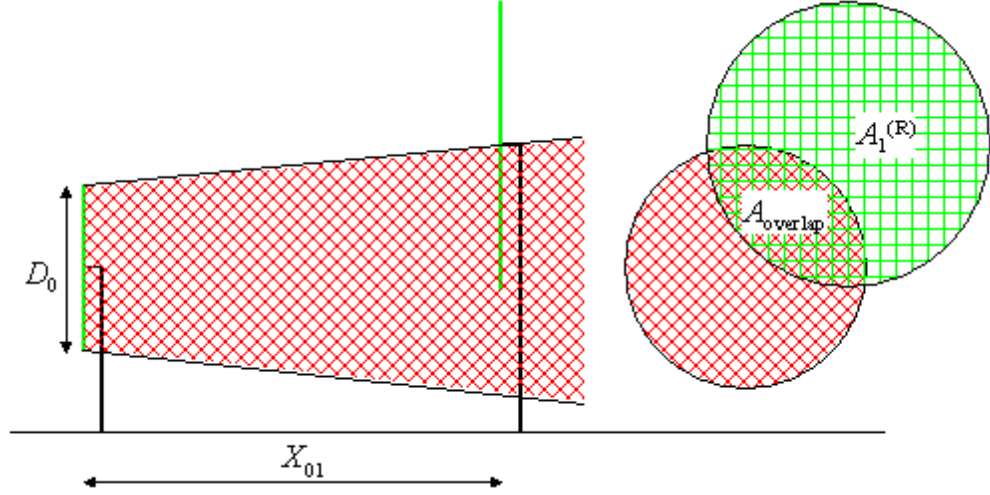
Figure 5.17. Flow field and wind farm geometry of N.O. Jensen's wake model (Jensen, 1983).

In WAsP model, the wind speed deficit at the down-wind wind turbine ("1") is calculated by:

$$\delta V_{01} = U_o(1 - \sqrt{1 - C_t})(\frac{D_o}{D_o + 2KX_{01}})^2 \frac{A_{overlap}}{A_1^R} \quad \text{(Jensen, 1983)}$$

$$\text{where } C_t = \frac{2F_t}{\rho \frac{\pi}{4} D_o^2 U_o^2} \quad \text{(Jensen, 1983)}$$

Here, U_0 denotes the wind speed at the up-wind turbine ("0"), D_0 as the rotor diameter, C_t as the thrust coefficient, K as the wake decay constant, X_{01} as the downwind horizontal distance between the wind turbines and $\frac{A_{overlap}}{A_1^R}$ denotes the overlapping fraction. For our study, the wake decay constant was considered to be 0.05.

5.4.1 Allocating Turbines According to Dominant Wind Direction

The selective zone was calculated and found to have 174.5 km^2. Based on this area, a minimum production from that extent was designed via allocating 134 turbines. These 134 turbines were chosen to have 3MW capacity individually. This results as estimation of 402 MW capacity offshore farm with 2.3 MW/ km^2 energy distribution per area. In our study, Vestas V112-3.0 MW model of turbine has been chosen which has a rotor diameter of 112 m and hub height of 84m. As at present, mostly used turbines are of around 3 MW for offshore wind technology, our turbine specification has been chosen accordingly (EWEA, 2013). Turbines were set in an equidistant of 10 diameter from each other as a way to let the wind recover from turbine to turbine.

Turbines front sides were also considered depending on the dominant wind directions. It was found to be 229.459^o, 218.015 for ASCAT and ASAR datasets respectively. The dominant direction for every sector has been determined by combining the wind speed and frequency generation of that respective sector and the opposite sector. In the below figure 5.18 the different wind farm layout based on the leading wind direction is presented where it shows a slight rotation of wind turbines formats.
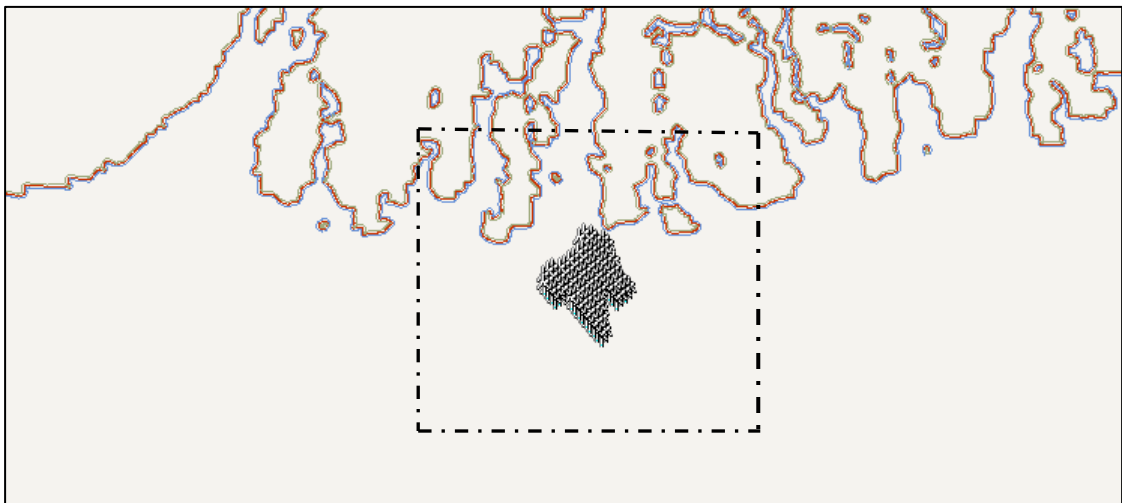
(a) Selected area of turbine allocation

| SAR (218.015°) | ASCAT (229.459°) | GWA (232.2°) |
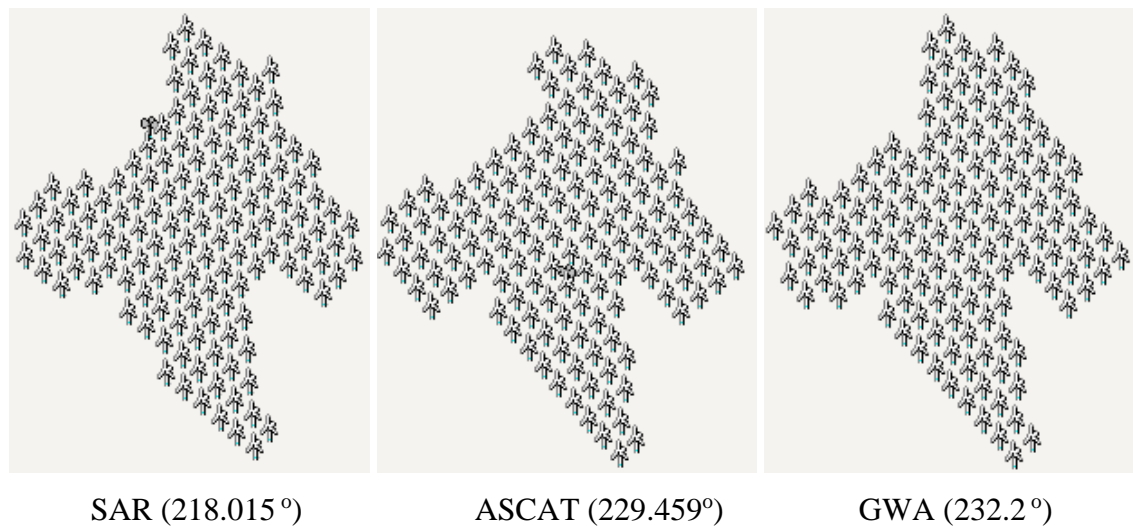
Figure 5.18. Wind farm layout

5.4.2 Calculation of AEP

In this WAsP project then, the selective wind farm grid has been inserted to calculate the gross and net annual energy production (AEP) along with the wake losses of the turbines. The Wind Farm insertion was a form of turbine cluster which specifies the power curve, generated power for a representative air density for each turbine at turbine hub height. The gross AEP is the energy production of a single turbine through corresponding wind distribution at the predicted hub height in the form of the supplied power curves. In gross AEP, the wake effect is not accounted. And for Net AEP case, the wake effect is counted as it the whole total annual energy of the farm. By the intricacy of this power curve and numerical wind distribution, each turbines annual energy production is calculated. Afterwards, by combing the each turbines annular energy and wake loses, the AEP is calculated for the whole wind farm.

Table 5.7. Twelve sectoral AEP using Moment 3 method

Source	Gross AEP (GWh)	Net AEP (GWh)	Wake Loss (%)
ASAR 12	1792	1693	5.52
ASAR 6	1793	1682	6.22

ASCAT 12	1385	1310	5.45
ASCAT 6	1379	1269	7.99
GWA	1352	1276	5.61

.

The above table (table 5.7) shows AEP estimation through MOM 3 method for all three datasets in 5 forms which are- ENVISAT ASAR for 12 sector and 6 sector, ASCAT for 12 sector and 6 sector and GWA. The results are quite similar among ASCAT and GWA, whereas ENVISAT ASAR datasets has an overestimation. While comparing the 12 sectors, it estimates a higher NET AEP, which leads to a higher error rate compared with (table 5.8). On the other hand, when the sectors are enlarged, the error rate is less specially in ASCAT scenario. But the wake losses are found to be in rise when it is 6 sector.

Table 5.8. Error Calculation of Satellite Datasets

Source	Sector	Error Rate (%)
ENVISAT ASAR	12	28
ENVISAT ASAR	12	27.6
ASCAT	6	2.6
ASCAT	6	0.5

For more detailed comparison of a 12 sectoral AEP estimation (based on MOM 3 fitting) has been presented hereafter(figure 5.18) where it shows a better comparison between the ASCAT and GWA values, whereas ENVISAT ASAR has an overestimation specifically in those sectors from where the NET AEP is high.
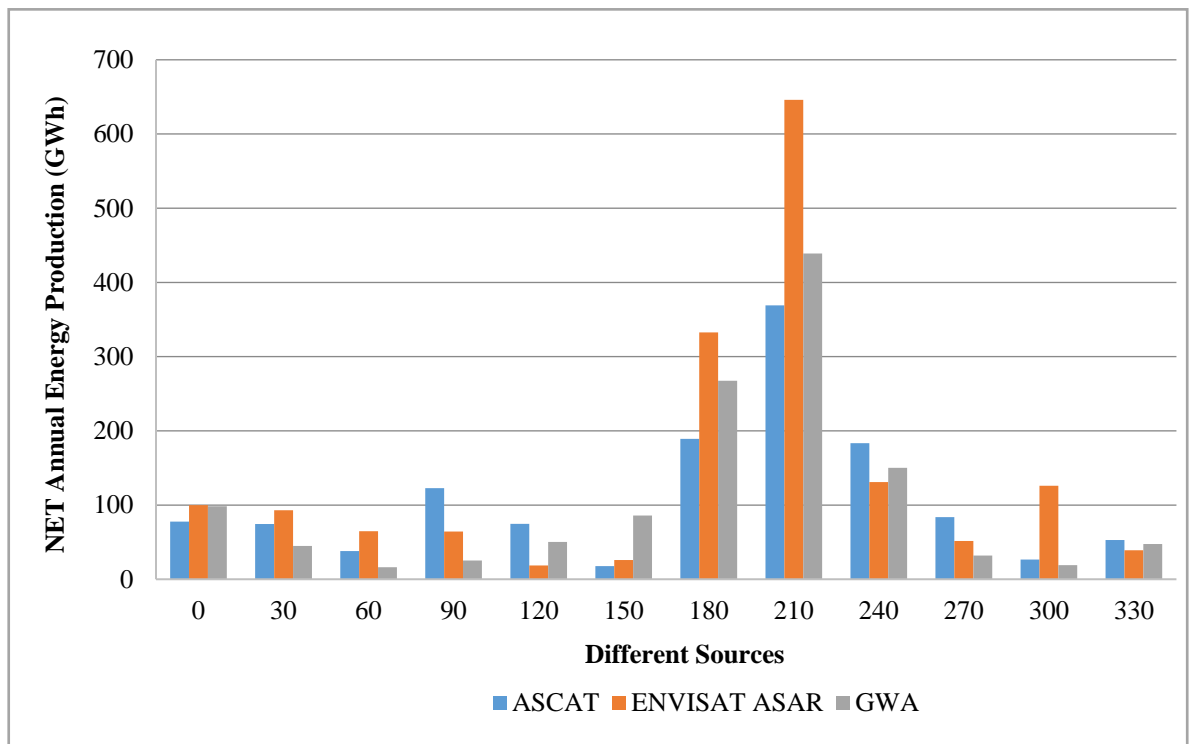
Figure 5.19. NET AEP comparison between different datasets

This result represents that when the sectors are enlarged, although there is a better fit to Weibull function due to more samples, the annual energy production in both gross and net form decreases than 12 sector estimation. As GWA is based on long term model data, it has been believed that it contains more realistic results and it has been taken as the Cooperative model. Nevertheless, the estimated energy production from ASCAT and GWA dataset matches well for the selective area along with a overestimation from ASAR; which demonstrates that more sample of data (over 500 in this case) gives more similar results to long term model statistics.

CHAPTER 6

DISCUSSION

For any precise study, higher number of samples are needed from SAR for wind resource assessment. Yet the sample number depends on the satellite archive, therefore nothing can be done in this study currently. But, Sentinel-1 A and B which is a new version of SAR technology, has started operating and collecting new images all over the globe. So there will be more data in the future and expected to be available for free. In addition, from previous studies it has been demonstrated that using satellite observations for wind resource estimation cases, the mean wind speed and the Weibull scale parameter (A) can be predicted well from around 70 samples considering an uncertainty of ±10% at a confidence level of 90% (Hasager et al., 2002). In other hand, to achieve the similar uncertainty and confidence level, the energy density and Weibull shape parameter (k) requires almost 2000 samples (Hasager et al., 2002). So, any location's wind energy density can be well predicted if the number of samples can be attained in a higher number.

In our study one of the critical scenario was to create a vector mapping of the Bay of Bengal as the topographic characteristic of the coastline has a really complex landscape scenario. Although it doesn't have high hills near coastlines but the excessive number of rivers and gates made it difficult to map the area. Nevertheless, a good elevation map has created finally and sensitively tested for the area along with 3 datasets. And from the result it shows that the map didn't affect the calculation significantly.

About, the datasets achieved from GWA found to have some complications in wind speed measurement near to the shore. In some specific points the GWA showed less wind speed at 50 m than 10 m height. Though this point is ignored as the hub height of our specified turbine is 84 m and interpolation of 100 m calculation is more effective on 84 meter prediction.

In wind energy meteorology, proper way to measurement should be dependent on the same time series of datasets. But, due to applying different remote sensing methods datasets, same time format could not be used. Rather than, the maximum number of samples from the obtained period has been accounted. But, it will be much more certain to use the same time of period for establishing a proper way of resource mapping. Also, from this study, our suggestion would be to use ASCAT and statistical models for offshore resource assessment and SAR winds to analyze the finer scale variability near the coast (e.g. effects of land topography).

While selecting an area for offshore wind farm, a location further from shore for a better wind could be selected, but there is not enough data from there and the planning was to have a wind farm without setting up a base station which requires less than 4 km

distance from the coastline. Though there will be higher rated turbines available soon, in our study, 3 MW capacity turbine was used in a reason to keep pace with the conventional technologies that are present in recent usage throughout the world. It is found from a press release[15] that, in Bay of Bengal at the eastern side, near coast area, wind farm is planned to be set up, while neither GWA nor our dataset shows any higher wind capacity area there, which can be recommended as a political policy of Bangladesh government only.

In the Weibull Statistical Analysis section, a four sectoral dataset was analyzed (45 degree each) considering the main wind directional paths, to observe the quality of wake modeling. But, the files could not be run by WAsP software which had to remove from the phases of statistical analysis reluctantly.

At the end, it can be said that, the combined 3 datasets for searching a potential location could have been more accurate if any in situ measurement could have been found. As GWA is also based on model results, it is not the desired data comparison. Yet this is the only dataset available for our selected location and wind engineers faces this problems in real life frequently.

CHAPTER 7

CONCLUSION

For a large offshore area, it is very difficult to define where should be focused on for planning of an offshore windfarm. Even we know, satellite measurements are new and has limited number of samples in any location, they are still the only representative of onsite measurements more than any of the models. Several models of satellites along with its higher number of samples can be used without any local measurements, although this can lead to very big uncertainties. But it can estimate a general region for further broad investigation.

---

[15]   http://www.windpowerengineering.com/construction/transportation/bangladesh-to-enter-the-wind-era/

Consequently, in this study three (ENVISAT ASAR, ASCAT and GWA) remote sensing measurements have been discussed and those datasets were used primarily to generate a wind Atlas of the Bay of Bengal and by utilizing that Atlas a potential zone has been found at a near shore area of the Bay of Bengal. Formerly, a case study has been performed to predict the Annual Energy Production of that particular area. Among these datasets, two (ENVISAT ASAR and ASCAT) are from satellite based and one (GWA) from long term mesoscale model measurement. The satellite datasets were compared with GWA, as no offshore wind farm has been established in the Bay of Bengal yet and there is no onsite data to have a suitable comparative study.

In our study, the data analysis on the satellite datasets has been performed along with different statistical methodology selected empirical state of the art moment fitting function to have a better estimation. The initial results with the current dataset shows similar shape and scale parameters for climate values. Therefore it can be understood that, with the limited number of sample datasets, even the simple empirical method are accepted to use. Furthermore, in this study, a potential location has been chosen to define if these data can be used for modeling. As a result all the datasets have given similar production values without directional information. When the directional information is added, less number of data samples were seen to create less quality as it is expected.

In the study, most of the calculation with their error is pointing towards the fact of directional view of wind (sectors) and lesser number of samples. Differences were accounted because of limited data in some sectors. So, reducing number of the sectors were suggested which showed improvement in Weibull fitting, though it has a slight increase in wake effects. Analysis shows that while there is not enough samples, all the methods shows similar results. One can understand from this result that, satellite data can be used to identify the highest density areas for a particular zone but it cannot be used exactly to estimate the highest region. As in our study, the satellite datasets were pointing the same location with GWA and one can make a preliminary analysis of the wind conditions by knowing that it can go up to 20% uncertainty.

From this study, it can be said that, satellite gives us the ability to identify the higher power density area so that we can utilize it for met mast set up. Even to find a potential zone for establishing mat mast is challenging and time worthy. The foundation of this thesis project is that, satellite datasets can be used to identify potential zone and it has a promising outcome of calculation capability of annual energy production, if compared with any long time statistical result and bathymetry data combination.

Furthermore, all three datasets used in this study comprises similar AEP (ASCAT better than ASAR) at the coastal area which indicates the selective location as a potential area and further researches regarding this study can lead towards a better future for the wind energy sector of Bangladesh.

REFERENCES

Amaya-Martínez, P.-A., Saavedra-Montes, A.-J., & Arango-Zuluaga, E.-I. (2014). A statistical analysis of wind speed distribution models in the aburrá valley, Colombia. *CT&F-Ciencia, Tecnología y Futuro, 5*(5), 121-136.

ASCAT, Metop Meteorological Missions. (2006). Retrieved 28 June 2016, from European SpaceAgency(ESA), Retrieved from http://www.esa.int/Our_Activities/Observing_the_Earth/The_Living_Planet_Pro gramme/Meteorological_missions/MetOp/About_ASCAT

Badger, M. (2015). *Wind resources*. Retrieved from Malmö:

Badger, M., Astrup, P., Hasager, C. B., Chang, R., & Zhu, R. (2014). *Satellite based wind resource assessment over the South China Sea.* Paper presented at the China Wind Power Conference 2014.

Bangladesh Energy Situation .Retrieved from https://energypedia.info/wiki/Bangladesh_Energy_Situation

Bay of Bengal. Google Earth. Retrieved from http://earth.google.com

Bay of Bengal Maritime Boundary Arbitration between Bangladesh and India, (2014).

Beaucage, P., Bernier, M., Lafrance, G., & Choisnard, J. (2008). Regional mapping of the offshore wind resource: Towards a significant contribution from space-borne synthetic aperture radars. *IEEE Journal of Selected Topics in Applied Earth Observations and Remote Sensing, 1*(1), 48-56.

Bingöl, F., Hassager, C. B., Badger, M., & Badger, J. (2013). RZGM2013-14.

Burton, T., Sharpe, D., Jenkins, N., & Bossanyi, E. (2001). *Wind energy handbook*: John Wiley & Sons.

Celeska, M., Najdenkoski, K., Stoilkov, V., Buchkovska, A., Kokolanski, Z., & Dimchev, V. (2015). *Estimation of Weibull parameters from wind measurement data by comparison of statistical methods.* Paper presented at the EUROCON 2015-International Conference on Computer as a Tool (EUROCON), IEEE.

Center for Renewable Energy and Sustainability, C. (Producer). Wind Power. Retrieved from http://renewable.uprrp.edu/index.php?page=wind-power

Christiansen, M. B. (2006). *Wind energy applications of synthetic aperture radar.* Institute of Geography, Faculty of Science, University of Copenhagen.

Christiansen, M. B., Koch, W., Horstmann, J., Hasager, C. B., & Nielsen, M. (2006). Wind resource assessment from C-band SAR. *Remote Sensing of Environment, 105*(1), 68-81.

COAPS, C. f. O.-A. P. S. (2003). Scatterometry and Ocean vector winds. Retrieved from https://coaps.fsu.edu/scatterometry/about/overview.php#ers

Dagestad, K.-F., Horstmann, J., Mouche, A., Perrie, W., Shen, H., Zhang, B., . . . Lehner, S. (2012). *Wind retrieval from synthetic aperture radar-an overview.* Paper presented at the 4th SAR Oceanography Workshop (SEASAR 2012).

Development of Renewable Energy Technologies by BPDB. Retrieved from http://www.bpdb.gov.bd

EWEA, E. W. E. A. (1999). *Wind Force 12: A blueprint to achieve 12% of the world's electricity from wind power by 2020.* Paper presented at the London: Forum for Energy and Development and Greenpeace International.

EWEA, E. W. E. A. (2013). Deep Water The next step for offshore wind energy. *European Wind Energy Association report, Brussels. See http://www. ewea. org.*

Global Wind Atlas. (2015). Retrieved from http://globalwindatlas.com/tutorials.html

GWEC, G. W. E. C. (2015). Global wind report, annual market update 2015: Global Wind Energy Council Brussels, Belgium.

Hasager, C. B., Astrup, P., Barthelmie, R., Dellwik, E., Mortensen, N. G., Nielsen, M., . . . Rathmann, O. (2002). *Validation of satellite SAR offshore wind speed maps to in-situ data, microscale and mesoscale model results*. Retrieved from http://orbit.dtu.dk/files/7726836/ris_r_1298.pdf

Hasager, C. B., Astrup, P., Christiansen, M. B., Nielsen, M., & Barthelmie, R. (2006). *Wind resources and wind farm wake effects offshore observed from satellite.* Paper presented at the Proceedings of the European Wind Energy Conference and Exhibition (EWEC).

Hasager, C. B., Badger, M., Mouche, A., Stoffelen, A., Driesenaar, T., Karagali, I., . . . Nielsen, M. (2012). Norsewind satellite wind climatology.

Hasager, C. B., Bingöl, F., Badger, M., Karagali, I., & Sreevalsan, E. (2011). *Offshore Wind Potential in South India from Synthetic Aperture Radar* (8755039081). Retrieved from http://orbit.dtu.dk/fedora/objects/orbit:87302/datastreams/file_7749647/content

Hasager, C. B., Mouche, A., Badger, M., Bingöl, F., Karagali, I., Driesenaar, T., . . . Longépé, N. (2015). Offshore wind climatology based on synergetic use of Envisat ASAR, ASCAT and QuikSCAT. *Remote Sensing of Environment, 156*, 247-263.

Hasager, C. B., Peña, A., Christiansen, M. B., Astrup, P., Nielsen, M., Monaldo, F., . . . Nielsen, P. (2008). Remote sensing observation used in offshore wind energy. *IEEE Journal of Selected Topics in Applied Earth Observations and Remote Sensing, 1*(1), 67-79.

Henderson, A. R., Morgan, C., Smith, B., Sørensen, H. C., Barthelmie, R. J., & Boesmans, B. (2003). Offshore wind energy in Europe-A review of the state-of-the-art. *Wind energy, 6*(1), 35-52.

Jensen, N. O. (1983). *A note on wind generator interaction*.

Kader, A., Chowdhury, M. Z. R., Uddin, M. M., Hoque, M. E., & Basak, S. C. (2013). Bathymetric study of the Bay of Bengal based on open source satellite and sounding data. *International Journal of Geomatics and Geosciences, 4*(1), 116.

Katic, I., Højstrup, J., & Jensen, N. O. (1986). *A simple model for cluster efficiency.* Paper presented at the European Wind Energy Association Conference and Exhibition.

Khan, M., Iqbal, M., & Mahboob, S. (2004). A wind map of Bangladesh. *Renewable Energy, 29*(5), 643-660.

Kidmo, D., Danwe, R., Doka, S., & Djongyang, N. (2015). Statistical analysis of wind speed distribution based on six Weibull Methods for wind power evaluation in Garoua, Cameroon. *Revue des Energies Renouvelables, 18*(1), 105-125.

Mathew, S. (2006). *Wind energy: fundamentals, resource analysis and economics* (Vol. 1): Springer.

Mortensen, N., Heathfield, D., Myllerup, L., Landberg, L., & Rathmann, O. (2007). Getting started with WAsP 9, Risø-I-2571 (EN). *Risø National Laboratory, Technical University of Denmark*.

Mukut, A. M. I., Islam, M. Q., & MahbubulAlam, M. (2008). Prospect of Wind Energy in the Coastal Belt of Bangladesh. *The Pacific Journal of Science and Technology, 9*(2), 442-451.

Peña, A., Hahmann, A., Hasager, C. B., Bingöl, F., Karagali, I., Badger, J., . . . Clausen, N.-E. (2011). *South Baltic Wind Atlas: South Baltic Offshore Wind Energy Regions Project*: Risø DTU-National Laboratory for Sustainable Energy.

Pramod, J. (2011). Wind energy engineering. *Mac Graw Hill*.

Ricciardulli, L., Wentz, F.J. (Producer). (April 2016, 20 June,2016). Remote Sensing Systems ASCAT C-2015 Daily Ocean Vector Winds on 0.25 deg grid, Version 02.1. Retrieved from www.remss.com/missions/ascat

SAF, O. (2013). ASCAT Wind Product User Manual. *Version, 1*, 23.

Small, D., Rosich, B., Schubert, A., Meier, E., & Nüesch, D. (2005). *Geometric validation of low and high-resolution ASAR imagery.* Paper presented at the Envisat & ERS Symposium.

Soisuvarn, S., Jelenak, Z., Chang, P. S., Alsweiss, S. O., & Zhu, Q. (2013). CMOD5. H— A high wind geophysical model function for C-band vertically polarized satellite scatterometer measurements. *IEEE Transactions on Geoscience and Remote Sensing, 51*(6), 3744-3760.

Solar and Wind Energy Resource Assessment (SWERA) Retrieved from http://en.openei.org/datasets/files/965/pub/swera_bangladesh_fullreport.pdf